UNIVERSITY OF CALIFORNIA

Los Angeles

Identification of determinants of aggressive prostate cancer

A dissertation submitted in partial satisfaction of the

requirements for the degree Doctor of Philosophy

in Molecular Biology

by

John Kyung Lee

2016

ABSTRACT OF THE DISSERTATION

Identification of determinants of aggressive prostate cancer

by

John Kyung Lee

Doctor of Philosophy in Molecular Biology

University of California, Los Angeles, 2016

Professor Owen N. Witte, Chair

Prostate cancer is a heterogeneous disease arising from the epithelial cells of the prostate gland. While most prostate cancers are considered to be indolent, subsets of these cancers are or will evolve to become aggressive with heightened proliferative and invasive capacity. Two features that accompany this lethal prostate cancer phenotype are (1) androgen-independent growth and, in many cases, (2) the acquisition of neuroendocrine differentiation. Few treatments are effective at this stage and a better understanding of the disease biology is required to develop therapeutics that extend and enhance life. To this end, we set out to characterize determinants of aggressive prostate cancer, with specific focus on the epithelial cell of origin of cancer, active kinase signaling networks, and the genetics of neuroendocrine prostate cancer (NEPC).

Our group has developed technology to isolate and transform basal cells from the human prostate epithelium using lentivirus to introduce defined oncogenic alterations into benign cells prior to

transplantation in mouse hosts. However, we were previously unable to assess the effect of oncogenic stress on luminal cells of the human prostate epithelium. We therefore adapted the human prostate transformation assay to use an intermediate organoid culture step to show that basal- and luminal-derived tumors arising from c-Myc overexpression and PI3K pathway activation exhibit distinct cancer differentiation states.

We have previously shown that global phosphorylation levels of tyrosine residues are increased in advanced prostate cancer relative to primary prostate cancer. To understand the active tyrosine kinase signaling networks in aggressive prostate cancer, we performed liquid chromatography tandem mass spectrometry to profile the tyrosine phosphoproteome of metastatic prostate cancer tissues obtained at rapid autopsy. We identified active and druggable targets/pathways including SRC, epidermal growth factor receptor (EGFR), rearranged during transfection (RET), anaplastic lymphoma kinase (ALK), and MAPK1/3 that may form the basis for future kinase inhibition studies in prostate cancer.

Finally, we used the human prostate transformation assay to define an important functional role for aberrant N-Myc expression in the setting of PI3K pathway activation in the initiation of NEPC. With this human NEPC model system, we established that epithelial cells can give rise to neuroendocrine cancer in the prostate gland and provided direct evidence of in vivo prostate cancer plasticity. Furthermore, N-Myc expression is required for maintenance of the cancer state and destabilizing N-Myc through inhibition of a kinase-independent interaction with Aurora A kinase may be a promising therapeutic strategy for NEPC.

The dissertation of John Kyung Lee is approved.

Christopher Denny

Thomas G. Graeber

Antoni Ribas

Michael Alan Teitell

Owen N. Witte, Committee Chair

University of California, Los Angeles

2016

DEDICATION

This dissertation is dedicated to my wife, Diana Rhee, my daughter, Penelope Lee, and my parents, Kwang Hoon and So Jong Lee.

TABLE OF CONTENTS

List of Figures

List of Tables

ACKNOWLEDGMENTS

I would like to thank my mentor, Dr. Owen Witte, for all of his support and mentorship. Owen has constantly challenged me to think critically and to focus on the clinical translational impact of my science. I am indebted to him for the unparalleled training and his backing of my career as a physician-scientist.

I would also like to thank the members of my doctoral committee: Christopher Denny, Thomas G. Graeber, Antoni Ribas, and Michael Alan Teitell. Each member provided significant expertise, advice, and support that proved invaluable during this period of scientific training.

Chapter 1 contains excerpts from the review article “Clinical targeting of mutated and wild-type protein tyrosine kinases in cancer” published in Molecular and Cellular Biology. Excerpts and figures are reproduced with permission.

Chapter 2 and 3 are reproduced with permission from the Proceedings of the National Academy of Sciences.

Chapter 4 is reproduced with permission from Cancer Cell.

I thank the sources of funding that have supported my research including the Specialty Training and Advanced Research Program at UCLA, the Division of Hematology-Oncology at UCLA, the Eli and Edythe Broad Center of Regenerative Medicine and Stem Cell Research and California

Institute for Regenerative Medicine Clinical Fellowship, the Tower Cancer Research Foundation Career Development Award, and the Prostate Cancer Foundation Young Investigator Award.

Finally, I thank my family and friends for their patience and support. The last few years have been emotionally difficult but you have always kept me centered and grounded to face life's challenges and grow from them.

VITA

2001	A.B. magna cum laude, Biochemical Sciences Harvard University Cambridge, Massachusetts
2004-2005	Award Recipient/Medical Student Howard Hughes Medical Institute-National Institutes of Health Research Scholars Program Bethesda, Maryland
2006	M.D., Medicine Geisel School of Medicine at Dartmouth Hanover, New Hampshire
2010-2016	Award Recipient/Trainee Specialty Training And Advanced Research Fellowship University of California, Los Angeles
2013, 2014	Diplomate in Internal Medicine and Medical Oncology The American Board of Internal Medicine
2014-2015	Award Recipient/Trainee California Institute for Regenerative Medicine Training Grant University of California, Los Angeles
2015-2016	Award Recipient Tower Cancer Research Foundation Career Development Award University of California, Los Angeles
2015-2018	Award Recipient Prostate Cancer Foundation Young Investigator Award University of California, Los Angeles

PUBLICATIONS

Drake, J. M., Graham, N. A., **Lee, J. K.**, Stoyanova, T., Faltermeier, C. M., Sud, S., Titz, B., Huang, J., Pienta, K. J., Graeber, T. G., & Witte, O. N. (2013). Metastatic castration-resistant prostate cancer reveals intrapatient similarity and interpatient heterogeneity of therapeutic kinase targets. *Proc Natl Acad Sci U S A, 110*(49), E4762-4769. doi: 10.1073/pnas.1319948110

Drake, J. M., **Lee, J. K.**, & Witte, O. N. (2014). Clinical targeting of mutated and wild-type protein tyrosine kinases in cancer. *Mol Cell Biol, 34*(10), 1722-1732. doi: 10.1128/mcb.01592-13

Park, J. W., **Lee, J. K.**, Phillips, J. W., Huang, P., Cheng, D., Huang, J., & Witte, O. N. (2016). Prostate epithelial cell of origin determines cancer differentiation state in an organoid transformation assay. *Proc Natl Acad Sci U S A, 113*(16), 4482-4487. doi: 10.1073/pnas.1603645113

Lee, J. K., Phillips, J. W., Smith, B. A., Park, J. W., Stoyanova, T., McCaffrey, E. F., Baertsch, R., Sokolov, A., Meyerowitz, J. G., Mathis, C., Cheng, D., Stuart, J. M., Shokat, K. M., Gustafson, W. C., Huang, J., & Witte, O. N. (2016). N-Myc Drives Neuroendocrine Prostate Cancer Initiated from Human Prostate Epithelial Cells. *Cancer Cell, 29*(4), 536-547. doi: 10.1016/j.ccell.2016.03.001

PRESENTATIONS

Oral Presentations:

2013:
Molecular Biology Institute Student Seminar

2014:
UCLA Stem Cell Club

2015:
Molecular Biology Institute Student Seminar
UCLA SPORE in Prostate Cancer Investigators' Meeting
UCLA Hematology-Oncology Didactic Seminar

Poster Presentations:

2015:
AACR Special Conference MYC: From Biology to Therapy
HHMI Science Meeting
UCLA BSCRC Annual Stem Cell Symposium
Broad Tri-Institutional Stem Cell Meeting
UCLA STAR Symposium
UCLA Department of Medicine Research Day

2016:
UCLA BSCRC Annual Stem Cell Symposium
UCLA Molecular Biology Institute Retreat

Chapter 1:

Introduction

Prostate cancer is the second leading cause of cancer mortality with approximately 26,120 deaths in the United States in 2016 [1]. Approximately 14% of all men will be diagnosed with prostate cancer during their lifetime, but most will be diagnosed at an early stage due to early detection from screening of serum prostate specific antigen (PSA) levels. In these cases, prostate cancer is usually localized to the prostate and can be cured with surgery and/or radiation therapy. In many men, however, the disease is either first identified after dissemination to distant sites or recurs some time later despite local therapies. At this advanced stage, prostate cancer is not considered curable. Depletion of androgens by castration [2], by either surgical or medical means, has been the single most effective treatment for advanced prostate cancer because of the dependence of prostate cancer on the androgen receptor (AR) signaling axis for proliferation and survival [3]. While nearly all patients respond to androgen deprivation, the response is usually short-lived and the disease recurs as castration-resistant prostate cancer (CRPC).

Data from the multi-institutional Stand Up To Cancer/Prostate Cancer Foundation/American Association for Cancer Research West Coast Prostate Cancer Dream Team indicates that inhibition of the AR signaling axis by blocking adrenal androgen production [4] or direct targeting of AR [5] may engender the evolution of aggressive variants of CRPC including neuroendocrine prostate cancer (NEPC) as a mechanism of adaptive resistance (unpublished data). NEPC has until recently been thought to represent an exceedingly rare subtype of prostate occurring in less than 1% of all primary prostate cancer, where conventional prostate adenocarcinoma is the overwhelmingly predominant histology seen. NEPC is distinguished by histologic features, variable expression of markers of neuroendocrine differentiation, absent AR expression, and loss of dependence on the AR signaling axis [6, 7]. Yet, autopsy series have

shown that NEPC is identified in up to 20-25% of all lethal metastatic prostate cancers [8]. Further, NEPCs are associated with poor clinical prognoses due an aggressive course and the lack of effective treatments.

In order to develop new therapeutics for lethal CRPC, we require a more complete understanding of the cellular and genetic components involved in the genesis and progression of prostate cancer. In the past decade, advances in high throughput sequencing technology and large sequencing initiatives have generated a sizable array of known and previously unknown genetic correlates of aggressive prostate cancer [9-11]. Transcriptome [12, 13] and proteome [14, 15] analyses of prostate cancer have also provided a wealth of information regarding global gene expression changes and oncogenic signaling activity that is not otherwise captured by genomic information. The ongoing challenge is to functionally characterize and validate these rich but complex oncogenic associations in the appropriate cellular contexts using forward genetics. Once relevant model systems have been developed that recapitulate aggressive prostate cancer biology, we can define vulnerabilities for therapeutic targeting.

1. The epithelial hierarchy of the benign prostate gland

The benign prostate gland is composed of three glandular zones, the peripheral zone, the central zone, and the transition zone [16]. All regions are composed of both non-glandular and glandular features. Glandular zones demonstrate defined architecture with the presence of both ducts and acini that are lined by two epithelial cell layers, namely an outer low cuboidal layer of basal cells (basal cytokeratin-positive and AR-negative) and an inner tall columnar mucin-secreting layer of

luminal cells (luminal cytokeratin-positive and AR-positive). Interspersed between the basal and luminal cell layers are rare neuroendocrine cells (neuroendocrine differentiation marker-positive and AR-negative) that generally reside in the basal layer but often demonstrate neurite-like extensions that extend into the luminal layer [17]. Basal, luminal, and neuroendocrine cells represent the three epithelial populations of the prostate gland (Figure 1).

Preliminary insight into the epithelial hierarchy and the presence of an epithelial stem cell arose from studies of hormone-responsiveness in the prostate. English et al. showed surgical castration of adult male rats produced prostate glandular involution with a significant reduction in number of luminal cells but not basal cells [18]. Upon supplementation of androgen via subcutaneous injection, the remaining cells that were castration-resistant, primarily basal cells and few luminal cells, could proliferate to regenerate full-fledged glands [18]. Further, Tsujimura et al. showed that this cycle of prostate involution-regeneration can be repeated over thirty times in animal models, indicating the presence of long-lived prostatic epithelial stem cells [19]. However, these studies could not unequivocally determine whether the putative epithelial stem cell population, defined by castration-resistance and tissue regenerative capacity, resided in the basal or luminal layers or perhaps both.

Subsequent work in defining the epithelial stem cell population in the prostate has largely relied on two different strategies: (1) the prospective isolation of cell populations coupled with an in vivo recombination assay and (2) lineage tracing in transgenic animals using cell-type specific reporters. Cunha and Lung originally developed a technique to combine tissue fragments of embryonic urogenital sinus mesenchyme (UGSM) and embryonic urogenital epithelial cells in a

graft that could be implanted under the kidney capsule of mice to regenerate functional prostate glands [20]. Our group subsequently adapted elements of this in vivo recombination technique to use dissociated mouse prostate epithelial cells and cultured embryonic UGSM to regenerate the branching tubular morphology of the prostate gland in vivo (Figure 2) [21]. Importantly, this advance has allowed the direct functional interrogation of specific prostate epithelial populations in glandular regeneration. Meanwhile, other groups have used lineage tracing to identify the contribution of different epithelial cell lineages to prostate gland development [22]. In these studies, genetically engineered mouse (GEM) models using basal cytokeratin (K5 or K14) promoters and luminal cytokeratin (K8 or K18) promoters are used to label basal or luminal cells with the expression of distinct fluorescent reporters that can be visualized to characterize progeny in situ (Figure 3).

Our group has shown that cell surface expression of Sca-1 (stem cell antigen-1) on mouse prostate epithelial cells enriches for the capacity to regenerate prostate tubular structures using the in vivo recombination assay [23]. This finding was simultaneously corroborated by Burger et al., who also found that Sca-1 expressing prostate cells highly express alpha-6-integrin and Bcl-2 which are markers of stem cells in other tissues [24]. We further demonstrated that $Lin^{-}Sca\text{-}1^{+}CD49f^{+}$ mouse prostate cells, localized to the basal layer of glands in the proximal region of ducts in the prostate, are substantially enriched in regenerative capacity [25]. As Sca-1 is not expressed in the human prostate, we identified Trop2 (TACSTD2) as an alternative marker of a subpopulation of basal cells in the mouse and human prostate with high regenerative activity and multi-lineage potential to generate basal, luminal, and neuroendocrine cells [26]. Importantly, we

have shown that human Trop2^{+}CD49f^{hi} basal cells but not Trop2^{+}CD49f^{lo} luminal cells can regenerate prostatic tubules in the context of the in vivo recombination assay [27].

While our studies have suggested that stem cell activity in the prostate is isolated to the basal layer, others using lineage tracing experiments have developed different conclusions. Notably, Wang et al. identified the first minority population of luminal cells, a castration-resistant Nkx3.1-expressing (CARN) cell, that can give rise to both basal and luminal cells [28]. Subsequent work from Choi et al. demonstrated that adult basal and luminal cells are self-sustaining lineages in mice through multiple rounds of prostate involution-regeneration [29]. However, Ousset et al. have convincingly shown through a systemic evaluation of the postnatal prostate development that the cellular hierarchy during this process is mediated by multipotent basal stem cells, in addition to unipotent basal and luminal cells [30]. In summary, a variety of models have been proposed to explain the epithelial hierarchy of the prostate during postnatal development and in homeostatic conditions (Figure 4).

Recent data suggests the presence of significant plasticity in epithelial cells of the prostate. This plasticity may be heightened during non-physiologic circumstances such as repair of the prostate epithelium after luminal cell anoikis [31], bacteria-induced prostatic inflammation [32], and a high-fat diet [33], all of which promote basal-to-luminal prostate epithelial differentiation. In addition, prospectively isolated basal and luminal cell populations subjected to three-dimensional organoid growth conditions produce outgrowths of cells with basal and luminal differentiation, indicating that both basal-to-luminal and luminal-to-basal differentiation may occur in certain contexts [34].

2. Epithelial stem or progenitor cells as cells of origin of prostate cancer

While most now accept that both basal and luminal epithelial cells in the prostate can assume stem or progenitor activity, the cell of origin of human prostate cancer remains debated [35, 36]. On one hand, controversy exists as to whether a stem cell, an intermediate progenitor cell, or a terminally differentiated cell is the cell of origin of cancer [37, 38]. On the other, multiple groups including ours have tried to reconcile whether basal cells, luminal cells, or both can be targets of transformation in the prostate [36, 39, 40]. As cancer occurs with advanced age and requires the acquisition of genetic abnormalities over time, it would seem logical that long-lived cells such as self-renewing stem cells in the prostate are likely cells of origin of prostate cancer. The question of whether prostate cancer arises from basal or luminal cells has long been influenced by the finding that typical prostate cancer, prostate adenocarcinoma, demonstrates a luminal keratin-positive and AR-positive phenotype with loss of the basal cell layer [41]. Thus, the conservative and widely accepted view has been that a luminal cell must be the cell of origin.

In vitro methods were developed first to propagate prostate epithelial cells for assessment of prostate epithelial transformation. However, two-dimensional culture of prostate epithelial cells has been primarily limited to outgrowths of cells with basal or basal intermediate phenotypes [42, 43]. The inability to grow luminal cells in these conditions has impeded studies comparing basal and luminal cells as targets of transformation. Recently, Karthaus et al. and Chua et al. developed defined three-dimensional organoid culture systems that support the proliferation and differentiation of both basal and luminal cells from the mouse and human prostate [34, 44]. This

technological advance should now facilitate and soon yield an improved understanding of the differential response of basal and luminal cell populations to oncogenic stresses in vitro.

In vivo studies investigating the cell of origin of prostate cancer can be divided into two classes: (1) the genetic modification of isolated cell populations coupled with an in vivo recombination assay and (2) GEM models using characterized promoters to introduce tissue-specific genetic alterations.

Our group has developed the former technique, in which basal and luminal cells from mouse or human prostates are isolated by fluorescence-activated cell sorting (FACS) based on surface marker expression, transduced with lentiviruses expressing oncogenes, then recombined with cultured embryonic UGSM before transplantation into immune-deficient mouse hosts either beneath the kidney capsule or in the subcutaneous space [45, 46]. Uniformly, basal cells but not luminal cells generate malignant outgrowths in this assay with evident basal-to-luminal cancer differentiation in response to oncogenes such as *AKT1*, *ERG*, *AR*, and *MYC* [23, 25, 45, 47].

Yet, in GEM models, Wang et al. have shown that the targeted deletion of the tumor suppressor *PTEN* in luminal CARN cells induces carcinoma [48] and Choi et al. demonstrated that disruption of *PTEN* in both CK5-positive basal or CK8-positive luminal cells of the prostate could produce carcinoma but basal cells appear more resistant to transformation [29]. In recent work, Wang et al. performed lineage tracing across a range of GEM models to show that luminal cells are favored as the cell of origin for these cancer models in situ but explanted basal cells from these models readily generate tumors in grafts [49]. In total, these findings indicate some

degree of assay dependence but suggest that both basal and luminal cells in the mouse can be cells of origin of prostate cancer.

However, inherent differences in the mouse and human prostate may limit the extrapolation of results from mouse transformation studies to human prostate cancer biology. For instance, mouse prostates are anatomically different, naturally do not develop prostate carcinoma, and generally involute with age in contrast to the aged human prostate which hypertrophies [50]. Recent cross-species bioinformatics analysis of luminal-derived and basal-derived GEM models of prostate cancer with human prostate cancers suggested that luminal-derived cancers are more aggressive than basal-derived cancers [51]. In contrast, our group has shown that aggressive human prostate cancers including CRPC and NEPC demonstrated a heightened basal stem cell signature score [52].

We are intrigued by the idea that the epithelial cell of origin of prostate cancer may determine features of the resultant cancer. If prostate cells across a range of epithelial differentiation states serve as targets of transformation, this could explain some of the highly heterogeneous nature of human prostate cancer. Our group has focused on isolating biologically distinct subsets of basal and luminal cells to interrogate how these populations respond in direct transformation studies and impart distinct prostate cancer phenotypes.

3. Genetic determinants of prostate cancer

Over the past two decades, many genetic alterations have been identified that play a role in prostate cancer initiation and progression. One of the most common pathways altered is the PI3K pathway which is activated in over 40% of primary prostate cancers and in 100% of metastatic prostate cancers [9]. Mechanisms of PI3K pathway activation commonly include loss of PTEN or activating mutations of PIK3CA, leading to the downstream activation of AKT [9, 11]. The MAPK pathway is also dysregulated in prostate cancer, oftentimes in concert with PI3K pathway activation, either from the loss of negative regulators of MAP kinases or activating mutations of MAP kinases [9]. Amplification and overexpression of *MYC* has also been identified in prostate cancer, even at the early stages of pre-malignant disease [53]. *MYC* plays a prominent role in late-stage disease as overexpression of *MYC* confers castration-resistance to prostate cancer [54]. Alterations in *TP53* and *RB1* are observed in prostate cancer but are more frequent in advanced disease [10, 11]. In addition, recurrent chromosomal rearrangement of ETS transcription factors such as *ERG* and *ETV1* have been found to occur in up to 50% of all prostate cancers [55]. AR signaling remains the most clinically relevant pathway in prostate cancer as it is a vital pathway for survival and proliferation [3]. Modulation of AR signaling with prostate cancer progression occurs through a variety of mechanisms that involve alterations in AR activity, function, and specificity [56].

GEM models of prostate-specific *PTEN* deletion [57], *MYC* overexpression [58], or concomitant inactivation of p53 and Rb1 [59] have been developed and recapitulate many aspects of prostate tumorigenesis. In addition, combinatorial models of Pten loss and MAPK activation [60], Pten loss and Smad4 loss [61], Pten loss and Myc overexpression [62], and Pten loss and p53 loss

[63] all produce progressive, metastatic prostate cancer indicating that interplay between these genetic events overcomes metastatic constraints in prostate cancer.

Our laboratory has used the in vivo recombination assay to similarly evaluate the capacity of individual and combinations of oncogenes to initiate cancer from mouse prostate epithelial cells. For instance, we have demonstrated that myristoylated AKT1 (myrAKT1) expression induces pre-malignant lesions [25] which progress to frank carcinoma in cooperation with AR [64], mutant Kras (G12D) [65], and ERG [66]. Interestingly, while ERG cooperates with myrAKT1 and also with AR to promote aggressive prostate cancer, it does not cooperate with p53 loss [66]. In addition, while overexpression of combinations of AR, mutant Kras (G12D), and myrAKT1 all synergize to promote the initiation and progression of prostate cancer, only the combination of AR and mutant Kras (G12D) drives expression of EZH2, a chromatin regulator overexpressed in aggressive prostate cancers and associated with a poor prognosis [65].

In direct transformation studies of the human prostate using the in vivo recombination assay, we have shown that enforced expression of myrAKT1 and ERG in basal cells initiates pre-malignant lesions while the combination of myrAKT1, ERG, and AR produces frank prostate cancer [27]. Furthermore, dysregulated expression of either c-Myc or myrAKT1 alone in human basal cells generates pre-malignant lesions but the two together results in a mixture of aggressive, poorly differentiated prostate adenocarcinoma and squamous cell carcinoma derived from a common clonal origin [47]. Evaluation of additional oncogenes and the development of technology to systematically knockout tumor suppressors using CRISPR/Cas9 technology [67] in our human prostate transformation assay are currently underway.

The recent use of next generation sequencing technologies has led to the identification of many more previously unknown genetic alterations in prostate cancer within the last five years. The Cancer Genome Atlas (TCGA) characterized 333 primary prostate cancers and identified seven molecular subtypes, some mutually exclusive, based on ETS fusions or mutations in *SPOP*, *FOXA1*, and *IDH1* [68]. Another recent finding is the recurrent deletion of *CHD1*, a regulator of genome stability, that may predispose prostate cancer cells to undergo chromoplexy, a process in which DNA translocations and deletions occur to disrupt cancer genes in a coordinated manner [69]. Furthermore, in two independent studies, Robinson et al. and TCGA identified that 20% of primary prostate cancers and metastatic CRPCs exhibit abnormalities in DNA repair pathways involving genes like *BRCA2*, *BRCA1*, and *ATM* [11, 68]. This finding is of immediate clinical relevance as an early-phase clinical trial of poly ADP ribose polymerase (PARP) inhibition in heavily pretreated metastatic CRPC with DNA repair defects showed significant activity [70]. Biological systems that effectively model these newly identified genetic abnormalities and pathways must be developed to understand their functional roles in prostate cancer progression and to develop new therapeutic approaches.

4. Pathogenesis of aggressive neuroendocrine prostate cancer

In the past, NEPC has been thought to make up less than 1% of all primary prostate cancers, representing an exceedingly rare subset of prostate cancer worthy of case reports. NEPC is most often identified in patients initially diagnosed with conventional prostate adenocarcinoma who recur during treatment, whether it be androgen-deprivation therapy or chemotherapy, often with

rapid metastatic progression of disease in visceral organs in the setting of a low PSA [7]. The entity has been described as treatment-related NEPC [71], although it is unclear whether primary NEPC and treatment-related NEPC represent distinct disease entities. While treatment-related NEPC was also thought to be fairly uncommon, autopsy series of patients with lethal metastatic CRPC suggest that up to 25% of patients have evidence of NEPC [8, 72].

NEPC is a heterogeneous group of neuroendocrine tumors but the most aggressive by histologic and clinical criteria is small cell neuroendocrine prostate carcinoma (SCNPC) [73]. The overall survival for patients with extensive stage SCNPC is approximately one year [74]. Patients will generally respond to initial treatment with radiation and/or combination cytotoxic chemotherapy but the response is short-lived and unrelenting progression leads to death [7]. No effective and standard treatment options are available for patients with this disease.

NEPC is defined by morphologic features and evidence of neuroendocrine differentiation. For instance, SCNPC distinctly demonstrates a high nuclear to cytoplasmic ratio, indistinct nucleoli, nuclear moulding, crush artifact, peripheral palisading, rosette formation, and multiple mitotic and apoptotic figures (Figure 5) [6]. Immunohistochemical studies to evaluate the expression of markers of neuroendocrine differentiation may also be performed to confirm the diagnosis. Commonly used markers include synaptophysin (SYP), chromogranins (CHGA and CHGB), neural cell adhesion molecule 1 (NCAM1 or CD56), and neuron specific enolase (NSE) [73]. In most cases, NEPC also demonstrates absence of expression of AR [75]. However, data from the Stand Up To Cancer/Prostate Cancer Foundation/American Association for Cancer Research

West Coast Dream Team suggests that some NEPCs retain AR expression despite the absence of downstream AR signaling genes (unpublished).

In up to 50% of cases of NEPC, the tumor is found to have a mixture of NEPC and conventional prostate adenocarcinoma [6]. The coexistence of NEPC and prostate adenocarcinoma has led many to question whether the two may be clonally related. In vitro studies have shown that the androgen-dependent LNCaP cell line can undergo differentiation to a neuroendocrine phenotype upon increases in intracellular cAMP [76] and androgen withdrawal [77], which indicated that prostate adenocarcinoma may exhibit plasticity. Recently, Lin et al. reported that an in vivo patient-derived xenograft of prostate adenocarcinoma transdifferentiated to lethal NEPC after androgen withdrawal [78]. Additional genetic studies of de novo human prostate cancer have similarly suggested a common clonal origin for both prostate adenocarcinoma and NEPC. Lotan et al. determined that *ERG* rearrangements occur in 45% of SCNPC, a frequency similar to that in prostate adenocarcinoma [79]. In the majority of cases in which SCNPC occurred concurrently with conventional prostate adenocarcinoma, *ERG* rearrangement was found in both components [79, 80]. Hansel et al. also reported that in a case of mixed SCNPC and prostate adenocarcinoma, both tumor components harbored an identical mutation (R175H) in *TP53* [81].

Based on these studies, it is widely believed that prostate adenocarcinoma can undergo a process of neuroendocrine differentiation to NEPC (Figure 6). However, in the lung, the pulmonary neuroendocrine cell is accepted as the primary cell of origin of small cell lung cancer (SCLC), although a subset of alveolar type 2 cells can also be transformed to SCLC [82]. Furthermore, targeted expression of the simian virus 40 large T antigen in the neuroendocrine cells of the

mouse prostate has been shown to initiate aggressive NEPC in mice [83]. Therefore, it seems likely that NEPC could arise from the transdifferentiation of prostate adenocarcinoma but also from the direct transformation of rare neuroendocrine prostate cells.

The molecular characterization of NEPC has led to the identification of multiple genetic factors that may be important in the pathogenesis of this disease. Tan et al. has shown that loss of Rb occurs in 90% of SCNPCs but only 7% of high-grade primary prostate adenocarcinomas [84]. In addition, they found loss of Pten in 63% of SCNPCs and mutations in *TP53* in 60% of SCNPCs [84]. Importantly, Beltran et al. identified that *MYCN* and *AURKA* are co-amplified and overexpressed in approximately 40% of NEPCs but in only 5% of prostate adenocarcinomas [12]. Further, amplification of *MYCN* and *AURKA* was found in 65% of patients with prostate adenocarcinoma who later developed NEPC but in only 5% of an unselected cohort [85]. In a study by Lapuk et al., diminished expression of the RE1-silencing transcription factor (REST), a master repressor of neuronal differentiation, was commonly identified in 50% of NEPCs [86]. Recent work has also implicated differential epigenetic regulation between NEPCs and prostate adenocarcinomas including enriched Polycomb-mediated silencing [87] and distinct global methylation profiles [13].

Model systems for the study of NEPC have centered on patient-derived xenografts (ie. LuCAP 49, WISH-PC2, MDA PCA 144-13, WM-4A and others) propagated in immune-deficient mice and GEM models that inactivate p53 and Rb in the prostate (Table 1) [88]. The first animal model of NEPC was the TRAMP model, in which the rat probasin promoter drives the expression of the simian virus 40 large and small T antigens [89]. The TRAMP model

reproducibly generated premalignant lesions, prostate adenocarcinoma, and anaplastic NEPC with metastases in a sequential, time-dependent course. Variation in the promoter and use of simian virus 40 T antigens has resulted in several other GEM models that generate NEPC including the 12T-10 LPB-Tag mouse [90], the FG-Tag model [91], the PSP94-TGMAP model [92], and the Cr2-Tag mouse [83]. Recently, Zhou et al. engineered a *TP53*$^{f/f}$ and *RB1*$^{f/f}$ mouse and crossed this onto probasin-Cre recombinase transgenic mice to conditionally knock out p53 and Rb in the prostate [93]. These mice develop NEPC but are dependent on a number of other secondary genetic alterations which have not been functionally validated [93].

Functional modeling of the genetic abnormalities identified NEPC, especially in a transformation model beginning with human prostate material, is critical to understand how they promote the pathogenesis of NEPC and how they can be targeted therapeutically.

5. Wild-type tyrosine kinases as mediators of advanced prostate cancer

The following is excerpted from a review article written by Drake J.M., Lee J.K., and Witte O.N. [94].

Since the discovery of v-SRC and v-ABL tyrosine phosphorylation 35 years ago [95, 96], considerable progress has been made in understanding how tyrosine phosphorylation contributes to normal cellular homeostasis and disease. Tyrosine phosphorylation is regulated by a family of enzymes known as tyrosine kinases. Tyrosine kinases are crucial mediators of normal cellular signal transduction functions, including cell proliferation, survival, migration, and apoptosis.

Humans express at least 90 tyrosine kinases, including 58 receptor tyrosine kinases (RTKs) [97]. RTKs are activated through binding of their extracellular domain to ligands, such as growth factors and cytokines. This ligand binding results in RTK dimerization/oligomerization [98] and subsequent tyrosine phosphorylation.

Despite the large number of signaling molecules recruited by RTKs, regulation of tyrosine kinases is tightly controlled to prevent aberrant cellular activities, usually through receptor-mediated ubiquitylation and degradation [99]. However, genetically altered mutations or pathway-activated mechanisms of tyrosine kinases can transform a cell from a normal state into a cancerous one. Over 50% of the 90 tyrosine kinases identified have been implicated in cancer despite the fact that tyrosine phosphorylation represents only 1% of the total phosphoproteome [100]. The disproportionate contribution of tyrosine kinases to cancer further highlights the need to understand the signaling networks initiated by tyrosine kinases as well as how to effectively target them.

Constitutive signals from either mutated or wild-type tyrosine kinases result in hyperactive pathways leading to continued cancer cell growth and survival. This reliance on the hyperactive pathway, known as pathway addiction, has provided unique opportunities for targeted inhibition of tyrosine kinases and has resulted in clinical successes (Table 2). Genetically altered tyrosine kinases can act as drivers in cancer through activating mutations [101-103], DNA translocations [104-106], or DNA amplifications [107] (Figure 7). However, wild-type or nonmutated tyrosine kinases can also function as critical nodes for pathway activation [108, 109] (Figure 7).

In prostate cancer, the overall somatic mutation rate is relatively low compared to other epithelial cancer types [110] and few mutations have been identified in tyrosine kinases [9, 10, 68]. Our laboratory has functionally demonstrated that overexpression of wild-type c-Src with AR in the mouse prostate transformation assay produces an aggressive carcinoma phenotype with evidence of epithelial-to-mesenchymal transition [111]. We have also shown that the overexpression of wild-type tyrosine kinases such as NTRK2 and MERTK in benign, immortalized RWPE-1 prostate cell line is capable of promoting metastasis [112]. Furthermore, immunohistochemical evaluation of global tyrosine phosphorylation shows increased tyrosine phosphorylation in CRPC relative to hormone naïve prostate cancer, pre-malignant lesions, or normal prostate [14]. These findings indicate that activation of wild-type tyrosine kinases by overexpression or pathway activation may be important in mediating prostate cancer progression.

Phosphoproteomics provides valuable information about the activation states of tyrosine kinases independent of genomic alterations, thereby uncovering tyrosine kinases that may be driving essential pathways in cancers that next-generation whole-genome or exome sequencing may miss [113]. We have implemented phosphoproteomics to investigate tyrosine kinase activity in mouse models of prostate tumorigenesis where we express nontyrosine kinase oncogenes [46]. We observed numerous activated tyrosine kinases, including SRC, EGFR, ABL, and JAK2, as well as tyrosine phosphorylation of MAPK1/3 and STAT3 [14]. Whether similar patterns of tyrosine kinase activation are observed in human prostate cancer is unknown.

The biggest challenge arising from this and other phosphoprofiling studies will be to determine if the activated tyrosine kinases identified via phosphoproteomics are drivers of cancer in a fashion

similar to that of genetically altered tyrosine kinases seen in other cancer types. In prostate cancer, the need for relevant in vivo models to assess the function of nonmutated activated tyrosine kinases is crucial to understanding the signaling pathways and nodes for appropriate therapy in this disease. In addition, the promiscuity of kinase inhibitors such as cabozantinib (VEGFR2, MET, or RET inhibitor) or sorafenib (RAF or VEGFR inhibitor) confounds the exact contribution of specific driver kinases in regulating survival and growth. However, this may be of therapeutic benefit, as multiple targets can be simultaneously inhibited with these agents, as suggested in chronic myeloid leukemia (CML) [114]. Finally, the evaluation of mechanisms of resistance to activated tyrosine kinases should also be assessed to predict combination or sequential therapies that could be tested clinically. This has been realized in certain cancers, such as targeting of the BCR-ABL translocation in CML, where sequential administration of new therapies circumvents common resistance mechanisms [115, 116].

Figure 1. Organization of epithelial cells in the prostate gland. Shown is a depiction of the organization of the three epithelial cell types (basal, luminal, and neuroendocrine) in a prostate acinus. (Modified from Goldstein et al., 2010, with kind permission from Elsevier)

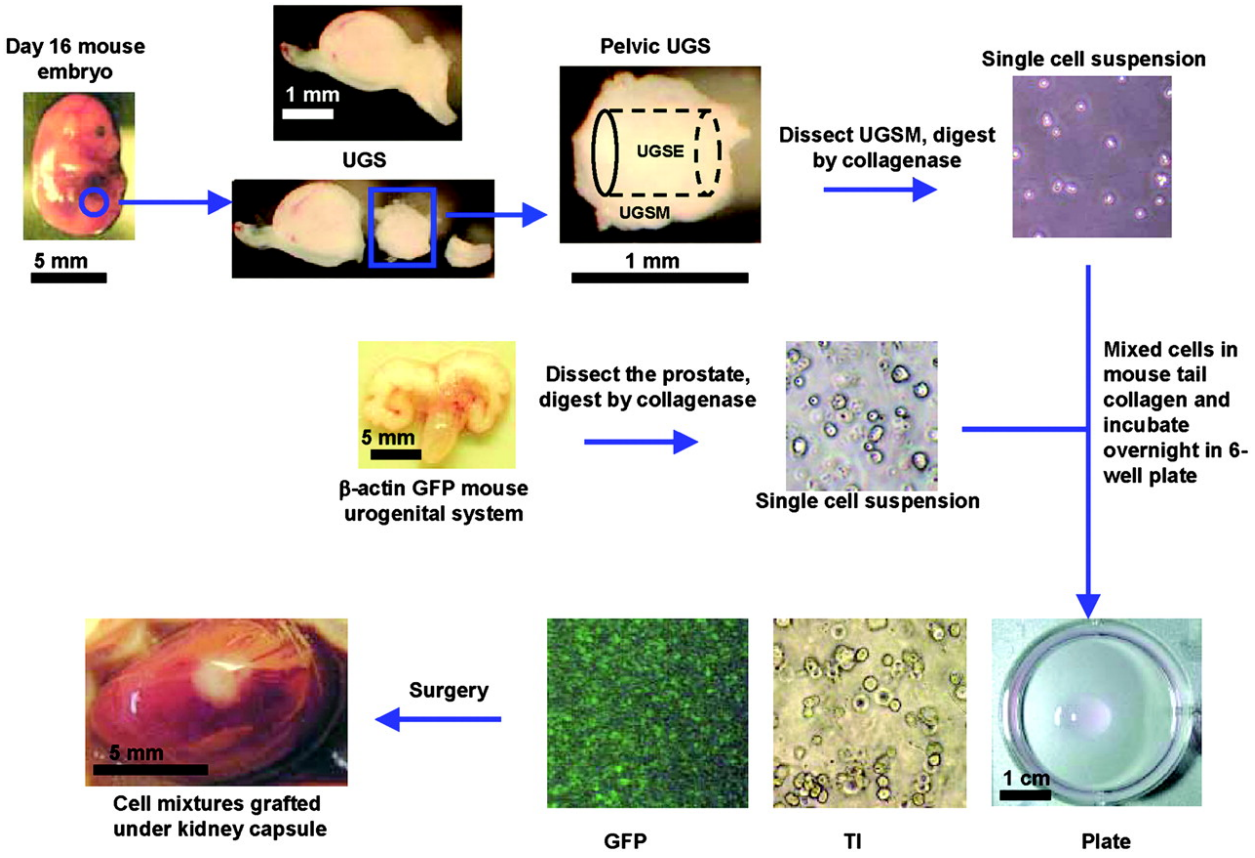

Figure 2. Overview of the in vivo mouse prostate recombination assay. Prepared single cell suspensions of adult mouse prostate epithelial cells and embryonic mouse urogenital sinus (UGS) mesenchyme are combined in collagen grafts and implanted under the kidney capsule of immune-deficient mice. (Reprinted from Xin et al., 2003, with kind permission from the National Academy of Sciences, USA, Copyright 2003)

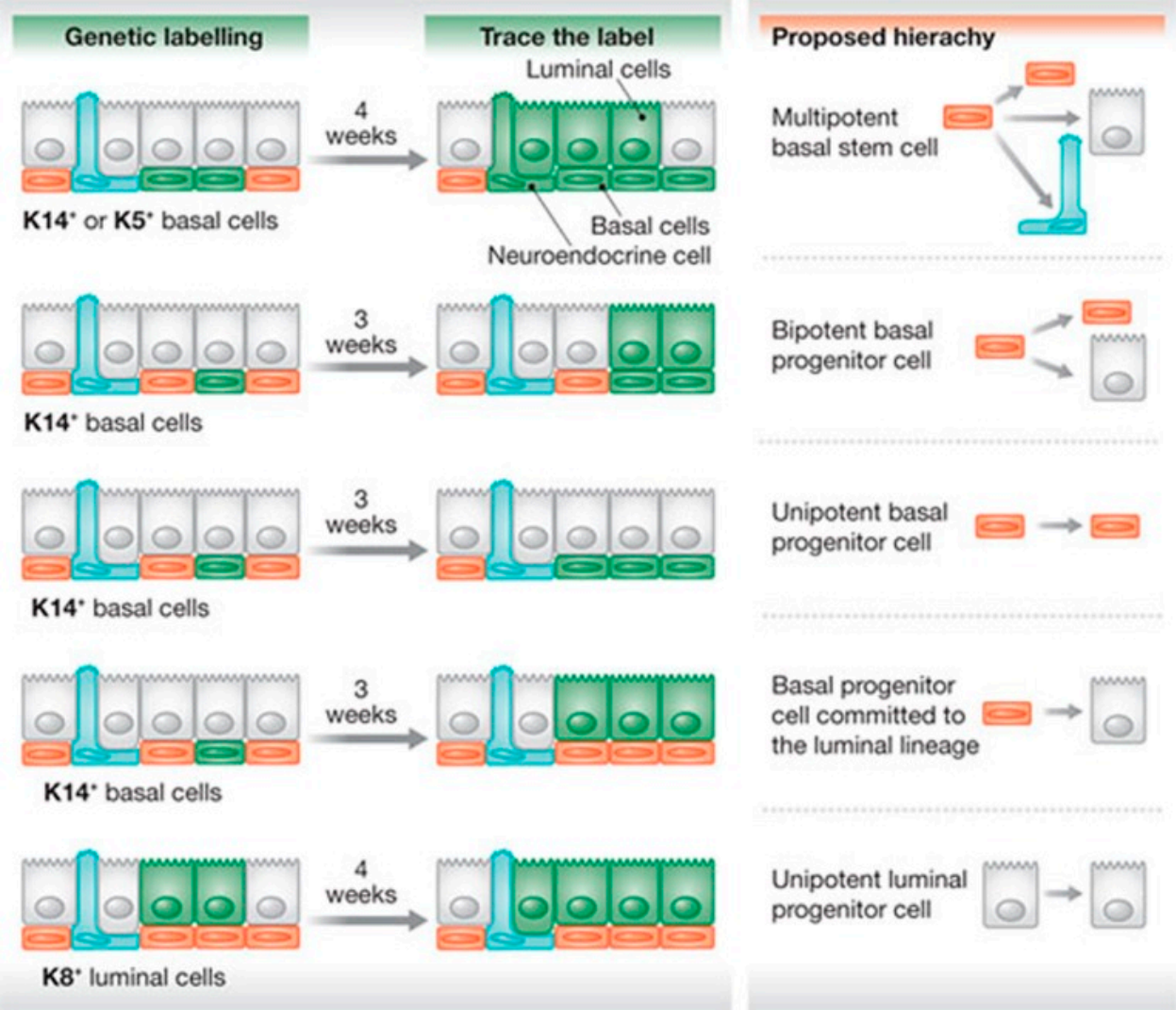

Figure 3. Overview of the genetic labeling of mouse prostate epithelial cells for lineage tracing. Shown is a schematic of lineage tracing studies of $K14^+$ or $K5^+$ basal cells and $K8^+$ luminal cells suggesting the presence of a multipotent basal stem cell and multiple intermediate progenitor cells. (Reprinted from Goldstein et al., 2012, with kind permission from the European Molecular Biology Organization)

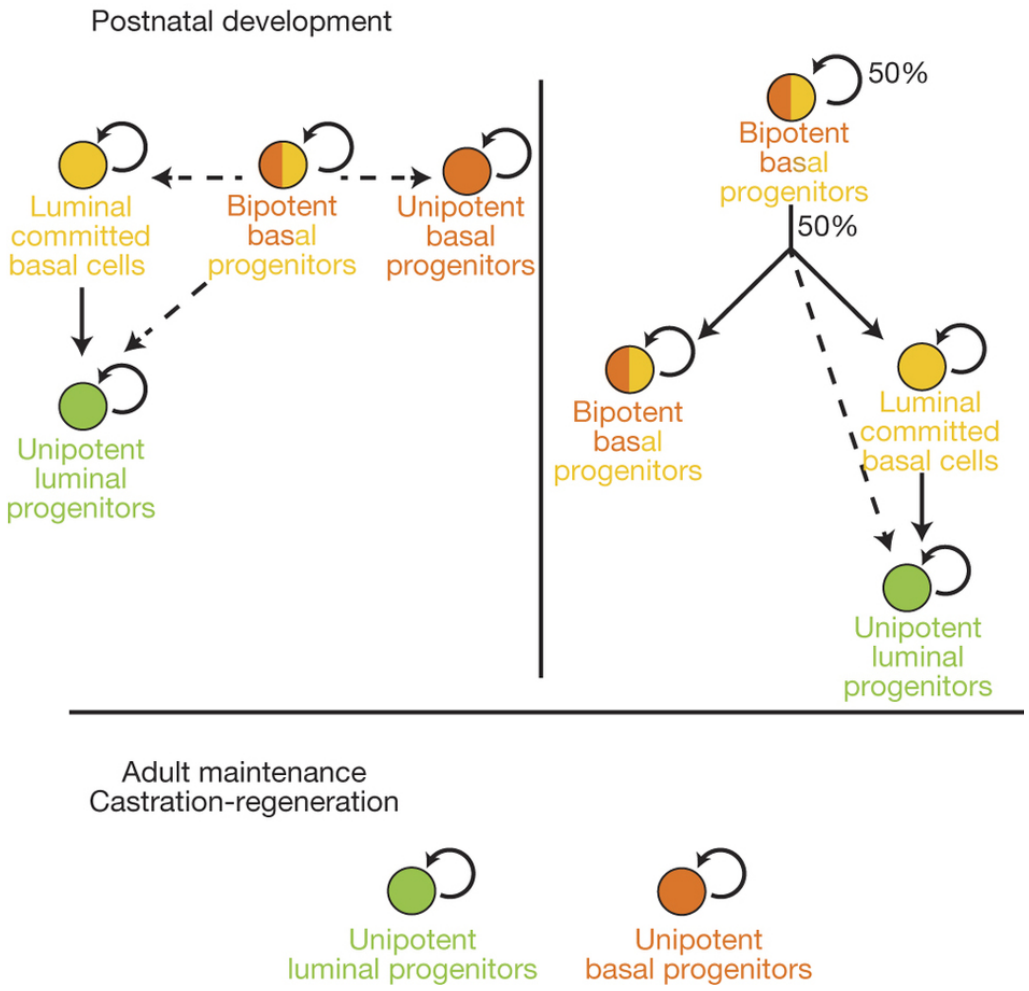

Figure 4. Proposed models of the epithelial hierarchy in the mouse prostate. Shown are two models of the epithelial hierarchy in postnatal development of the prostate. In the first model on the left, basal cells consist of unipotent and bipotent progenitors. In the second model on the right, a single bipotent basal progenitor can give rise to additional bipotent basal progenitors or unipotent luminal progenitor or a luminal committed cell. In homeostatic conditions in the adult prostate shown on the bottom, unipotent luminal and basal progenitors replenish luminal and basal cell lineages. (Reprinted from Ousset et al., 2012, with kind permission from the Nature Publishing Group)

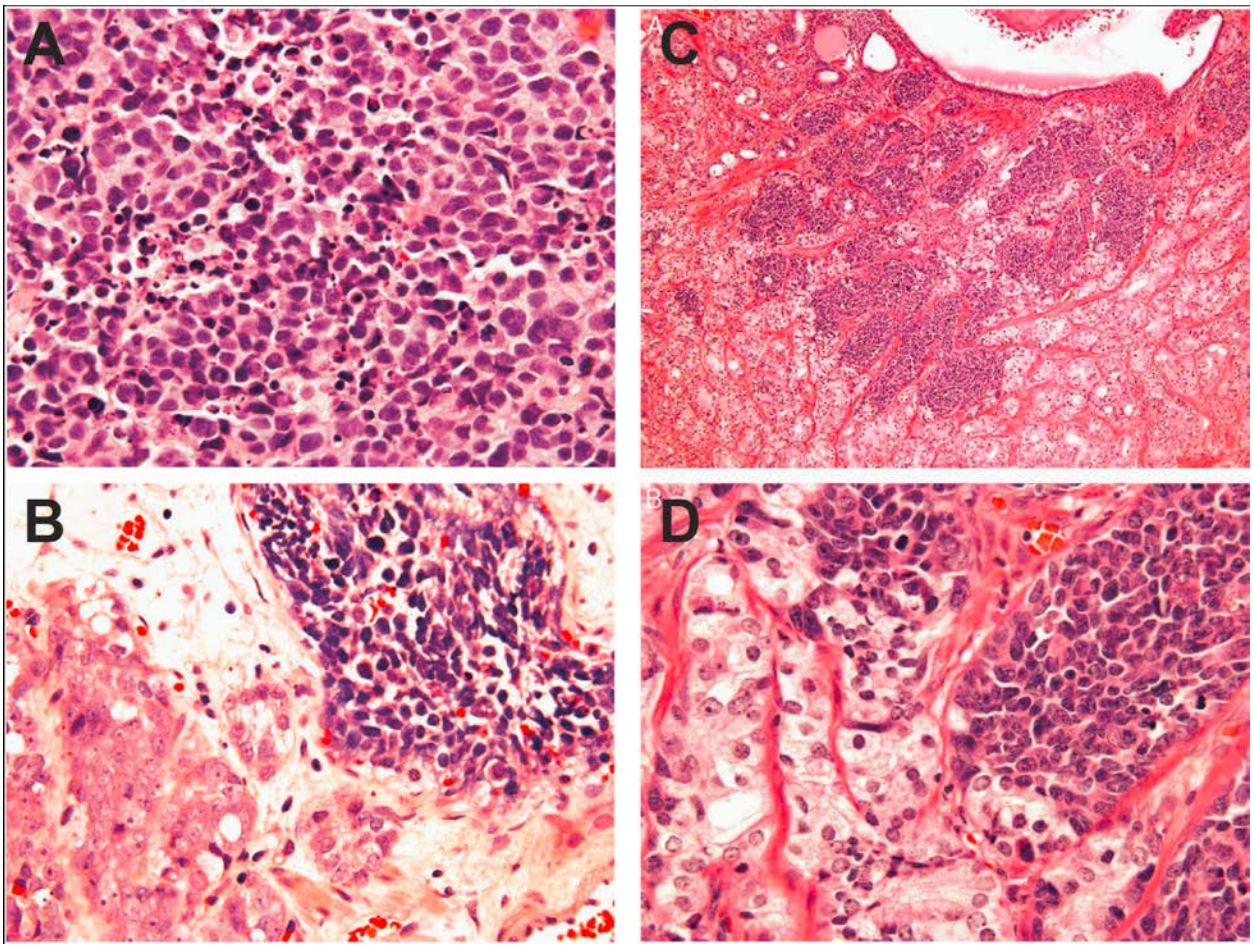

Figure 5. Comparison of the histology of NEPC and prostate adenocarcinoma. Shown are photomicrographs of hematoxylin and eosin stained tissue sections of (A) pure small cell neuroendocrine prostate cancer (SCNPC), (B) mixed high-grade acinar adenocarcinoma on the left and SCNPC on the right, (C) low magnification images and (D) high magnification images of mixed usual prostate adenocarcinoma on the left and SCNPC on the right. Small cell carcinoma cells have scant cytoplasm, hyperchromatic nuclei with salt and pepper chromatin without prominent nucleoli. Also note numerous mitoses and apoptotic bodies. (Adapted from Wang et al., 2008, with kind permission from Wolters Kluwer Health, Inc.)

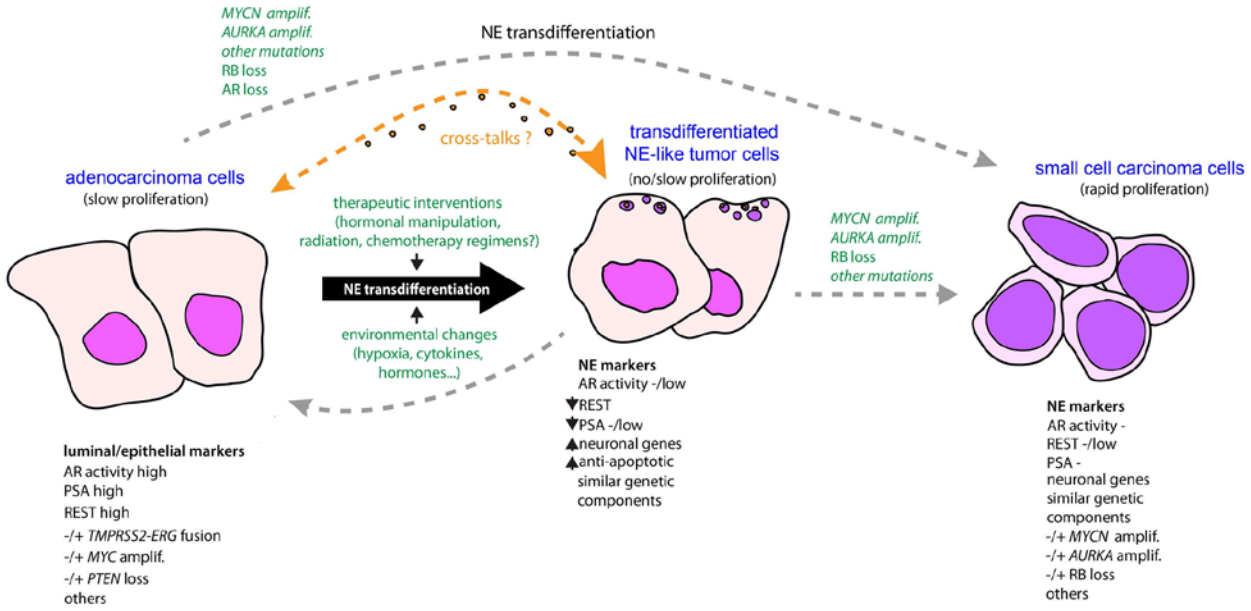

Figure 6. Model of the transdifferentiation from prostate adenocarcinoma to NEPC. Adenocarcinoma cells may accumulate genetic damage to transdifferentiate to a neuroendocrine-like state. Additional genetic alterations including *MYCN* and *AURKA* amplification and Rb loss may further push the evolution to small cell carcinoma. Alternatively, small cell carcinoma can arise directly from the transformation of adenocarcinoma cells. (Adapted from Terry and Beltran, 2014, with kind permission from Frontiers Media)

Name	Details	Species/Type	Author and Year
NCI H660	Lymph node metastasis of NEPC	Human cell line	Mertz et al., 2007
PC-3	Bone metastasis of prostate adenocarcinoma	Human cell line	Tai et al., 2011
LUCAP 49	Omental metastasis of NEPC	Human xenograft	True et al., 2002
WISH-PC2	Resected NEPC	Human xenograft	Pinthus et al., 2000
UCRU-PR-2	Biospy of NEPC	Human xenograft	van Haaften-Day et al., 1987
WM-4A	Resected tumor with mixed NEPC	Human xenograft	Agemy et al., 2008
MDA PCA 144	Resected tumor with mixed NEPC	Human xenograft	Aparicio et al., 2011
LTL352	Resected urethral metastasis of NEPC	Human xenograft	Lin et al., 2014
LTL 370	Resected penile metastasis of NEPC	Human xenograft	Lin et al., 2014
TRAMP	Rat probasin promoter-SV40 large and small T antigens	GEMM	Greenberg et al., 1995
12T-10 LPB-Tag	Large probasin promoter-SV40 large T antigen	GEMM	Masumori et al., 2001
12T-7f LPB-Tag/ PB-hepsin	Large probasin promoter-SV40 large T antigen/rat probasin promoter-hepsin	GEMM	Klezovitch et al., 2004
FG-Tag	Fetal globin promoter-SV40 large and small T antigens	GEMM	Perez-Stable et al., 1996
PSP-TGMAP	PSP94 promoter-SV40 large and small T antigens	GEMM	Gabril et al., 2002
PSP-KIMAP	PSP94 promoter-knock in of SV40 large and small T antigens	GEMM	Duan et al., 2005
CR2-Tag	Cryptdin-2 promoter-SV40 large and small T antigens	GEMM	Garabedian et al., 1998
$p53^{f/f}$;$Rb^{f/f}$;Pb-Cre	Conditional knockout of p53 and Rb in mouse prostate	GEMM	Zhou et al., 1996

Table 1. Established model systems for the study of NEPC.

Activating genetic alterations of tyrosine kinases and FDA-approved targeted inhibitors in human malignancies[a]

Genetic alteration	Kinase	Disease(s)	FDA-approved inhibitor(s)
Mutation(s)			
Exons 19, 21	EGFR	NSCLC	Erlotinib, afatinib
Exons 8, 9, 11, 13, 17	c-KIT	GIST	Imatinib, sunitinib
Exons 12, 14, 18	PDGFRα	GIST	Imatinib, sunitinib
Exons 10, 11, 13, 14	RET	Medullary thyroid carcinoma	Vandetinib, cabozantinib
V617F	JAK2	Myeloproliferative neoplasms	Ruxolitinib
Translocation(s)			
BCR-ABL1 fusion	ABL1	CML	Imatinib, dasatinib, nilotinib, bosutinib, ponatinib
RET/PTC family fusions	RET	PTC	Vandetinib
EML4-ALK fusion	ALK	NSCLC	Crizotinib
Amplification(s): increased copy no. and/or overexpression	ERBB2	Breast cancer, gastric cancer	Trastuzumab, lapatinib, ado-trastuzumab emtansine, pertuzumab
Pathway activation			
B-cell receptor signaling	BTK	CLL B-cell non-Hodgkin's lymphoma	Ibrutinib
Angiogenesis	VEGFR	CCRCC, soft-tissue carcinoma	Sorafenib, sunitinib, pazopanib, axitinib

[a] Abbreviations: NSCLC, non-small-cell lung cancer; GIST, gastrointestinal stromal tumor; CML, chronic myelogenous leukemia; PTC, papillary thyroid carcinoma; CCRCC, clear cell renal cell carcinoma; CLL, chronic lymphocytic leukemia.

Table 2. Activating genetic alterations of tyrosine kinases and FDA-approved targeted inhibitors in human malignancies. (Reprinted from Drake et al., 2013, with kind permission from the American Society for Microbiology)

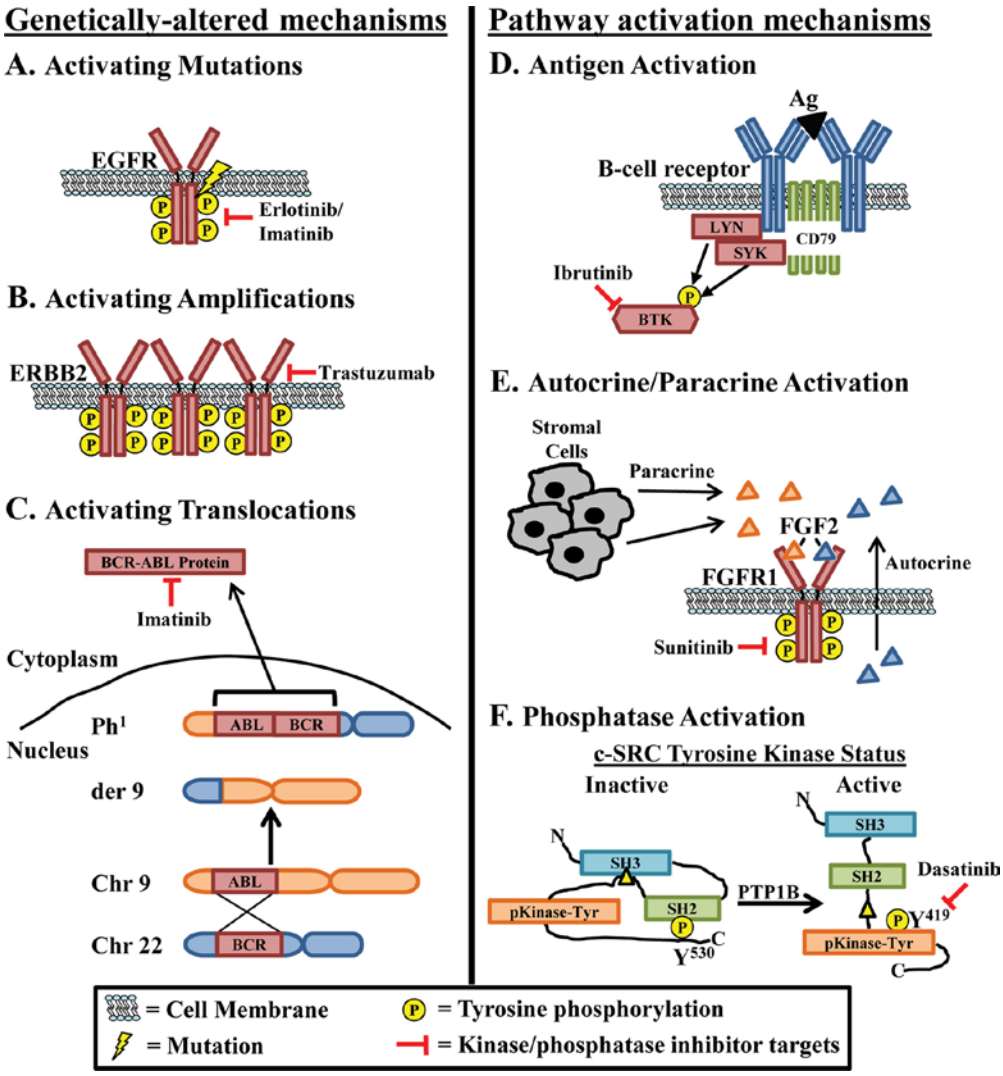

Figure 7. Mechanisms of mutated and wild-type tyrsone kinase activation in cancer. Three prototypical mechanisms of genetically altered tyrosine kinase activation as evidenced through genetic alterations. Shown are examples of mutations (A), amplifications (B), or translocations (C) that render a kinase constitutively active and thus contribute to the addiction of tumor cells on pathways driven by the genetically altered kinase. In the absence of genetic alterations (D to F), nonmutated tyrosine kinases can be activated via many different mechanisms and contribute to pathway signaling. In all cases, this pathway addiction leads to increased tumor cell proliferation and survival. In some cases, highly potent therapies that inhibit (red) the altered protein kinase have resulted in robust clinical outcomes. RTK, receptor tyrosine kinase; Chr, chromosome; Ph1, Philadelphia chromosome; BCR, breakpoint cluster region; Ag, antigen; BTK, Bruton's tyrosine kinase; PTP1B, protein tyrosine phosphatase 1B. (Reprinted from Drake et al., 2013, with kind permission from the American Society for Microbiology)

References

1. Siegel, R.L., K.D. Miller, and A. Jemal, *Cancer statistics, 2016.* CA Cancer J Clin, 2016. **66**(1): p. 7-30.

2. Huggins, C., *EFFECT OF ORCHIECTOMY AND IRRADIATION ON CANCER OF THE PROSTATE.* Ann Surg, 1942. **115**(6): p. 1192-200.

3. Heinlein, C.A. and C. Chang, *Androgen receptor in prostate cancer.* Endocr Rev, 2004. **25**(2): p. 276-308.

4. de Bono, J.S., et al., *Abiraterone and increased survival in metastatic prostate cancer.* N Engl J Med, 2011. **364**(21): p. 1995-2005.

5. Scher, H.I., et al., *Increased survival with enzalutamide in prostate cancer after chemotherapy.* N Engl J Med, 2012. **367**(13): p. 1187-97.

6. Wang, W. and J.I. Epstein, *Small cell carcinoma of the prostate. A morphologic and immunohistochemical study of 95 cases.* Am J Surg Pathol, 2008. **32**(1): p. 65-71.

7. Aggarwal, R., et al., *Neuroendocrine prostate cancer: subtypes, biology, and clinical outcomes.* J Natl Compr Canc Netw, 2014. **12**(5): p. 719-26.

8. Tanaka, M., et al., *Progression of prostate cancer to neuroendocrine cell tumor.* Int J Urol, 2001. **8**(8): p. 431-6; discussion 437.

9. Taylor, B.S., et al., *Integrative genomic profiling of human prostate cancer.* Cancer Cell, 2010. **18**(1): p. 11-22.

10. Grasso, C.S., et al., *The mutational landscape of lethal castration-resistant prostate cancer.* Nature, 2012. **487**(7406): p. 239-43.

11. Robinson, D., et al., *Integrative clinical genomics of advanced prostate cancer.* Cell, 2015. **161**(5): p. 1215-28.

12. Beltran, H., et al., *Molecular characterization of neuroendocrine prostate cancer and identification of new drug targets.* Cancer Discov, 2011. **1**(6): p. 487-95.

13. Beltran, H., et al., *Divergent clonal evolution of castration-resistant neuroendocrine prostate cancer.* Nat Med, 2016. **22**(3): p. 298-305.

14. Drake, J.M., et al., *Oncogene-specific activation of tyrosine kinase networks during prostate cancer progression.* Proc Natl Acad Sci U S A, 2012. **109**(5): p. 1643-8.

15. Drake, J.M., et al., *Metastatic castration-resistant prostate cancer reveals intrapatient similarity and interpatient heterogeneity of therapeutic kinase targets.* Proc Natl Acad Sci U S A, 2013. **110**(49): p. E4762-9.

16. McNeal, J.E., *Normal histology of the prostate.* Am J Surg Pathol, 1988. **12**(8): p. 619-33.

17. Abrahamsson, P.A. and P.A. di Sant'Agnese, *Neuroendocrine cells in the human prostate gland.* J Androl, 1993. **14**(5): p. 307-9.

18. English, H.F., R.J. Santen, and J.T. Isaacs, *Response of glandular versus basal rat ventral prostatic epithelial cells to androgen withdrawal and replacement.* Prostate, 1987. **11**(3): p. 229-42.

19. Tsujimura, A., et al., *Proximal location of mouse prostate epithelial stem cells: a model of prostatic homeostasis.* J Cell Biol, 2002. **157**(7): p. 1257-65.

20. Cunha, G.R. and B. Lung, *The possible influence of temporal factors in androgenic responsiveness of urogenital tissue recombinants from wild-type and androgen-insensitive (Tfm) mice.* J Exp Zool, 1978. **205**(2): p. 181-93.

21. Xin, L., et al., *In vivo regeneration of murine prostate from dissociated cell populations of postnatal epithelia and urogenital sinus mesenchyme.* Proc Natl Acad Sci U S A, 2003. **100 Suppl 1**: p. 11896-903.

22. Kwon, O.J. and L. Xin, *Prostate epithelial stem and progenitor cells.* Am J Clin Exp Urol, 2014. **2**(3): p. 209-18.

23. Xin, L., D.A. Lawson, and O.N. Witte, *The Sca-1 cell surface marker enriches for a prostate-regenerating cell subpopulation that can initiate prostate tumorigenesis.* Proc Natl Acad Sci U S A, 2005. **102**(19): p. 6942-7.

24. Burger, P.E., et al., *Sca-1 expression identifies stem cells in the proximal region of prostatic ducts with high capacity to reconstitute prostatic tissue.* Proc Natl Acad Sci U S A, 2005. **102**(20): p. 7180-5.

25. Lawson, D.A., et al., *Isolation and functional characterization of murine prostate stem cells.* Proc Natl Acad Sci U S A, 2007. **104**(1): p. 181-6.

26. Goldstein, A.S., et al., *Trop2 identifies a subpopulation of murine and human prostate basal cells with stem cell characteristics.* Proceedings of the National Academy of Sciences, 2008.

27. Goldstein, A.S., et al., *Identification of a cell of origin for human prostate cancer.* Science, 2010. **329**(5991): p. 568-71.

28. Wang, X., et al., *A luminal epithelial stem cell that is a cell of origin for prostate cancer.* Nature, 2009. **461**(7263): p. 495-500.

29. Choi, N., et al., *Adult murine prostate basal and luminal cells are self-sustained lineages that can both serve as targets for prostate cancer initiation.* Cancer Cell, 2012. **21**(2): p. 253-65.

30. Ousset, M., et al., *Multipotent and unipotent progenitors contribute to prostate postnatal development.* Nat Cell Biol, 2012. **14**(11): p. 1131-8.

31. Toivanen, R., A. Mohan, and M.M. Shen, *Basal Progenitors Contribute to Repair of the Prostate Epithelium Following Induced Luminal Anoikis.* Stem Cell Reports, 2016.

32. Kwon, O.J., et al., *Prostatic inflammation enhances basal-to-luminal differentiation and accelerates initiation of prostate cancer with a basal cell origin.* Proc Natl Acad Sci U S A, 2014. **111**(5): p. E592-600.

33. Kwon, O.J., et al., *High fat diet promotes prostatic basal-to-luminal differentiation and accelerates initiation of prostate epithelial hyperplasia originated from basal cells.* Stem Cell Res, 2016. **16**(3): p. 682-691.

34. Karthaus, W.R., et al., *Identification of multipotent luminal progenitor cells in human prostate organoid cultures.* Cell, 2014. **159**(1): p. 163-75.

35. Huang, J. and O.N. Witte, *A seminal finding for prostate cancer?* N Engl J Med, 2010. **362**(2): p. 175-6.

36. Lee, S.H. and M.M. Shen, *Cell types of origin for prostate cancer.* Curr Opin Cell Biol, 2015. **37**: p. 35-41.

37. Packer, J.R. and N.J. Maitland, *The molecular and cellular origin of human prostate cancer.* Biochim Biophys Acta, 2016. **1863**(6 Pt A): p. 1238-60.

38. White, A.C. and W.E. Lowry, *Refining the role for adult stem cells as cancer cells of origin.* Trends Cell Biol, 2015. **25**(1): p. 11-20.

39. Goldstein, A.S., T. Stoyanova, and O.N. Witte, *Primitive origins of prostate cancer: in vivo evidence for prostate-regenerating cells and prostate cancer-initiating cells.* Mol Oncol, 2010. **4**(5): p. 385-96.

40. Moscatelli, D. and E.L. Wilson, *PINing down the origin of prostate cancer.* Sci Transl Med, 2010. **2**(43): p. 43ps38.

41. Okada, H., et al., *Keratin profiles in normal/hyperplastic prostates and prostate carcinoma.* Virchows Arch A Pathol Anat Histopathol, 1992. **421**(2): p. 157-61.

42. Stonington, O.G. and H. Hemmingsen, *Culture of cells as a monolayer derived from the epithelium of the human prostate: a new cell growth technique.* J Urol, 1971. **106**(3): p. 393-400.

43. Garraway, L.A., et al., *Intermediate basal cells of the prostate: in vitro and in vivo characterization.* Prostate, 2003. **55**(3): p. 206-18.

44. Chua, C.W., et al., *Single luminal epithelial progenitors can generate prostate organoids in culture.* Nat Cell Biol, 2014. **16**(10): p. 951-61, 1-4.

45. Lukacs, R.U., et al., *Isolation, cultivation and characterization of adult murine prostate stem cells.* Nat Protoc, 2010. **5**(4): p. 702-13.

46. Goldstein, A.S., et al., *Purification and direct transformation of epithelial progenitor cells from primary human prostate.* Nat Protoc, 2011. **6**(5): p. 656-67.

47. Stoyanova, T., et al., *Prostate cancer originating in basal cells progresses to adenocarcinoma propagated by luminal-like cells.* Proc Natl Acad Sci U S A, 2013. **110**(50): p. 20111-6.

48. Wang, X., et al., *A luminal epithelial stem cell that is a cell of origin for prostate cancer.* Nature, 2009. **461**(7263): p. 495-500.

49. Wang, Z.A., et al., *Luminal cells are favored as the cell of origin for prostate cancer.* Cell Rep, 2014. **8**(5): p. 1339-46.

50. Hensley, P.J. and N. Kyprianou, *Modeling prostate cancer in mice: limitations and opportunities.* J Androl, 2012. **33**(2): p. 133-44.

51. Wang, Z.A., et al., *Lineage analysis of basal epithelial cells reveals their unexpected plasticity and supports a cell-of-origin model for prostate cancer heterogeneity.* Nat Cell Biol, 2013. **15**(3): p. 274-283.

52. Smith, B.A., et al., *A basal stem cell signature identifies aggressive prostate cancer phenotypes.* Proc Natl Acad Sci U S A, 2015. **112**(47): p. E6544-52.

53. Fleming, W.H., et al., *Expression of the c-myc protooncogene in human prostatic carcinoma and benign prostatic hyperplasia.* Cancer Res, 1986. **46**(3): p. 1535-8.

54. Bernard, D., et al., *Myc confers androgen-independent prostate cancer cell growth.* J Clin Invest, 2003. **112**(11): p. 1724-31.

55. Tomlins, S.A., et al., *Recurrent fusion of TMPRSS2 and ETS transcription factor genes in prostate cancer.* Science, 2005. **310**(5748): p. 644-8.

56. Shen, M.M. and C. Abate-Shen, *Molecular genetics of prostate cancer: new prospects for old challenges.* Genes Dev, 2010. **24**(18): p. 1967-2000.

57. Wang, S., et al., *Prostate-specific deletion of the murine Pten tumor suppressor gene leads to metastatic prostate cancer.* Cancer Cell, 2003. **4**(3): p. 209-21.

58. Ellwood-Yen, K., et al., *Myc-driven murine prostate cancer shares molecular features with human prostate tumors.* Cancer Cell, 2003. **4**(3): p. 223-38.

59. Gingrich, J.R., et al., *Metastatic prostate cancer in a transgenic mouse.* Cancer Res, 1996. **56**(18): p. 4096-102.

60. Mulholland, D.J., et al., *Pten loss and RAS/MAPK activation cooperate to promote EMT and metastasis initiated from prostate cancer stem/progenitor cells.* Cancer Res, 2012. **72**(7): p. 1878-89.

61. Ding, Z., et al., *SMAD4-dependent barrier constrains prostate cancer growth and metastatic progression.* Nature, 2011. **470**(7333): p. 269-73.

62. Hubbard, G.K., et al., *Combined MYC Activation and Pten Loss Are Sufficient to Create Genomic Instability and Lethal Metastatic Prostate Cancer.* Cancer Res, 2016. **76**(2): p. 283-92.

63. Cho, H., et al., *RapidCaP, a novel GEM model for metastatic prostate cancer analysis and therapy, reveals myc as a driver of Pten-mutant metastasis.* Cancer Discov, 2014. **4**(3): p. 318-33.

64. Xin, L., et al., *Progression of prostate cancer by synergy of AKT with genotropic and nongenotropic actions of the androgen receptor.* Proc Natl Acad Sci U S A, 2006. **103**(20): p. 7789-94.

65. Cai, H., et al., *Collaboration of Kras and androgen receptor signaling stimulates EZH2 expression and tumor-propagating cells in prostate cancer.* Cancer Res, 2012. **72**(18): p. 4672-81.

66. Zong, Y., et al., *ETS family transcription factors collaborate with alternative signaling pathways to induce carcinoma from adult murine prostate cells.* Proc Natl Acad Sci U S A, 2009. **106**(30): p. 12465-70.

67. Jinek, M., et al., *A programmable dual-RNA-guided DNA endonuclease in adaptive bacterial immunity.* Science, 2012. **337**(6096): p. 816-21.

68. TCGA, *The Molecular Taxonomy of Primary Prostate Cancer.* Cell, 2015. **163**(4): p. 1011-25.

69. Baca, S.C., et al., *Punctuated evolution of prostate cancer genomes.* Cell, 2013. **153**(3): p. 666-77.

70. Mateo, J., et al., *DNA-Repair Defects and Olaparib in Metastatic Prostate Cancer.* N Engl J Med, 2015. **373**(18): p. 1697-708.

71. Wang, H.T., et al., *Neuroendocrine Prostate Cancer (NEPC) progressing from conventional prostatic adenocarcinoma: factors associated with time to development of NEPC and survival from NEPC diagnosis-a systematic review and pooled analysis.* J Clin Oncol, 2014. **32**(30): p. 3383-90.

72. Shah, R.B., et al., *Androgen-independent prostate cancer is a heterogeneous group of diseases: lessons from a rapid autopsy program.* Cancer Res, 2004. **64**(24): p. 9209-16.

73. Epstein, J.I., et al., *Proposed Morphologic Classification of Prostate Cancer With Neuroendocrine Differentiation.* The American journal of surgical pathology, 2014. **38**(6): p. 756-767.

74. Spiess, P.E., et al., *Treatment outcomes of small cell carcinoma of the prostate: a single-center study.* Cancer, 2007. **110**(8): p. 1729-37.

75. Beltran, H., et al., *Aggressive variants of castration-resistant prostate cancer.* Clin Cancer Res, 2014. **20**(11): p. 2846-50.

76. Bang, Y.J., et al., *Terminal neuroendocrine differentiation of human prostate carcinoma cells in response to increased intracellular cyclic AMP.* Proc Natl Acad Sci U S A, 1994. **91**(12): p. 5330-4.

77. Yuan, T.C., et al., *Androgen deprivation induces human prostate epithelial neuroendocrine differentiation of androgen-sensitive LNCaP cells.* Endocr Relat Cancer, 2006. **13**(1): p. 151-67.

78. Lin, D., et al., *High fidelity patient-derived xenografts for accelerating prostate cancer discovery and drug development.* Cancer Res, 2014. **74**(4): p. 1272-83.

79. Lotan, T.L., et al., *ERG gene rearrangements are common in prostatic small cell carcinomas.* Mod Pathol, 2011. **24**(6): p. 820-8.

80. Williamson, S.R., et al., *ERG-TMPRSS2 rearrangement is shared by concurrent prostatic adenocarcinoma and prostatic small cell carcinoma and absent in small cell carcinoma of the urinary bladder: evidence supporting monoclonal origin.* Mod Pathol, 2011. **24**(8): p. 1120-7.

81. Hansel, D.E., et al., *Shared TP53 gene mutation in morphologically and phenotypically distinct concurrent primary small cell neuroendocrine carcinoma and adenocarcinoma of the prostate.* Prostate, 2009. **69**(6): p. 603-9.

82. Sutherland, K.D., et al., *Cell of origin of small cell lung cancer: inactivation of Trp53 and Rb1 in distinct cell types of adult mouse lung.* Cancer Cell, 2011. **19**(6): p. 754-64.

83. Hu, Y., et al., *Molecular characterization of a metastatic neuroendocrine cell cancer arising in the prostates of transgenic mice.* J Biol Chem, 2002. **277**(46): p. 44462-74.

84. Tan, H.L., et al., *Rb loss is characteristic of prostatic small cell neuroendocrine carcinoma.* Clin Cancer Res, 2014. **20**(4): p. 890-903.

85. Mosquera, J.M., et al., *Concurrent AURKA and MYCN gene amplifications are harbingers of lethal treatment-related neuroendocrine prostate cancer.* Neoplasia, 2013. **15**(1): p. 1-10.

86. Lapuk, A.V., et al., *From sequence to molecular pathology, and a mechanism driving the neuroendocrine phenotype in prostate cancer.* J Pathol, 2012. **227**(3): p. 286-97.

87. Clermont, P.L., et al., *Polycomb-mediated silencing in neuroendocrine prostate cancer.* Clin Epigenetics, 2015. **7**(1): p. 40.

88. Berman-Booty, L.D. and K.E. Knudsen, *Models of neuroendocrine prostate cancer.* Endocr Relat Cancer, 2015. **22**(1): p. R33-49.

89. Greenberg, N.M., et al., *Prostate cancer in a transgenic mouse.* Proceedings of the National Academy of Sciences, 1995. **92**(8): p. 3439-3443.

90. Kasper, S., et al., *Development, progression, and androgen-dependence of prostate tumors in probasin-large T antigen transgenic mice: a model for prostate cancer.* Lab Invest, 1998. **78**(6): p. i-xv.

91. Perez-Stable, C., et al., *Prostate, adrenocortical, and brown adipose tumors in fetal globin/T antigen transgenic mice.* Lab Invest, 1996. **74**(2): p. 363-73.

92. Gabril, M.Y., et al., *Prostate targeting: PSP94 gene promoter/enhancer region directed prostate tissue-specific expression in a transgenic mouse prostate cancer model.* Gene Ther, 2002. **9**(23): p. 1589-99.

93. Zhou, Z., et al., *Synergy of p53 and Rb deficiency in a conditional mouse model for metastatic prostate cancer.* Cancer Res, 2006. **66**(16): p. 7889-98.

94. Drake, J.M., J.K. Lee, and O.N. Witte, *Clinical targeting of mutated and wild-type protein tyrosine kinases in cancer.* Mol Cell Biol, 2014. **34**(10): p. 1722-32.

95. Witte, O.N., A. Dasgupta, and D. Baltimore, *Abelson murine leukaemia virus protein is phosphorylated in vitro to form phosphotyrosine.* Nature, 1980. **283**(5750): p. 826-31.

96. Hunter, T. and B.M. Sefton, *Transforming gene product of Rous sarcoma virus phosphorylates tyrosine.* Proc Natl Acad Sci U S A, 1980. **77**(3): p. 1311-5.

97. Manning, G., et al., *The protein kinase complement of the human genome.* Science, 2002. **298**(5600): p. 1912-34.

98. Ullrich, A. and J. Schlessinger, *Signal transduction by receptors with tyrosine kinase activity.* Cell, 1990. **61**(2): p. 203-12.

99. Kirkin, V. and I. Dikic, *Role of ubiquitin- and Ubl-binding proteins in cell signaling.* Curr Opin Cell Biol, 2007. **19**(2): p. 199-205.

100. Del Rosario, A.M. and F.M. White, *Quantifying oncogenic phosphotyrosine signaling networks through systems biology.* Curr Opin Genet Dev, 2010. **20**(1): p. 23-30.

101. Nakahara, M., et al., *A novel gain-of-function mutation of c-kit gene in gastrointestinal stromal tumors.* Gastroenterology, 1998. **115**(5): p. 1090-5.

102. Yamamoto, Y., et al., *Activating mutation of D835 within the activation loop of FLT3 in human hematologic malignancies.* Blood, 2001. **97**(8): p. 2434-9.

103. da Cunha Santos, G., F.A. Shepherd, and M.S. Tsao, *EGFR mutations and lung cancer.* Annu Rev Pathol, 2011. **6**: p. 49-69.

104. Rowley, J.D., *Letter: A new consistent chromosomal abnormality in chronic myelogenous leukaemia identified by quinacrine fluorescence and Giemsa staining.* Nature, 1973. **243**(5405): p. 290-3.

105. Sozzi, G., et al., *A t(10;17) translocation creates the RET/PTC2 chimeric transforming sequence in papillary thyroid carcinoma.* Genes Chromosomes Cancer, 1994. **9**(4): p. 244-50.

106. Soda, M., et al., *Identification of the transforming EML4-ALK fusion gene in non-small-cell lung cancer.* Nature, 2007. **448**(7153): p. 561-6.

107. Slamon, D.J., et al., *Human breast cancer: correlation of relapse and survival with amplification of the HER-2/neu oncogene.* Science, 1987. **235**(4785): p. 177-82.

108. Cartwright, C.A., et al., *pp60c-src activation in human colon carcinoma.* J Clin Invest, 1989. **83**(6): p. 2025-33.

109. Herman, S.E., et al., *Bruton tyrosine kinase represents a promising therapeutic target for treatment of chronic lymphocytic leukemia and is effectively targeted by PCI-32765.* Blood, 2011. **117**(23): p. 6287-96.

110. Alexandrov, L.B., et al., *Signatures of mutational processes in human cancer.* Nature, 2013. **500**(7463): p. 415-21.

111. Cai, H., et al., *Invasive prostate carcinoma driven by c-Src and androgen receptor synergy.* Cancer Res, 2011. **71**(3): p. 862-72.

112. Faltermeier, C.M., et al., *Functional screen identifies kinases driving prostate cancer visceral and bone metastasis.* Proc Natl Acad Sci U S A, 2016. **113**(2): p. E172-81.

113. Olsen, J.V., et al., *Global, in vivo, and site-specific phosphorylation dynamics in signaling networks.* Cell, 2006. **127**(3): p. 635-48.

114. Wong, S., et al., *Sole BCR-ABL inhibition is insufficient to eliminate all myeloproliferative disorder cell populations.* Proc Natl Acad Sci U S A, 2004. **101**(50): p. 17456-61.

115. Talpaz, M., et al., *Dasatinib in imatinib-resistant Philadelphia chromosome-positive leukemias.* N Engl J Med, 2006. **354**(24): p. 2531-41.

116. Cortes, J.E., et al., *A phase 2 trial of ponatinib in Philadelphia chromosome-positive leukemias.* N Engl J Med, 2013. **369**(19): p. 1783-96.

Chapter 2:

Prostate Epithelial Cell of Origin Determines Cancer Differentiation State in an Organoid Transformation Assay

Proc Natl Acad Sci USA (2016) 113:4482-7

Prostate epithelial cell of origin determines cancer differentiation state in an organoid transformation assay

Jung Wook Park[a], John K. Lee[b,c], John W. Phillips[a], Patrick Huang[a], Donghui Cheng[d], Jiaoti Huang[d,e,1], and Owen N. Witte[a,c,d,f,g,2]

[a]Department of Microbiology, Immunology, and Molecular Genetics, David Geffen School of Medicine, University of California, Los Angeles, CA 90095; [b]Division of Hematology and Oncology, Department of Medicine, David Geffen School of Medicine, University of California, Los Angeles, CA 90095; [c]Molecular Biology Institute, David Geffen School of Medicine, University of California, Los Angeles, CA 90095; [d]Eli and Edythe Broad Center of Regenerative Medicine and Stem Cell Research, University of California, Los Angeles, CA 90095; [e]Department of Pathology and Laboratory Medicine, David Geffen School of Medicine, University of California, Los Angeles, CA 90095; [f]Department of Molecular and Medical Pharmacology, David Geffen School of Medicine, University of California, Los Angeles, CA 90095; and [g]Howard Hughes Medical Institute, University of California, Los Angeles, CA 90095

Contributed by Owen N. Witte, March 4, 2016 (sent for review February 9, 2016; reviewed by Beatrice S. Knudsen and Calvin Kuo)

The cell of origin for prostate cancer remains a subject of debate. Genetically engineered mouse models have demonstrated that both basal and luminal cells can serve as cells of origin for prostate cancer. Using a human prostate regeneration and transformation assay, our group previously demonstrated that basal cells can serve as efficient targets for transformation. Recently, a subpopulation of multipotent human luminal cells defined by CD26 expression that retains progenitor activity in a defined organoid culture was identified. We transduced primary human prostate basal and luminal cells with lentiviruses expressing c-Myc and activated AKT1 (myristoylated AKT1 or myrAKT1) to mimic the *MYC* amplification and *PTEN* loss commonly detected in human prostate cancer. These cells were propagated in organoid culture before being transplanted into immunodeficient mice. We found that c-Myc/myrAKT1–transduced luminal xenografts exhibited histological features of well-differentiated acinar adenocarcinoma, with strong androgen receptor (AR) and prostate-specific antigen (PSA) expression. In contrast, c-Myc/myrAKT1–transduced basal xenografts were histologically more aggressive, with a loss of acinar structures and low/absent AR and PSA expression. Our findings imply that distinct subtypes of prostate cancer may arise from luminal and basal epithelial cell types subjected to the same oncogenic insults. This study provides a platform for the functional evaluation of oncogenes in basal and luminal epithelial populations of the human prostate. Tumors derived in this fashion with defined genetics can be used in the preclinical development of targeted therapeutics.

human prostate cancer | cells of origin | luminal cell | cancer differentiation | oragnoid culture

The human prostate has two main epithelial cell types, basal and luminal, as well as a minor population of neuroendocrine cells. Primary prostate cancer nearly always has a luminal phenotype characterized by atypical glands, strong androgen receptor (AR) signaling, and an absence of basal cells (1). This histological description suggests that prostate cancer has a luminal cell of origin. Animal studies in genetically engineered mouse models have shown that basal and luminal populations can both serve as cells of origin for prostate cancer (2, 3). Isolation and in vivo transplantation of oncogene-transduced epithelial populations has produced similar results (4, 5). In the human prostate, however, only basal cells have been shown to be efficient targets for transformation (6, 7). In this study, we sought to establish whether human prostate luminal cells could also serve as cells of origin for prostate cancer in an organoid culture assay with enforced oncogene expression.

The development of organotypic culture conditions has greatly aided the study of normal tissue development in diverse epithelial tissues. The use of 3D ex vivo culture systems of purified epithelial cells have made it possible to define stem-like characteristics of cellular subpopulations. Organoid culture has allowed the identification of minimal sets of signaling molecules required for normal growth, self-renewal, and differentiation (8–11).

Along with providing insight into developmental processes, organoid systems also have facilitated studies of carcinogenesis. One distinct advantage of these assays is that they begin with primary benign cells, removing much of the genetic complexity in traditional cell line xenograft assays. Organoid culture has allowed the functional validation of carcinogenic loci identified in genomic studies of pancreatic, gastric, and colon cancers. In one study, *APC*, *TP53*, *KRAS* (G12D), and *SMAD4* mutations were shown to be required for progressive transformation to adenocarcinoma-like phenotypes in organoid culture and for tumorigenicity in vivo (9).

Recent work has established organoid culture conditions for mouse and human prostate epithelial cells (12). These conditions allow the continuous propagation of basal cells ($CD49f^{Hi}$) and luminal cells ($CD26^{+}$). Purified populations of each cell type were cultured separately, but after expansion in vitro, both populations generated mixtures of $CK5^{+}$ basal cells and $CK8^{+}$ luminal cells. However, only purified luminal cells were able to

Significance

This study demonstrates that both primary human basal and luminal epithelial cells are cells of origin for prostate cancer through the use of a prostate organoid culture system. This technology enables the monitoring of early stages of prostate tumorigenesis in vitro and the interrogation of human prostate epithelial populations with synonymous oncogenic stimuli. The combination of c-Myc overexpression and activation of the PI3K/AKT pathway drives high-grade prostate adenocarcinoma in basal cell-derived tumors; however, the same oncogenic stress causes low-grade prostate adenocarcinoma in luminal cell-derived tumors. These findings indicate inherent context-specific and lineage-dependent differences in the response of human prostate epithelial cells to oncogenic stimuli.

Author contributions: J. W. Park, J.K.L., J. W. Phillips, and O.N.W. designed research; J. W. Park, P.H., and D.C. performed research; J. W. Park, J.K.L., J. W. Phillips, J.H., and O.N.W. analyzed data; and J. W. Park, J.K.L., J. W. Phillips, J.H., and O.N.W. wrote the paper.

Reviewers: B.S.K., Cedars Sinai Medical Center; and C.K., Stanford University.

The authors declare no conflict of interest.

Freely available online through the PNAS open access option.

[1]Present address: Department of Pathology, Duke University School of Medicine, Durham, NC 27710.

[2]To whom correspondence should be addressed. Email: owenwitte@mednet.ucla.edu.

generate organoids with glandular architecture. Consistent with previous mouse studies (2, 13), Karthaus et al. (12) postulated the existence of luminal stem/progenitor cells capable of regenerating the normal glandular architecture of the human prostate.

In the present study, we demonstrate that luminal cells can be propagated after oncogene transduction in organoid culture. These transduced cells produce atypical glandular structures when xenografted in immunodeficient mice [NSG; NOD.Cg-*Prkdc*^{scid} *Il2rg*^{tm1Wjl}/SzJ (14)]. The structures display strong AR and prostate-specific antigen (PSA) expression, but lack tumor protein p63 (p63) expression. Xenografts derived from c-Myc/AKT1–transduced basal cells showed histological features of poorly differentiated adenocarcinoma, whereas xenografts from luminal cell organoids transduced with the same two oncogenes exhibited features of low-grade prostate adenocarcinoma. Our findings suggest that prostate epithelial lineages respond differentially to the same oncogenic insults to generate distinct types of human prostate cancer.

Results

Establishment of Oncogene-Transduced Human Primary Prostate Basal and Luminal Organoids. We previously demonstrated that human prostate basal cells are efficient targets for transformation upon the ectopic expression of selected oncogenes (6, 7). In those studies, we transduced primary human basal cells with oncogenes and immediately implanted them s.c. into NSG mice. Overexpression of AR, ERG, and myrAKT1 in the basal cells produced a transformed phenotype of low-grade adenocarcinoma; however, we failed to transform primary human luminal cells (6). We surmised that the different transformation potentials of the cell types in our assay could be either cell-intrinsic or modified by cell-extrinsic environmental cues that preferentially facilitate transformation of basal cells. To address these issues, we adapted a recently described prostate organoid culture system (12) to provide a permissive environment for recovery and growth after the introduction of oncogenes in epithelial populations freshly isolated from primary human prostate tissues.

To isolate basal and luminal cells from benign human prostate tissues, we used antibodies targeting the cell surface markers CD49f and CD26, to differentiate the populations by fluorescence-activated cell sorting (FACS). More than 50% of the dissociated epithelial cells from human prostates were CD49f^{Hi} basal cells, and only 7–16% were CD26^{+} luminal cells (Fig. S1*A*). A postsort analysis of the basal and luminal cell populations was performed to measure cross-contamination from each population. The cross-contamination rate of basal cells in the sorted luminal population was <0.1%. No cross-contamination of luminal cells was detected in the purified basal cell population (0 out of 2,000 total events) (Fig. S1*A*).

We transduced basal and luminal cells with an empty vector or vectors bearing c-Myc and myrAKT1. This oncogene pair mimics *MYC* amplification and *PTEN* loss, two alterations commonly seen in prostate cancer (15–17). *PTEN* loss in basal and luminal cells drives tumor development in a genetically engineered mouse model (18). We previously showed that c-Myc/myrAKT1 can transform human prostate basal cells to poorly differentiated adenocarcinoma and squamous cell carcinoma in vivo in immune-defective mice (7). After transduction of isolated basal and luminal cells, the populations were propagated separately in organoid culture for 2 wk (Fig. 1*A* and Fig. S2*A*).

In the empty vector condition, basal cells grew as solid spherical structures, whereas luminal cells developed gland-like structures with a central lumen (Fig. S2*B*). Despite starting with the same number of cells on culture initiation, basal cells were approximately 50-fold enriched in organoid-forming capacity compared with luminal cells (461 ± 90 out of 1,000 basal cells and 9 ± 2 out of 1,000 luminal cells; Fig. S2*C*). This finding is consistent with a previous report (12).

To assess transduction efficiency, we measured green fluorescent protein (GFP) or red fluorescent protein (RFP) as a

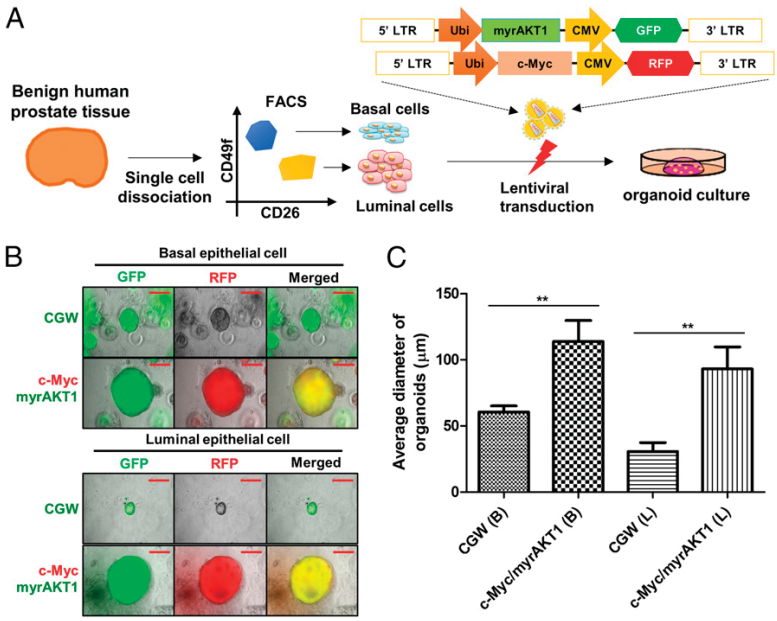

Fig. 1. Expression of c-Myc and myrAKT1 induced growth of basal and luminal cells in organoid culture. (*A*) Schematic of an organoid culture of human primary basal and luminal cells with lentiviral transduction. Ubi, human ubiquitin C promoter; CMV, cytomegalovirus promoter; LTR, long terminal repeat. (*B*) Representative images of c-Myc and myrAKT1–transduced basal or luminal organoids. CGW, empty vector. (Scale bar, 50 μm.) (*C*) Average diameter of c-Myc/myrAKT1–transduced basal and luminal organoids. B, basal cell; L, luminal cell. $^{**}P < 0.05$.

surrogate marker for oncogene expression, because these are coexpressed from the proviral sequence (Fig. 1*A*). On average, 18% of the basal organoids and 16% of the luminal organoids were GFP- and RFP-positive at 3 d after transduction (Fig. S1*B*). After 2 wk in culture, the diameter of the double-transduced basal or luminal organoids was significantly larger than that of the empty vector organoids, suggesting a growth advantage after the introduction of c-Myc and myrAKT1 (Fig. 1*C*).

We measured the organoid-forming efficiency of c-Myc/myrAKT1–transduced basal or luminal cells from four independent patient specimens. Initial experiments starting with 1,000 luminal cells did not yield any GFP/RFP-positive organoids. After increasing the number of starting luminal cells to 10,000 per assay, we detected 5–22 GFP/RFP doubly transduced luminal organoids (0.05–0.22% in Table 1). In the basal population, 1,000 initiating cells yielded 11–30 GFP/RFP doubly transduced basal organoids (1.1–3.0% in Table 1).

c-Myc/myrAKT1–Transduced Basal and Luminal Organoids Display Histological and Molecular Features of Human Prostate Cancer. c-Myc/myrAKT1–transduced basal organoids grew as solid spherical structures (Figs. 1*B* and 2*A*). We observed that oncogene-transduced luminal cells also grew as solid spherical structures with loss of the central lumen seen in the empty vector condition (Fig. S2*B*). Both oncogene-transduced basal and luminal cell organoids displayed vague/absent glandular structures with poorly formed lumens. Some c-Myc/myrAKT1–transduced luminal organoids showed adenosquamous differentiation (Fig. 2*A*).

We confirmed the expression of c-Myc and myrAKT1 oncogenes in the basal and luminal organoids by immunohistochemistry (IHC) (Fig. S3). c-Myc/myrAKT1–transduced basal and luminal organoids displayed molecular phenotypes of human prostate adenocarcinoma, including strong expression of cytokeratin 8 (CK8) and low/absent expression of p63 and cytokeratin 5 (CK5). Focal expression of p63 and CK5 was detected along the rim of the oncogene-transduced basal and luminal organoids (Fig. 2*A*). This could represent basal cell differentiation that may be activated by direct contact with the Matrigel basal membrane matrix in the organoid culture system. AR and PSA expression was low in the oncogene-transduced basal and luminal organoids (Fig. 2*A*). The observation of basal-to-luminal differentiation during tumorigenesis is consistent with previous studies (4, 6, 7). Measurement of the Ki67 cell proliferation marker showed that c-Myc/myrAKT1 basal organoids harbored more Ki67-positive cells compared with c-Myc/myrAKT1 luminal organoids (40% vs. 20%; Fig. 2*B*). We found no significant difference in expression of cleaved-caspase 3 (Cas3), a marker of apoptosis, between c-Myc/myrAKT1–transduced basal and luminal organoids (Fig. 2*A*). We were able to maintain the oncogene-transduced basal and luminal organoids for at least three passages, with 2 wk of culture between each passage.

Human Luminal Cells Develop a Less Aggressive Phenotype Than Basal Cells with the Same Oncogenic Stimuli. We collected intact c-Myc/myrAKT1–transduced basal and luminal cell organoids by enzymatic digestion of the Matrigel. We combined these organoids with murine urogenital sinus mesenchyme (UGSM) cells and implanted these cell grafts s.c. into NSG mice (19) (Fig. 3*A*).

Xenografts of the c-Myc/myrAKT1–transduced basal organoids formed large outgrowths (>1 cm in diameter) within 8 wk of transplantation. In contrast, the oncogene-transduced luminal organoids developed small tumor grafts (<0.5 mm) with a longer latency of 5–8 mo. The xenografts derived from c-Myc/AKT1–transduced basal and luminal cell organoids showed expression of GFP and RFP (Fig. 3*B*). Whereas basal cell-derived xenograft tumors were uniformly fluorescent, only two to six fluorescent foci were found in the luminal cell-derived xenografts from four independent human specimens. Necropsy revealed that all tumors were limited to the s.c. space, with no evidence of gross metastasis.

c-Myc/myrAKT1 xenografts derived from basal cells showed histological features of a poorly differentiated Gleason score 9 or 10 (4 + 5 or 5 + 5) adenocarcinoma. They exhibited a vague/absent glandular structure with poorly formed lumens in a diffuse pattern with solid cell nests. Adenosquamous differentiation was observed as well (Fig. 3*B*). This mixed tumor phenotype was also seen in our previous study (7). The basal organoid xenografts displayed histological features of human prostate cancer, with strong CK8 expression, absent p63 and CK5 expression, and low/absent AR and PSA expression (Fig. 3*C*). Expression of the oncogenes c-Myc and myrAKT1 in the xenografts was confirmed by IHC (Fig. S3).

In contrast to the basal xenografts, the c-Myc/myrAKT1 luminal xenografts exhibited clear glandular structure with well-formed lumens. We found a single cell layer and absence of basal cells on the microscopic appearance of the luminal xenografts stained using H&E. Loss of the basal cell layer is an essential diagnostic feature of prostate carcinoma (20–23). The tumors were well differentiated and exhibited histological features of a well-differentiated Gleason score 6 (3 + 3) adenocarcinoma (Fig. 3*B*).

IHC analysis of the luminal cell-derived tumors showed uniform expression of the luminal cell marker CK8, as well as the absence of basal cell markers CK5 and p63 (Fig. 3*C*). Unlike the basal cell-derived tumors, the luminal cell-derived tumors showed high levels of nuclear AR staining and evidence of AR pathway activation, with strong staining for PSA (Fig. 3*C*). Xenografts produced from c-Myc/myrAKT1–transduced luminal organoids using the tissue of a second patient produced a mixed adenosquamous carcinoma in the luminal xenografts (Fig. S4). These results suggest that luminal cells respond to the oncogenes c-Myc and myrAKT1 similarly to basal cells in terms of their ability to differentiate to adenocarcinoma and squamous cell carcinoma during tumorigenesis.

We found a significantly higher frequency of Ki67-positive cells in basal cell organoid xenografts than in luminal cell organoid xenografts (>80% vs. 5–10%; Fig. 3*C*). This finding implies that the differences in tumor latency and tumor size between c-Myc/myrAKT–transduced basal- and luminal-derived xenografts may be explained in part by differences in cellular proliferation rate. We detected Cas3-positive cells in basal cell organoid xenografts, but not in luminal cell organoid xenografts (Fig. 3*C*).

Table 1. Efficiency of GFP/RFP double-positive luminal and basal cell organoids

Type	No. of cells seeded	Average no. of GFP/RFP double-positive organoids (range)
$CD26^{+}$ luminal cell	10,000	12 (5–22)
$CD49f^{Hi}$ basal cell	10,000	>200
$CD26^{+}$ luminal cell	1,000	0
$CD49f^{Hi}$ basal cell	1,000	21 (11–30)

Discussion

Our previous studies have shown that primary basal epithelial cells from human prostate tissues can be readily transformed by select oncogenes in a transplantation assay. Until now, we have been unable to show that human prostate luminal cells also can be a direct target of transformation (6, 7). We have adapted an organoid culture system that enables the propagation of basal cells and rare luminal progenitor cells to transform both populations of cells. Our studies provide evidence that human prostate luminal cells can serve as cells of origin of prostate cancer, as has been suggested by previous work with mouse models (24, 25).

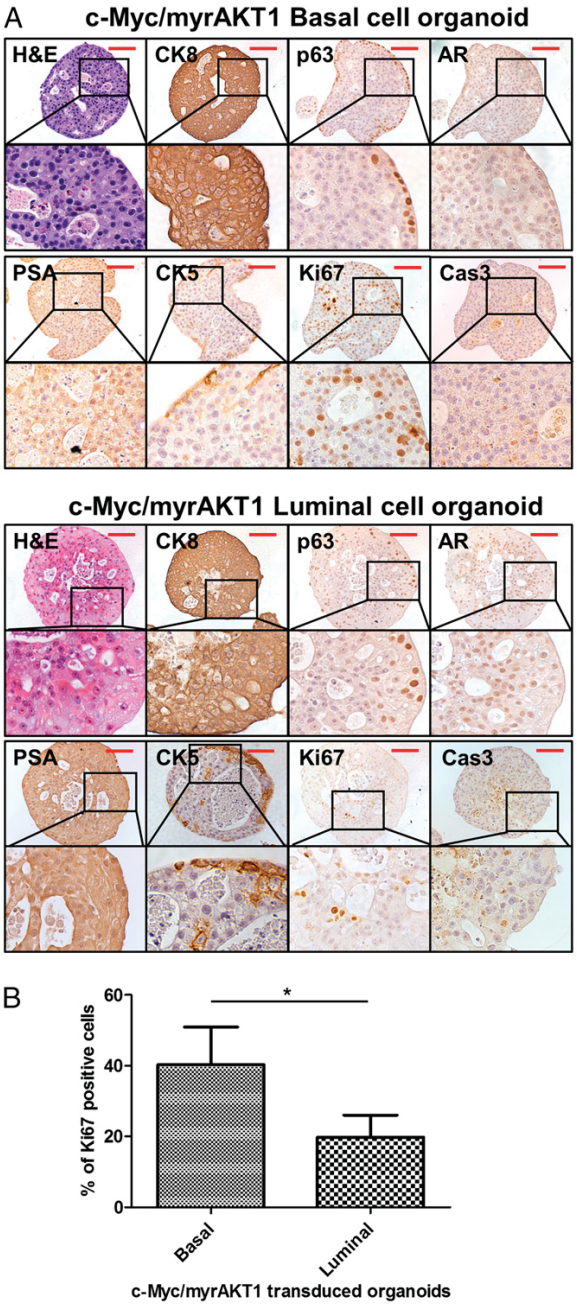

Fig. 2. Molecular characterization of c-Myc/myrAKT1–transduced basal and luminal organoids. (*A*) Representative images of c-Myc/myrAKT1–transduced basal and luminal organoids with H&E and IHC staining for CK8, p63, AR, PSA, CK5, Ki67, and Cas3. (*B*) Percentage of $Ki67^+$ cells in c-Myc/myrAKT1 basal, and luminal cell organoids. $*P < 0.05$. (Scale bar, 100 μm.)

Intriguingly, human basal- and luminal-derived tumors demonstrate histologically distinct phenotypes when challenged with the same oncogenes, *MYC* and *AKT1*. Tumors derived from basal cells are of a higher grade than tumors derived from luminal cells. This finding is consistent with previous observations of slower disease progression and decreased cellular proliferation and tumor invasion in luminal-derived prostate tumors compared with basal-derived tumors in the context of *PTEN* loss (18). It also coincides with our recent report that aggressive human prostate cancers are enriched for a basal stem cell expression signature (26). In contrast, however, another study found that tumors of luminal origin were more aggressive than tumors of basal origin based on cross-species bioinformatics analyses (3). A similar cell-of-origin effect has been demonstrated in breast cancer. One study identified human $CD10^+$ basal cells of the breast as precursors to rare metaplastic tumors, and $EpCAM^+/CD49f^-$ luminal cells as leading to common forms of estrogen receptor-positive and -negative human breast cancer (27). Other recent studies have demonstrated that basal and luminal cells of the mouse mammary gland can be transformed by mutant $PIK3CA^{H1047R}$ overexpression (28, 29). Mutant PIK3CA in basal cells evoked benign tumors, such as adenomyoepithelioma and fibroadenoma, in contrast to the mostly aggressive mammary tumors, including adenosquamous carcinoma and carcinosarcoma, when it was expressed in luminal cells. Mutant PIK3CA caused a different spectrum of tumor types when expressed in basal or luminal cells. These findings suggest that the cell of origin could dictate the aggressiveness and heterogeneity of various tumors driven by the same oncogenic event (28, 29). Although it is widely accepted that combinations of oncogenic events have a major role in determining tumor phenotype, our findings and those of other studies suggest that the differentiation state and cell context in which oncogenic events are expressed play significant roles in defining the molecular subtype of the resulting tumor in human prostate cancer.

Previous efforts to transform prostate epithelial cells have been limited to basal and transit-amplifying or intermediate basal cells, owing to their enhanced ability to endure and proliferate in a variety of in vitro and in vivo conditions (6, 7). Although current growth factor-enriched prostate organoid culture conditions have begun to overcome this limitation, the low frequency of luminal progenitor cell propagation suggests the need for further optimization. In future work, single-cell RNA sequencing technology will allow us to better identify distinct epithelial cell subpopulations within the basal and luminal cells. We suspect that multiple cells of origin within the classic basal and luminal epithelial dichotomy may play a significant role in explaining the heterogeneity of human prostate cancer. As we identify new subpopulations within the epithelial hierarchy of the human prostate, it also will be necessary to understand and mimic in organoid culture the critical stromal interactions and signaling pathways that promote the survival and growth of these cells.

Next-generation sequencing technology has revealed significant genetic heterogeneity in human prostate cancer (30–32). Importantly, Baca et al. (33) defined sequential somatic DNA alterations in the natural history of human prostate cancer development and progression, and identified mutations in *FOXA1* and *SPOP*, loss of *NKX3.1*, and rearrangement of the *ERG* gene as among the earliest events in prostate cancer development. Mutations of *TP53*, *CDKN1A*, *CDKN1B*, *CHD1*, and *PTEN* follow these early events (33). The genomic amplification of *MYCN* has been associated with neuroendocrine prostate cancer (34). Using a tissue recombination model, N-Myc and myrAKT1 overexpression in primary human basal cells was able to initiate a mixed phenotype of neuroendocrine carcinoma and adenocarcinoma (35). Defining the functional consequences of sequential oncogenic events in human prostate cancer development will provide insight into human prostate cancer progression and aggressiveness at the molecular level.

In summary, we have provided evidence of the direct transformation of human prostate luminal cells using an organoid culture. This culture system enables the real-time visualization of early events during tumorigenesis and a direct comparison of human prostate basal and luminal epithelial cell transformation, which was not possible with previous technologies. Our finding

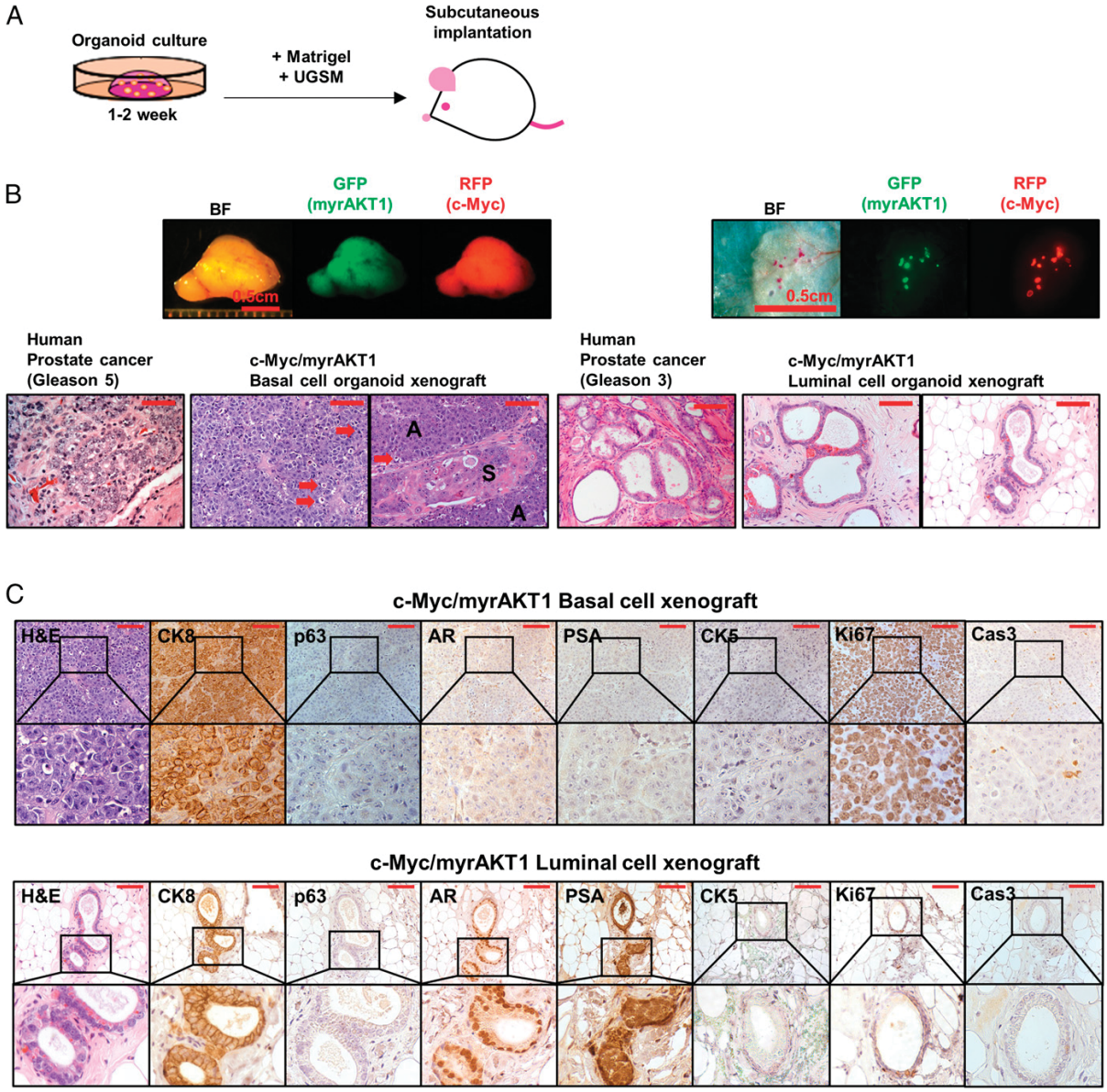

Fig. 3. Comparison of tumors derived from c-Myc/myrAKT1 basal and luminal cell organoids. (*A*) Schematic of the process of establishing xenografts by s.c. injection. (*B*) Representative human prostate cancers and c-Myc/myrAKT1 xenografts. (Scale bar, 100 μm.) Shown are photomicrographs of tumor sections of c-Myc/myrAKT1 basal and luminal xenografts. Red arrows indicate vague/absent glandular structure with poorly formed lumens. A, adenocarcinoma; S, squamous cell carcinoma. (*C*) IHC staining for CK8, p63, AR, PSA, CK5, Ki67, and Cas3. (Scale bar, 100 μm.)

that basal- and luminal-derived tumors demonstrate different phenotypes when challenged with the same oncogenic stimuli suggests that identifying alternative cells of origin for prostate cancer may provide a way to subclassify prostate cancers and facilitate investigation of human prostate cancer heterogeneity.

Methods

Lentiviral Vectors. The myristoylated AKT vector has been described previously (4), as has the c-Myc vector (7).

Organoid Culture of Primary Human Prostate Cells. Patient tissue was provided in a deidentified manner and thus was exempt from Institutional Review Board approval. Acquisition and processing of human tissue, dissociation and isolation of distinct epithelial subsets, and lentiviral transduction have been described in detail previously (19). Between 1,000 and 10,000 FACS-sorted cells were plated in 20–30 μL of growth factor-reduced Matrigel (Corning) after lentiviral transduction. Organoid culture was performed as described previously (36).

In Vivo Implantation of Organoids. Organoids were harvested by dissociation of Matrigel with 1 mg/mL Dispase. The organoids were washed three times with PBS and then mixed with 100,000 UGSM cells in 20–30 μL of Matrigel. The preparation of UGSM cells has been described previously (37). The organoid-Matrigel mixture was implanted s.c. in immunodeficient mice using a 28-gauge syringe.

IHC. Organoids and xenografts were fixed in 10% buffered formalin for 6–24 h and then embedded in HistoGel (Thermo Fisher Scientific) and paraffin, sectioned (4 μm thickness), and mounted on glass slides (Thermo Fisher Scientific). IHC was performed as described previously (6).

Antibodies. Antibodies used for flow cytometry included CD49f-PE and HLA-A/B/C-biotin (eBiosciences), CD49f-Alexa Fluor 647 and CD26-FITC (BioLegend), and Trop2-APC (R&D Systems). Antibodies used for IHC included CK5 (PRB-160P; Covance), CK8 (MMS-162P; Covance), p63 and AR (SC-8431 and SC-816; Santa Cruz Biotechnology), CD26/DPP4 (LS-C122983; LifeSpan Biosciences), c-Myc (ab32072, Abcam), pAKT (9271; Cell Signaling), PSA (A056201-2; Dako), Ki67 (ab16667; Abcam), and Cas3 (9664; Cell Signaling).

Animal Work. NOD.Cg-*Prkdc*^{scid} *Il2rg*^{tm1Wjl}/SzJ (NSG) mice were originally purchased from the Jackson Laboratories and were housed and bred under the care of the Division of Laboratory Animal Medicine at the University of California, Los Angeles. Subcutaneous injections were performed according to protocols approved by the university's Animal Research Committee.

ACKNOWLEDGMENTS. J. W. Park is supported by the Eli and Edythe Broad Center of Regenerative Medicine and Stem Cell Research at University of California, Los Angeles (UCLA) Training Program. J.K.L. is supported by the Tower Cancer Research Foundation Career Development Award, a Prostate Cancer Foundation Young Investigator Award, and the UCLA Subspecialty Training and Advanced Research Program. J. W. Phillips is supported by UCLA Tumor Cell Biology Training Grant T32CA09056. J.H. is supported by the National Institutes of Health (Grants 5R01 CA172603-02, 2P30 CA016042-39, 1R01 CA181242-01A1, and 1R01 CA195505), the Department of Defense Prostate Cancer Research Program (Grant W81XWH-12-1-0206), UCLA Specialized Program of Research Excellence (SPORE) in Prostate Cancer, the Prostate Cancer Foundation's Honorable A. David Mazzone Special Challenge Award, and a UCLA Jonsson Comprehensive Cancer Center Impact Grant. O.N.W. is an Investigator of the Howard Hughes Medical Institute supported by National Institutes of Health Grant U01 CA164188-01A and a Prostate Cancer Foundation Challenge Award. J.H. and O.N.W. are supported by Stand Up To Cancer/Prostate Cancer Foundation/Prostate Dream Team Translational Cancer Research Grant SU2C-AACR-DT0812. This research grant is made possible by the generous support of the Movember Foundation. Stand Up To Cancer is a program of the Entertainment Industry Foundation administered by the American Association for Cancer Research.

1. Humphrey PA (2012) Histological variants of prostatic carcinoma and their significance. *Histopathology* 60(1):59–74.
2. Wang X, et al. (2009) A luminal epithelial stem cell that is a cell of origin for prostate cancer. *Nature* 461(7263):495–500.
3. Wang ZA, et al. (2013) Lineage analysis of basal epithelial cells reveals their unexpected plasticity and supports a cell-of-origin model for prostate cancer heterogeneity. *Nat Cell Biol* 15(3):274–283.
4. Xin L, Lawson DA, Witte ON (2005) The Sca-1 cell surface marker enriches for a prostate-regenerating cell subpopulation that can initiate prostate tumorigenesis. *Proc Natl Acad Sci USA* 102(19):6942–6947.
5. Lawson DA, Xin L, Lukacs RU, Cheng D, Witte ON (2007) Isolation and functional characterization of murine prostate stem cells. *Proc Natl Acad Sci USA* 104(1):181–186.
6. Goldstein AS, Huang J, Guo C, Garraway IP, Witte ON (2010) Identification of a cell of origin for human prostate cancer. *Science* 329(5991):568–571.
7. Stoyanova T, et al. (2013) Prostate cancer originating in basal cells progresses to adenocarcinoma propagated by luminal-like cells. *Proc Natl Acad Sci USA* 110(50):20111–20116.
8. Shin K, et al. (2011) Hedgehog/Wnt feedback supports regenerative proliferation of epithelial stem cells in bladder. *Nature* 472(7341):110–114.
9. Li X, et al. (2014) Oncogenic transformation of diverse gastrointestinal tissues in primary organoid culture. *Nat Med* 20(7):769–777.
10. McCracken KW, et al. (2014) Modelling human development and disease in pluripotent stem cell-derived gastric organoids. *Nature* 516(7531):400–404.
11. Gregorieff A, Liu Y, Inanlou MR, Khomchuk Y, Wrana JL (2015) Yap-dependent reprogramming of Lgr5(+) stem cells drives intestinal regeneration and cancer. *Nature* 526(7575):715–718.
12. Karthaus WR, et al. (2014) Identification of multipotent luminal progenitor cells in human prostate organoid cultures. *Cell* 159(1):163–175.
13. Korsten H, Ziel-van der Made A, Ma X, van der Kwast T, Trapman J (2009) Accumulating progenitor cells in the luminal epithelial cell layer are candidate tumor-initiating cells in a Pten knockout mouse prostate cancer model. *PLoS One* 4(5):e5662.
14. Shultz LD, Ishikawa F, Greiner DL (2007) Humanized mice in translational biomedical research. *Nat Rev Immunol* 7(2):118–130.
15. Gurel B, et al. (2008) Nuclear MYC protein overexpression is an early alteration in human prostate carcinogenesis. *Mod Pathol* 21(9):1156–1167.
16. King JC, et al. (2009) Cooperativity of TMPRSS2-ERG with PI3-kinase pathway activation in prostate oncogenesis. *Nat Genet* 41(5):524–526.
17. Carver BS, et al. (2009) Aberrant ERG expression cooperates with loss of PTEN to promote cancer progression in the prostate. *Nat Genet* 41(5):619–624.
18. Lu TL, et al. (2013) Conditionally ablated Pten in prostate basal cells promotes basal-to-luminal differentiation and causes invasive prostate cancer in mice. *Am J Pathol* 182(3):975–991.
19. Goldstein AS, et al. (2011) Purification and direct transformation of epithelial progenitor cells from primary human prostate. *Nat Protoc* 6(5):656–667.
20. Humphrey PA (2007) Diagnosis of adenocarcinoma in prostate needle biopsy tissue. *J Clin Pathol* 60(1):35–42.
21. Algaba F, et al. (1996) Assessment of prostate carcinoma in core needle biopsy: Definition of minimal criteria for the diagnosis of cancer in biopsy material. *Cancer* 78(2):376–381.
22. Epstein JI (1995) Diagnostic criteria of limited adenocarcinoma of the prostate on needle biopsy. *Hum Pathol* 26(2):223–229.
23. Epstein JI (2004) Diagnosis and reporting of limited adenocarcinoma of the prostate on needle biopsy. *Mod Pathol* 17(3):307–315.
24. Wang ZA, Toivanen R, Bergren SK, Chambon P, Shen MM (2014) Luminal cells are favored as the cell of origin for prostate cancer. *Cell Reports* 8(5):1339–1346.
25. Chua CW, et al. (2014) Single luminal epithelial progenitors can generate prostate organoids in culture. *Nat Cell Biol* 16(10):951–961.
26. Smith BA, et al. (2015) A basal stem cell signature identifies aggressive prostate cancer phenotypes. *Proc Natl Acad Sci USA* 112(47):E6544–E6552.
27. Keller PJ, et al. (2012) Defining the cellular precursors to human breast cancer. *Proc Natl Acad Sci USA* 109(8):2772–2777.
28. Van Keymeulen A, et al. (2015) Reactivation of multipotency by oncogenic PIK3CA induces breast tumour heterogeneity. *Nature* 525(7567):119–123.
29. Koren S, et al. (2015) PIK3CA(H1047R) induces multipotency and multi-lineage mammary tumours. *Nature* 525(7567):114–118.
30. Taylor BS, et al. (2010) Integrative genomic profiling of human prostate cancer. *Cancer Cell* 18(1):11–22.
31. Grasso CS, et al. (2012) The mutational landscape of lethal castration-resistant prostate cancer. *Nature* 487(7406):239–243.
32. Barbieri CE, et al. (2012) Exome sequencing identifies recurrent SPOP, FOXA1 and MED12 mutations in prostate cancer. *Nat Genet* 44(6):685–689.
33. Baca SC, et al. (2013) Punctuated evolution of prostate cancer genomes. *Cell* 153(3):666–677.
34. Beltran H, et al. (2011) Molecular characterization of neuroendocrine prostate cancer and identification of new drug targets. *Cancer Discov* 1(6):487–495.
35. Lee JK, et al. (2016) N-Myc drives neuroendocrine prostate cancer initiated from human prostate epithelial cells. *Cancer Cell*, 10.1016/j.ccell.2016.03.001.
36. Drost J, et al. (2016) Organoid culture systems for prostate epithelial and cancer tissue. *Nat Protoc* 11(2):347–358.
37. Lukacs RU, Goldstein AS, Lawson DA, Cheng D, Witte ON (2010) Isolation, cultivation and characterization of adult murine prostate stem cells. *Nat Protoc* 5(4):702–713.

Supporting Information

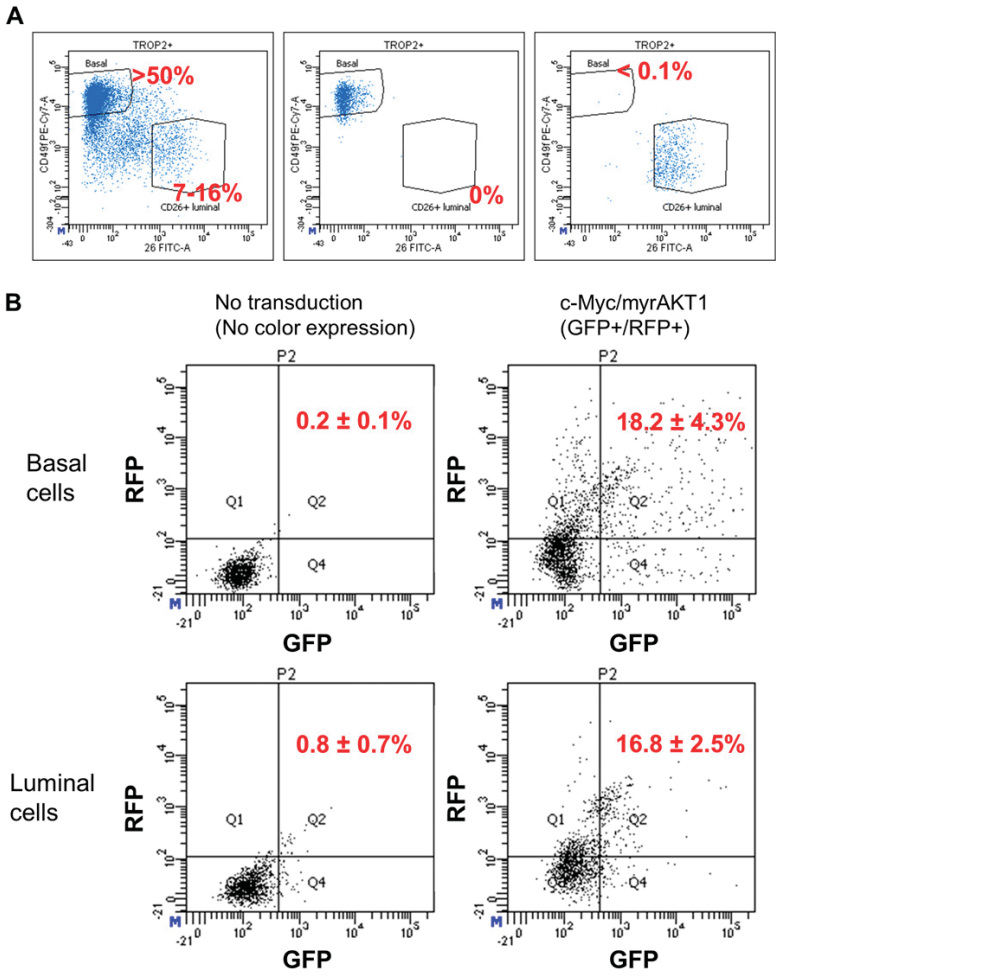

Fig. S1. Isolation of primary human prostate basal and luminal epithelial cells and assessment of lentiviral transduction efficiency. (*A*) Flow cytometry analysis for CD49f and CD26 dissociated human prostate tissue as gated during the sort (*Left*) and postsort of basal (*Middle*) and luminal (*Right*) cells before organoid culture. (*B*) Representative plots of dissociated organoids at 2 d after lentivial transduction cells with no lentiviral transduction were used as a negative control to make a positive gate for GFP/RFP doubly transduced cells.

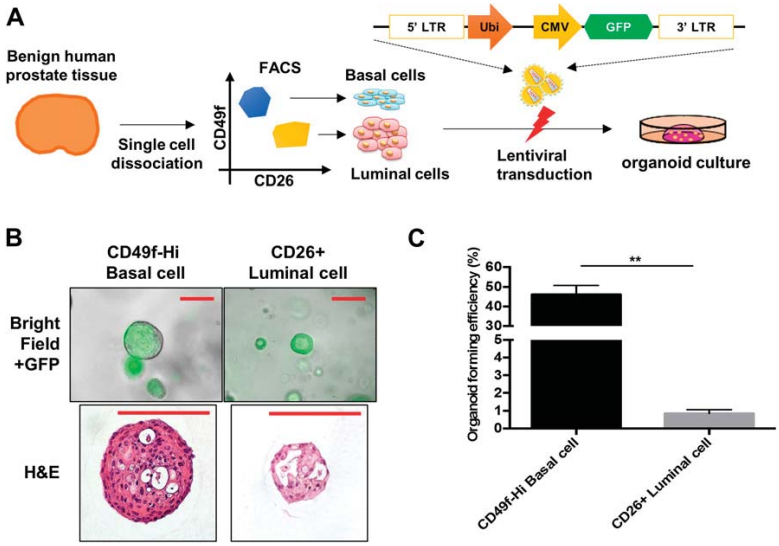

Fig. S2. Basal cells are more efficient than luminal cells at forming organoids. (*A*) Schematic of organoid culture of human primary basal and luminal cells lentivirally transduced with empty vector. (*B*) Representative merged images (bright and GFP fluorescence fields) of organoids of basal and luminal cells. (Scale bar, 50 μm.) (*C*) Organoid-forming efficiency of basal and luminal cells transduced with empty vector. $^{**}P < 0.05$.

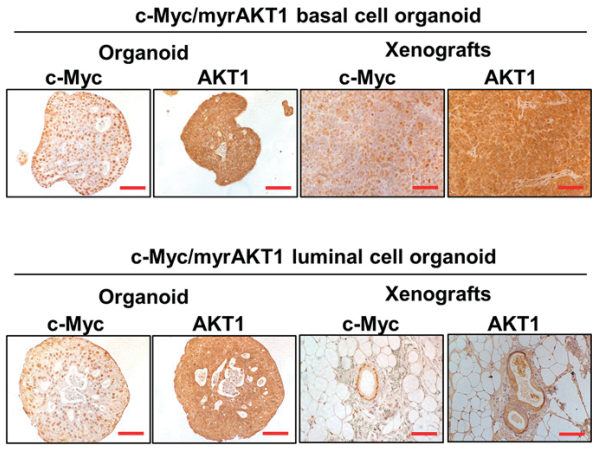

Fig. S3. Expression c-Myc and myrAKT1 oncogenes in xenografts of oncogene-transduced basal and luminal organoids. Representative IHC images for anti–c-Myc and AKT1 are shown. (Scale bar, 100 μm.)

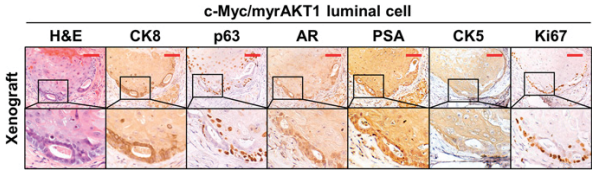

Fig. S4. Mixed adenosquamous cell carcinoma in c-Myc/myrAKT luminal xenografts and IHC for luminal cell markers (CK8, AR, and PSA), basal cell markers (p63 and CK5), and an index of cell proliferation (Ki67). (Scale bar, 100 μm.)

Chapter 3:

Metastatic Castration-Resistant Prostate Cancer Reveals Intrapatient Similarity and Interpatient Heterogeneity of Therapeutic Kinase Targets

Proc Natl Acad Sci USA (2013) 110:E4762-9

Metastatic castration-resistant prostate cancer reveals intrapatient similarity and interpatient heterogeneity of therapeutic kinase targets

Justin M. Drake[a], Nicholas A. Graham[b,c], John K. Lee[d,e], Tanya Stoyanova[a], Claire M. Faltermeier[e], Sudha Sud[f], Björn Titz[b,c], Jiaoti Huang[g,h,i], Kenneth J. Pienta[f,j], Thomas G. Graeber[b,c,g,k,l], and Owen N. Witte[a,c,l,m,1]

[a]Department of Microbiology, Immunology, and Molecular Genetics, [b]Crump Institute for Molecular Imaging, [c]Department of Molecular and Medical Pharmacology, [d]Division of Hematology and Oncology, Department of Medicine, [e]Molecular Biology Institute, [g]Jonsson Comprehensive Cancer Center, [h]Department of Pathology and Laboratory Medicine, [i]Eli and Edythe Broad Center of Regenerative Medicine and Stem Cell Research, [k]Institute for Molecular Medicine, [l]California NanoSystems Institute, and [m]Howard Hughes Medical Institute, David Geffen School of Medicine, University of California, Los Angeles, CA 90095; [j]The Brady Urological Institute, Johns Hopkins School of Medicine, Baltimore, MD 21231; and [f]Department of Internal Medicine, University of Michigan Medical School, Ann Arbor, MI 48109

Contributed by Owen N. Witte, October 23, 2013 (sent for review September 5, 2013)

In prostate cancer, multiple metastases from the same patient share similar copy number, mutational status, erythroblast transformation specific (ETS) rearrangements, and methylation patterns supporting their clonal origins. Whether actionable targets such as tyrosine kinases are also similarly expressed and activated in anatomically distinct metastatic lesions of the same patient is not known. We evaluated active kinases using phosphotyrosine peptide enrichment and quantitative mass spectrometry to identify druggable targets in metastatic castration-resistant prostate cancer obtained at rapid autopsy. We identified distinct phosphopeptide patterns in metastatic tissues compared with treatment-naive primary prostate tissue and prostate cancer cell line-derived xenografts. Evaluation of metastatic castration-resistant prostate cancer samples for tyrosine phosphorylation and upstream kinase targets revealed SRC, epidermal growth factor receptor (EGFR), rearranged during transfection (RET), anaplastic lymphoma kinase (ALK), and MAPK1/3 and other activities while exhibiting intrapatient similarity and interpatient heterogeneity. Phosphoproteomic analyses and identification of kinase activation states in metastatic castration-resistant prostate cancer patients have allowed for the prioritization of kinases for further clinical evaluation.

metastasis | resistance | personalized medicine | combination therapy | phosphotyrosine

Mutational and copy number analyses from epithelial tumors have identified several activating tyrosine kinase mutations and amplifications, such as epidermal growth factor receptor (EGFR) mutations in lung adenocarcinoma and erythroblastic leukemia viral oncogene homolog 2 (*ERBB2 or HER2/neu*) gene amplification in breast cancer (1). The dependence on these tyrosine kinases for tumor growth and survival has led to successful clinical treatment with tyrosine kinase inhibitors (TKIs) (2, 3). However, recent genomic analyses of prostate adenocarcinoma revealed that activating tyrosine kinase mutations or amplifications are very rare (1, 4–6).

Despite the scarcity of tyrosine kinase amplifications or activating mutations in prostate cancer, tyrosine kinase expression and activity has been shown to play an important role in disease progression. For example, coexpression of wild-type SRC tyrosine kinase and androgen receptor (AR) can synergistically drive the formation of mouse prostate adenocarcinoma (7). Evaluation of nontyrosine-kinase–initiated mouse models of prostate cancer further identified activation of the nonreceptor tyrosine kinases SRC, ABL1, and Janus kinase 2 (JAK2) (8). We also observed increased tyrosine phosphorylation in nearly 50% of castration-resistant prostate cancer (CRPC) tissues examined compared with hormone-naïve prostate cancer (8). These studies suggest that comprehensive evaluation of metastatic CRPC samples for tyrosine kinase activity may lead to the identification of new drug targets.

Studies in melanoma and breast cancer have revealed that despite heterogeneity in primary, localized disease, metastases seem to arise from a single precursor cell (9, 10). The multifocal nature of organ-confined prostate cancer poses a question as to the clonality of metastatic disease (11). Investigation into clonality in metastatic CRPC has found that tumors isolated from anatomically different lesions in the same patient bear similar copy number, mutational status, erythroblast transformation specific (ETS) rearrangements, and methylation patterns from multiple metastatic lesions supporting their clonal origins (6, 12–14). In addition, these studies found a remarkable amount of interpatient heterogeneity, suggesting that personalized medicine approaches may be necessary to efficiently target metastatic lesions. Previous observations of intrapatient similarity hold promise with regard to treatment strategies for metastatic CRPC patients by means of systematically attacking the cancer cell clone contributing to disease.

This led us to investigate whether actionable targets such as tyrosine kinases also maintain similar activation patterns across anatomically distinct metastases from the same patient. With

Significance

Metastatic castration-resistant prostate cancer (CRPC) remains incurable due to the lack of effective therapies. The need to identify new actionable targets in CRPC is crucial as we begin to examine the resistance mechanisms related to androgen withdrawal. Here, we report an unbiased quantitative phosphoproteomic approach to identify druggable kinases in metastatic CRPC. These kinase activation patterns revealed intrapatient similarity and interpatient heterogeneity across a large panel of targets. Interestingly, these kinase activities are not a result of mutation but rather pathway activation within the tumors themselves. The observation that similar kinase activities are present in most if not all anatomically disparate metastatic lesions from the same patient suggests that CRPC patients may benefit from individualized, targeted combination therapies.

Author contributions: J.M.D., N.A.G., K.J.P., T.G.G., and O.N.W. designed research; J.M.D., N.A.G., J.K.L., T.S., C.M.F., and S.S. performed research; J.M.D., N.A.G., J.K.L., C.M.F., B.T., and J.H. analyzed data; and J.M.D., N.A.G., J.K.L., and O.N.W. wrote the paper.

The authors declare no conflict of interest.

Freely available online through the PNAS open access option.

Data deposition: The MS proteomics data have been deposited in ProteomeXchange, www.proteomexchange.org (accession no. PXD000238).

[1]To whom correspondence should be addressed. E-mail: owenwitte@mednet.ucla.edu.

access to rare metastatic CRPC tissue from the University of Michigan's Rapid Autopsy Program (15), we evaluated global tyrosine phosphorylation patterns in lethal metastatic CRPC patients. Phosphotyrosine peptide enrichment and quantitative mass spectrometry (MS) identified diverse phosphorylation events in the metastatic tissues compared with naive primary prostate tissue and prostate cancer cell line-derived xenografts. Validation of activated kinases that were identified via either MS or kinase–substrate relationships revealed intrapatient similarity and interpatient heterogeneity across a large panel of targets. Interestingly, these kinase activities are a result not of mutation (6) but rather of pathway activation within the tumors themselves. In summary, the observation that similar tyrosine kinase activities are present in most if not all anatomically disparate metastatic lesions from the same patient reveals that (*i*) CRPC lesions may be clonal in origin and (*ii*) kinase activation patterns observed in these lesions should be prioritized for further evaluation as new targeted therapeutic strategies.

Results

Phosphotyrosine Peptide Signatures Are Dramatically Different Between Prostate Cancer Cell Line-Derived Xenografts and Treatment-Naïve or Metastatic CRPC Tissues. To identify and discover unique kinase targets in metastatic CRPC, we analyzed 16 metastatic CRPC samples from 13 different patients obtained at rapid autopsy (15) by quantitative label-free phosphotyrosine MS (Fig. 1). These included eight anatomically unique sites as well as two or three distinct sites from three separate patients. Each sample contained greater than 50% tumor content as determined by histological analyses. We also analyzed one benign prostatic hyperplasia (BPH), six treatment-naïve matched benign and cancerous prostates, and metastatic or s.c. xenograft tumors derived from the androgen-insensitive 22Rv1 and androgen-sensitive LNCaP cell lines (Dataset S1) (8). From three separate phosphotyrosine enrichment preparations and MS analyses, we identified 297 unique phosphopeptides corresponding to 185 unique proteins (Dataset S2).

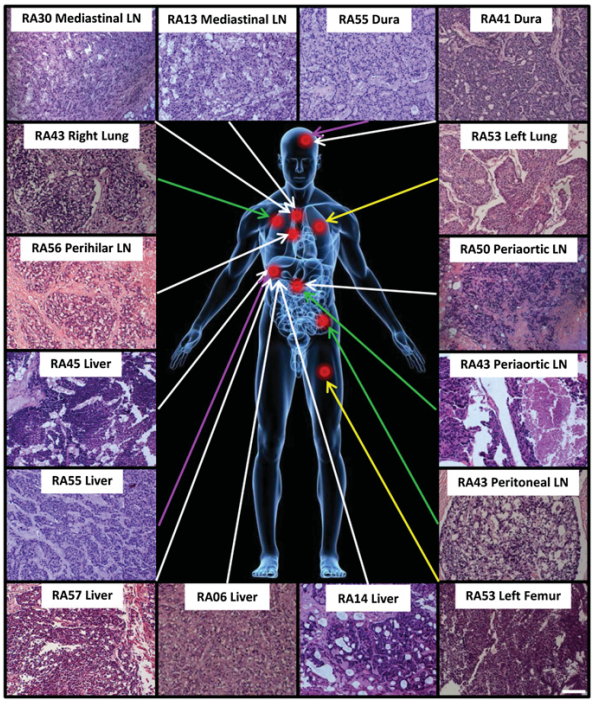

Fig. 1. Anatomical location and histological characterization of metastatic CRPC samples used for phosphoproteomics. Metastatic CRPC tissues were obtained from the Rapid Autopsy Program at the University of Michigan. Sixteen samples from 12 different patients are represented and prepared as previously described for phosphoproteomics (8). Red dots indicate the approximate location of the metastatic lesions analyzed. Same-colored lines represent tissues from the same patient. Patient RA53 left lung and left femur were combined due to limiting material (yellow lines). Only tissues with greater than 350 mg and 50% tumor content were evaluated. (Scale bar, 50 μm.)

To compare different models and stages of prostate cancer, we included cell line-derived xenografts, treatment-naïve primary prostate benign and cancerous tissues, and metastatic CRPC in a single phosphotyrosine enrichment preparation. Unsupervised hierarchical clustering revealed three separate clusters. In particular, the cell line-derived xenografts formed a distinct group compared to the primary tissues, indicating that these xenografts are poor representations of primary patient tissue (Fig. 2*A*). In addition, unsupervised hierarchical clustering also did not distinguish between the patient-matched benign or cancerous prostates, indicating that tyrosine phosphorylation remains relatively unchanged in treatment-naïve benign or cancerous prostates (Fig. 2*A* and Figs. S1 and S2). This suggests that evaluation of phosphotyrosine activity in metastatic CRPC tissues is crucial to testing potential new therapeutic treatments.

Phosphoproteomic Profiling and Kinase/Substrate Enrichment Analyses Identifies Several Druggable Nonmutated Kinase Targets and Pathways in Metastatic CRPC Lesions. Most patients with metastatic CRPC present with metastases at multiple sites, creating a therapeutic dilemma (15). We set out to examine heterogeneity in a cohort of metastatic CRPC patients including those with multiple, anatomically distinct metastatic sites for activated kinase targets. Several metastatic CRPC patients that we evaluated contained similar anatomic sites of involvement including tumors in the liver, lung, dura, and distant lymph nodes. Unsupervised hierarchical clustering of the tyrosine phosphorylation patterns of 10 metastatic lesions, including two patients for which we had two independent metastatic lesions, grouped samples by both patient and metastatic site (Fig. 2*B* and Fig. S3).

Phosphotyrosine peptide identification directly identified several activated kinases and phosphatases [tyrosine kinase 2 (TYK2) Y^{292}, protein tyrosine kinase 2 beta (PTK2B) Y^{579}, MAPK1/3 $Y^{187/204}$, discoidin domain receptor tyrosine kinase 1 (DDR1) Y^{796}, the JAK2/SRC kinase target STAT3 Y^{705}, and protein tyrosine phosphatase, non-receptor type 11 (PTPN11) $Y^{62/63}$]. Kinase–substrate relationship analyses, which predict kinase activity based on phosphopeptide motifs (8), have also identified putative upstream kinases and phosphatases [anaplastic lymphoma kinase (ALK), EGFR, PTK6, SRC, and PTPN2] that were active in individual metastatic CRPC samples (Figs. S1–S3 and Datasets S3–S5). These identifications were notable because of the US Food and Drug Administration–approved late-stage clinical trial of available kinase inhibitors targeting SRC (dasatinib/bosutinib/ponatinib) (16–18), EGFR (erlotinib) (19), ALK (crizotinib) (20), the MAPK1/3 upstream pathway kinases mitogen-activated protein kinase kinase 1/2 (MEK1/2) (trametinib) (21), or the STAT3 upstream kinase JAK2 (ruxolitinib) (22). Western blot analyses from five different patients confirmed the activation states of some of these kinases and also revealed interpatient heterogeneity as each patient evaluated displayed a unique phosphopattern (Fig. 2*C*). As expected, when evaluating prospectively the mutational status of a subset of our samples, we observed little to no activating mutations in these kinases. We did find one patient, RA57 Liver, to have two mutations [one in ephrin type-A receptor 4 (EPHA4) and one in mast/stem cell growth factor receptor (SCFR or KIT)] (6). However, our kinase/substrate enrichment scores did not predict kinase activity of either EPHA4 or KIT, again suggesting

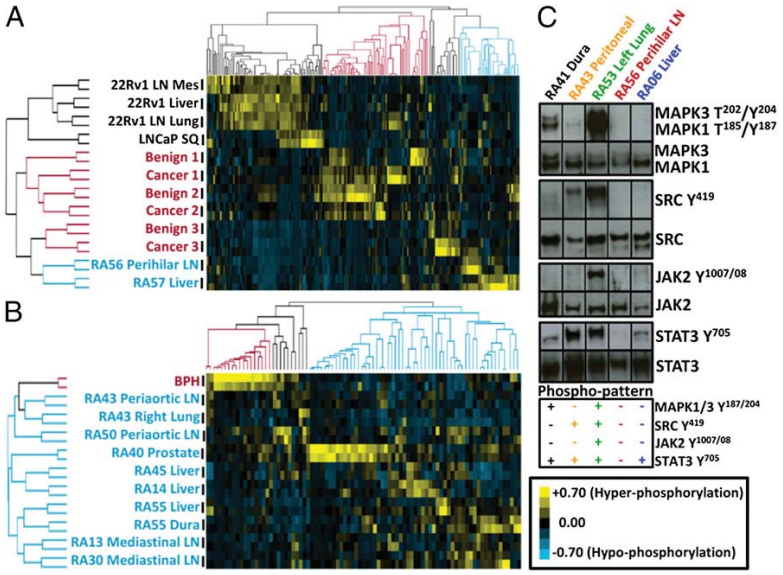

Fig. 2. Phosphoproteomic analyses of cell line-derived xenografts, treatment-naïve prostate cancer, and metastatic CRPC reveal distinct phosphopatterns. (*A*) Unsupervised hierarchical clustering of phosphotyrosine-enriched peptides separates cell line-derived xenograft tumors from primary prostate or metastatic tissue. (*B*) Further evaluation of a separate run of 10 metastatic CRPC lesions reveals patient-specific and metastatic site similarity of phosphotyrosine peptide patterns. (*C*) Western blot validation of four different activated kinases identified from both phosphoproteomics and inferred kinase activities confirms the heterogeneity observed across five different patients, as each patient exhibited a unique phosphopattern. Western blot data were separated to highlight each individual patient but were performed on the same western blot. Yellow, hyperphosphorylation; blue, hypophosphorylation. Intensity bar in Fig. 2*B* is applicable to Fig. 2*A*.

that these mutations did not lead to any detectable levels of activation of these kinases in this tissue sample.

Correlation analysis of the phosphotyrosine signaling patterns revealed a significant level of similarity in the phosphotyrosine profiles from lesions derived from a single patient, despite the fact that these lesions were derived from distinct anatomical sites (Fig. S4). Comparing three liver metastases, we also observed high levels of similarity between two of three lesions (Fig. S4). These MS–based phosphoproteomic data suggest that metastatic CRPC lesions isolated from the same patient may exhibit highly similar tyrosine kinase activation patterns but do not exclude the possibility that anatomical location may also drive similar phosphotyrosine signaling patterns in CRPC. This aspect is further analyzed below.

Large-Scale Analyses of Kinase Activation Patterns Reveals Intrapatient Similarity Across Multiple, Anatomically Distinct Metastases. To determine if signaling patterns were more similar within anatomically distinct metastatic lesions from the same CRPC patient or within sites of metastasis, we examined a larger, independent set of patients that included 28 distinct metastatic lesions from seven different CRPC patients (Fig. S5). Western blot analysis of phosphoproteins identified by MS and kinase/substrate enrichment analysis or the activated states of receptor tyrosine kinase (RTK) targets [EGFR Y^{1173}, ERBB2 Y^{1221}, and hepatocyte growth factor receptor (HGFR or MET) Y^{1234}] for which there are clinical inhibitors available confirmed our initial observation of intrapatient similarities (Fig. 3 and Fig. S6 *A–C*). Comparison of different patients revealed dramatically different kinase activation patterns. This ranged from SRC Y^{419}, STAT3 Y^{705}, MAPK1/3 $T^{185/202}/Y^{187/204}$, and AKT S^{473}, activated upon phosphatase and tensin homolog (*PTEN*) loss in the majority of prostate cancers, for patient RA43 to only STAT3 Y^{705} for patient RA55 (Fig. 3). These unique phosphopatterns suggest that shared kinase activities exist in metastatic CRPC lesions isolated from the same patient.

To determine if this pattern of intrapatient similarity across metastases remains consistent with a larger set of other RTK and intracellular kinases, we evaluated five previously analyzed sets of patient metastases using RTK and phosphokinase arrays from R&D Systems. Analysis of three or four anatomically distinct metastatic lesions from each patient revealed signaling patterns that were qualitatively similar within a patient's set of metastatic lesions (Fig. 4*A*). Patient-specific patterns included (*i*) tyrosine phosphorylation of ALK, RYK, and the activation site of AKT T^{308} in patient RA37; (*ii*) hemopoietic cell kinase (HCK) pY^{411} from patient RA56; and (*iii*) cellular RET (c-RET) phosphorylation in RA33 (Fig. 4*A*). Quantitation of these arrays revealed intrapatient similarities for nine phospho- and total proteins (Fig. 4*B*). Principal component analysis (PCA) of the kinases and proteins with detectable phosphorylation or expression ($n = 11$) demonstrated highly similar intrapatient grouping (Fig. 4*C* and Fig. S7). Surprisingly, the signaling patterns found in these metastatic lesions appear to be substantially cell autonomous as lesions from similar anatomical sites did not group together (Fig. 4*D*). Statistical analysis of pairwise correlation coefficients confirmed that metastatic CRPC lesions isolated from the same patient have strongly similar signaling patterns, more so than lesions from similar anatomical sites in different patients (Fig. S8).

Phosphorylation of Neuronal RTK RET in Metastatic CRPC Lesions with a Small Cell Neuroendocrine Carcinoma Phenotype. Further evaluation of the phospho-RTK arrays revealed tyrosine phosphorylation of RET in patient RA33 (Fig. 3*A*). RET is expressed in neuronal cell types, suggesting this patient may have suffered from a rare small cell neuroendocrine carcinoma (SCNC) phenotype (23). Indeed histological analyses of patient RA33 confirmed SCNC as evidenced by a diffuse, solid growth pattern with darkly stained nucleus, a homogeneous chromatin pattern, high nuclear/cytoplasmic (N/C) ratio, lack of nucleoli, and frequent mitotic figures (Fig. S9 *A* and *B*, arrows). These are in sharp contrast

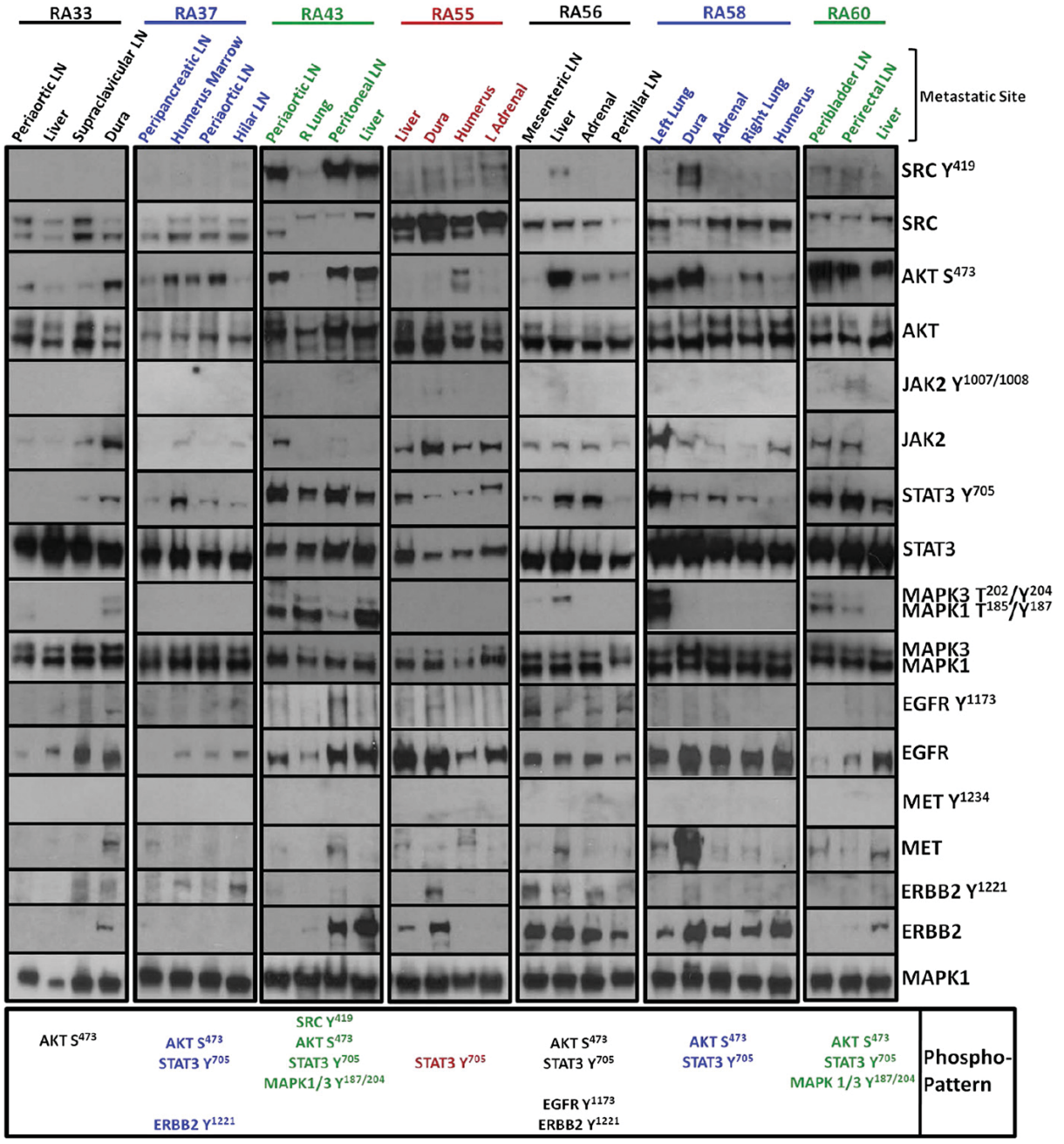

Fig. 3. Related phosphokinase and substrate expression patterns are observed within distinct anatomical metastatic lesions of the same patient. Western blot analyses from seven different sets of patients with three or four distinct metastatic lesions were evaluated for kinase activation patterns that were identified in the phosphoproteomic datasets and kinase–substrate relationships or RTKs that have been previously targeted clinically. Each patient expressed similar activated kinase patterns independent of the anatomical location of the metastatic lesions. The unique phosphopatterns are also depicted schematically below the Western blot data.

to the conventional prostatic adenocarcinoma that shows glandular formation (Fig. S9*C*, dashed circle), nuclear morphology consisting of open and vesicular chromatin patterns, and prominent nuclei (Fig. S9*C*, arrow). These data suggest that the molecular phenotyping of SCNC, as indicated by phospho-RET activity, may drive novel therapeutic strategies for this rarer subtype of prostate cancer.

Stratification of Metastatic CRPC Patients' Kinase Activation Patterns Suggests That Simultaneous Targeting of SRC and MEK Kinases May Be of Potential Therapeutic Value. To predict potential kinase inhibitor combination therapies for metastatic CRPC patients, we evaluated all 16 individual metastatic CRPC lesions that had been analyzed by phosphoproteomics. We pooled kinases that were

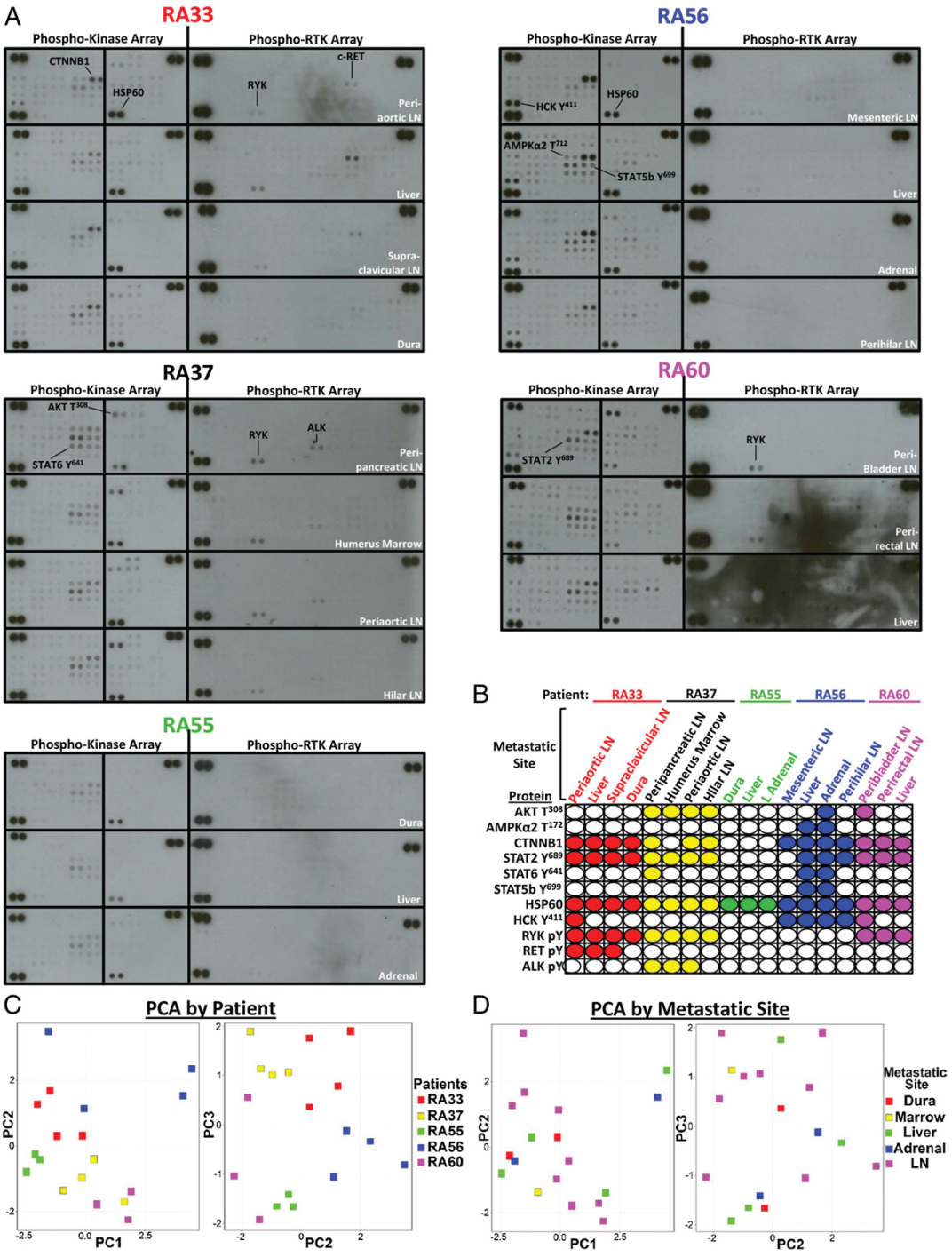

Fig. 4. Large-scale analyses of kinase activation patterns confirm intrapatient similarity across multiple, anatomically distinct metastases. (*A*) Phosphokinase and phospho-RTK arrays were used to analyze metastatic lesions from five different patients from anatomically distinct metastatic lesions. (*B*) Unique phosphopatterns were observed for each patient, and similar patterns were observed within the same patient, as shown with like-colored circles. Each observable phospho- or total protein spot from the phosphokinase and RTK arrays were used for PCA. LN, lymph node. (*C*) PCA analysis of all five patients confirms intrapatient kinase expression similarity and interpatient dissimilarity. (*D*) Grouping metastatic lesions by similar anatomical site shows no significant grouping of samples. Each phosphokinase and phospho-RTK array are spotted in duplicate, and positive control spots are located in the top left, right, and bottom left of each array. The first three principal components represent 77% of the total variance. Adrenal, adrenal gland lesions; LN, distant lymph node lesions; marrow, bone marrow lesion.

Table 1. Kinase and inhibitor stratification of metastatic CRPC patients

Patient number and metastatic location	Identified kinases via MS and western blot plus inferred kinases via kinase–substrate relationships*	Potential clinical inhibitors				
		Dasatinib†	Erlotinib‡	Crizotinib§	Ruxolitinib¶	Trametinib‖
RA06 Liver	EPHA3-7, SRC, PDGFR	X				
RA13 Mediastinal LN	ALK, FLT3/CSF1R/KIT, INSR, MAPK1, MAP3K2, PTK6, SRC	X		X		X
RA14 Liver	EGFR, MAPK1, MAP3K2, PTK6	X	X			X
RA30 Mediastinal LN	ALK, FLT3/CSF1R/KIT, MAP3K2, PTK6, SRC	X		X		X
RA40 Prostate	EGFR, MAPK1/3, MAP2K2, MAP3K2, PTK6, SRC	X	X			X
RA41 Dura	FLT3/CSF1R/KIT, MAPK1/3, SRC	X				X
RA43 Peritoneal and Right Lung	ALK, EGFR, EPHA3-7, MAPK1/3, PTK6, SRC	X	X	X		X
RA43 Periaortic LN	MAPK1/3, SRC	X				X
RA43 Right Lung	EGFR, FLT3/CSF1R/KIT, MAPK1/3, MAP2K2	X	X			X
RA45 Liver	ALK, MAP3K2			X		X
RA50 Periaortic LN	MAPK1/3, MAP3K2					X
RA53 Left Femur and Left Lung	ALK, EPHA3-7, JAK2, MAPK1/3, PDGFR, PTK6, SRC	X		X	X	X
RA55 Liver	ALK, EGFR, EPHA3, MAPK1/3, MAP2K2, MAP3K2, PTK6	X	X	X		X
RA55 Dura	EGFR, PTK6	X	X			
RA56 Perihilar LN	EGFR, HCK, TYK2	X	X		X	
RA57 Liver	EPHA7, MAP3K2, TYK2	X			X	X

*Kinases corresponding to identified phosphopeptides observed as >twofold over benign tissues, via western blotting, or kinase–substrate relationships ($P < 0.1$) as shown in Dataset S4.
†SRC family kinase, KIT, PDGFR, and EPHA receptor inhibitor.
‡EGFR inhibitor.
§ALK inhibitor.
¶JAK2 inhibitor.
‖MEK inhibitor.

identified from MS, western blot, and predicted kinase–substrate relationships to reveal a wide range of predicted kinase activities across the patient samples (Table 1). Mapping clinically available inhibitors to these kinases revealed 11 different TKI combinations with overlap between four sets of inhibitor combinations (Table 1). Notably, the SRC inhibitor dasatinib and the MEK inhibitor trametinib were predicted therapeutic strategies in 14 of 16 (87.5%) or 13 of 16 (81.2%) patients, respectively. If we consider combination therapy, 11 of 16 (68.8%) patients would be predicted to benefit from both SRC and MEK inhibitors, whereas 5 of 16 (31.2%) patients would not. There are no current clinical trials in prostate cancer evaluating the efficacy of SRC and MEK combination therapy in metastatic CRPC, but if initiated, stratification of patients based on activation of these two kinases would be necessary. Overall, the kinases identified in metastatic CRPC patients using phosphoproteomic analyses (*i*) may guide the molecular stratification of patients to direct the proper course of treatment with kinase inhibitor combinations, (*ii*) confirm the complexity observed across patients, and (*iii*) suggest that individualized therapy needs to be considered before clinical treatment decisions.

Discussion

From our study, we were able to measure protein phosphorylation in 41 metastatic CRPC samples from 17 patients including 16 samples by quantitative phosphotyrosine MS. Our phosphokinase profiling and evaluation of active kinases suggests that kinase activity patterns are patient-specific and are maintained across multiple metastatic lesions within the same patient. These data support previous studies suggesting that metastatic disease arises from a single precursor cancer cell or focal mass located at the primary tumor site (6, 12–14). Our findings add actionable information to this perspective. Kinase inhibitor treatment regimens guided by the biopsy of a single accessible metastatic lesion may be sufficient to predict the responses of multiple sites, leading to a more efficacious use of single agents or multidrug combinations, although this concept is still untested.

The development of new targeted therapies for metastatic CRPC presents a number of clinical questions. Major challenges include effective stratification of patients who will benefit from selected treatments and recognition of context-specific molecular targets. One approach to address these issues is the serial sampling and molecular characterization of malignant tissue from patients during the course of their disease. The increasing availability of high-throughput tools has enabled the genomic and transcriptomic profiling of large numbers of clinical carcinoma samples of different subtypes (4, 24, 25). Phosphoproteomic technology, particularly mass spectroscopy–based proteomics, is also rapidly advancing and has recently been applied to the elucidation of tyrosine-kinase–driven pathways in cell lines (26–29) or the discovery of activated kinases that may be useful for therapy in human cancers (30, 31).

Our analysis of phosphotyrosine signaling patterns in primary tumors and xenografts indicates that the prostate cell line-derived xenografts evaluated have different phosphorylation patterns compared with primary tissues. Supporting this notion, gene expression studies in small-cell lung cancer (SCLC) also identified primary tumor-specific signatures that were lost upon transitioning to cell culture (32), and proteomic analyses in colorectal cancer suggest that xenograft tumors are dramatically different from their cell line counterparts (33). This suggests that the stratification and prioritization of therapeutic targets for CRPC will require analysis of primary tissue, rather than cell lines or cell line-derived xenografts.

Interestingly, very few patient sets were positive for the activated states of EGFR, ERBB2, or MET, although they were detected in prostate cancer cell lines. Drugs targeting EGFR and ERBB2 did not produce significant results in CRPC patients (34,

35), however the MET inhibitor cabozantinib has shown promise in the clinic (36). This is in contrast to our observation that MET activity is not detected in our analyzed metastatic CRPC tissues. One explanation is that our sampling of metastatic CRPC tissues is too small or that MET activity was lost before tissue collection and we were not able to detect it. Two other possibilities are that cabozantinib activity in metastatic CRPC is not targeted toward epithelial MET but rather to MET expressed in osteoblasts or other mesenchymal cells in the bone microenvironment (36) and that cabozantinib is inhibiting another tyrosine kinase such as VEGFR2 or RET (37). Although we did not evaluate VEGFR2 activity, we did observe RET activity in SCNC, suggesting this kinase may be potentially targeted by cabozantinib in metastatic CRPC patients.

Rapid autopsy programs have paved the way for studies in genomic mutations, copy number alterations, and splicing variants from metastatic tissues that are otherwise difficult to obtain (4, 6, 15, 38, 39). Although we evaluated many soft tissue metastatic lesions, we were only able to evaluate five bone metastases. Although bone metastases are evident in over 90% of metastatic CRPC patients (15), metastatic bone tumors are hard to study because tumor material is lodged into hard, calcified bone, preventing the procurement of quality material for analysis. This is also especially difficult considering the large amount of tissue (>350 mg) required for phosphoproteomic preparations. A potential outcome could be that kinase patterns are principally determined by site of metastasis due to signals initiated by the surrounding local microenvironment creating a pre-metastatic niche (40). Tissue-specific kinase activation patterns were not observed in our study, but further evaluation of bone metastases in patients also harboring soft tissue metastases will be necessary to extend these findings.

Materials and Methods

Tissue Culture of Prostate Cancer Cell Lines and Derivation of Xenograft Tumors. 22Rv1 cells were grown in RPMI medium supplemented with L-glutamine, FBS, and nonessential amino acids (NEAAs). LNCaP, DU145, and C4-2 cells were grown in DMEM supplemented with L-glutamine, FBS, and NEAA. Thirty 15-cm plates were collected from each cell line and treated with 2 mM Vanadate for 30 min. Cells were subsequently lysed in 9 M Urea lysis buffer and used for phosphoproteomic analysis.

To generate metastatic tumors, 1×10^5 22Rv1 cells were injected intracardially as previously described, and dissemination was monitored using bioluminescence imaging (41). After 8 wks, tumors were extracted from the metastatic locations including the liver and lymph nodes in the mesenteric and lung regions. Also, to evaluate primary tumor growth, 1×10^6 LNCaP cells were injected s.c. and excised once they reached Division of Laboratory Animal Medicine (DLAM) limits.

Acquisition of Clinically Matched Benign and Cancerous Primary Prostate Tissues and Metastatic CRPC Samples. Patient samples were obtained from the University of California–Los Angeles (UCLA) Translational Pathology Core Laboratory, which is authorized by the UCLA Institutional Review Board to distribute anonymized tissues to researchers as described previously (42–44). Cancer and benign areas were clearly marked on the frozen section slides, and prostate tissue containing the cancer region was separated from the benign area before collecting for phosphoproteomic analyses.

The Rapid Autopsy program at the University of Michigan has been previously described (11, 39). Frozen tissues from the Rapid Autopsy program were sent overnight on dry ice for phosphotyrosine peptide analysis. Sections were stained with hematoxylin and eosin for representative histology.

Quantitative Analysis of Phosphotyrosine Peptides by MS. Tissue lysis was performed as previously described (8). Briefly, greater than 350 mg of frozen tumor mass was homogenized and sonicated in urea lysis buffer (20 mM Hepes pH 8.0, 9 M urea, 2.5 mM sodium pyrophosphate, 1.0 mM beta-glycerophosphate, 1% *N*-octyl glycoside, 2 mM sodium orthovanadate). Total protein was measured using the bicinchoninic acid (BCA) Protein Assay Kit (Thermo Scientific/Pierce), and 25 mg of total protein was used for phosphoproteomic analysis. The remaining protein lysate was frozen for subsequent western blot analyses.

Phosphotyrosine peptide enrichment and liquid chromatography tandem MS (LC-MS/MS) analysis was performed as previously described (8, 26, 45). Phosphopeptides were identified using the Proteome Discoverer software (version 1.4.0.88, Thermo Fisher Scientific). MS/MS fragmentation spectra were searched using SEQUEST against the Uniprot human reference proteome database with canonical and isoform sequences (downloaded January 2012 from uniprot.org). Search parameters included carbamidomethyl cysteine (*C) as a static modification. Dynamic modifications included phosphorylated tyrosine, serine, or threonine (pY, pS, and pT, respectively) and oxidized methionine (*M). The Percolator node of Protein Discoverer was used to calculate false discovery rate (FDR) thresholds, and the FDR for the datasets was adjusted to 1% (version 1.17, Thermo Scientific). The Percolator algorithm uses a target-decoy database search strategy and discriminates true and false identifications with a support vector machine (46). The PhosphoRS 2.0 node was used to more accurately localize the phosphate on the peptide (47). Only phosphopeptides with at least one phosphotyrosine assignment with a reported probability above 20% were considered. MS2 spectra for all reported phosphopeptides are deposited to the ProteomeXchange Consortium with the dataset identifier PXD000238 (48).

Data Analysis. Data analysis was performed as previously described (8). For clustering, we removed any peptides that had an ANOVA score greater than 0.2. Hierarchical clustering of phosphotyrosine data was performed using the Cluster program with the Pearson correlation and pairwise complete linkage analysis (49) and visualized using Java TreeView (50). Quantitative data for each phosphopeptide can be found in Dataset S5, *Batch 1–3*. To evaluate the significance of intrapatient and anatomical site similarity, the Pearson correlation coefficient was calculated for each pair of phosphotyrosine samples, and the resulting correlation matrix was clustered using the pHeatmap package in R. Statistical significance was assessed against the null hypothesis that the correlation was not different from zero.

Prediction of Kinase–Substrate Relationships and Enrichment Analysis of Kinase Activity. Predictions, enrichment, and permutation analyses have been previously described (8). Phosphotyrosine peptides were ranked by the signal-to-noise ratio observed for a given perturbation (e.g., metastatic CRPC compared with benign prostate or BPH). The enrichment scores for all putative upstream kinases are shown in Dataset S4, *Batch 1–3*.

Western Blot. For western blots, equal protein amounts of metastatic CRPC tissue urea lysates (20 or 30 μg) were used from tissues prepared as described previously (8). Antibodies were diluted as follows: AKT (1:1,000, Santa Cruz), pAKT S^{473} (1:2,000, Cell Signaling), EGFR (1:1,000, Cell Signaling), pEGFR Y^{1173} (1:1,000, Cell Signaling), STAT3 (1:1,000, Cell Signaling), pSTAT3 Y^{705} (1:2,000, Cell Signaling), JAK2 (1:1,000, Cell Signaling), pJAK2 $Y^{1007/1008}$ (1:500, Cell Signaling), MAPK1/3 (1:1,000, Cell Signaling), MAPK1/3 $T^{185/202}$/$Y^{187/204}$ (1:2,000, Cell Signaling), SRC (1:1,000, Millipore), pSRC Y^{419} (1:1,000, Cell Signaling), ERBB2 (1:1,000, Cell Signaling), pERBB2 $Y^{1221/1222}$ (1:1,000, Cell Signaling), MET (1:1,000, Cell Signaling), and pMET Y^{1234} (1:1,000, Cell Signaling). ECL substrate (Millipore) was used for detection and development on GE/Amersham film.

Phospho-RTK and Phosphokinase Arrays. Human Phospho-RTK (R&D Sytems) and phosphokinase (R&D Systems) arrays were used according to the manufacturer's instructions. Briefly, 300 μg of 9 M urea lysate for each metastatic sample was diluted in the kit-specific dilution buffer to a final concentration of 0.85 M urea and incubated with blocked membranes overnight. The membranes were washed and exposed to chemiluminescent reagent and developed on GE/Amersham film. Quantitation of each array was performed using Image J. To evaluate the significance of intrapatient and anatomical site similarity, the Pearson correlation coefficient was calculated for each pair of samples using only the kinases and proteins with detectable phosphorylation or expression (n = 11), and the correlation coefficients were clustered using the pHeatmap package in R. Statistical similarity of intrapatient lesions was assessed against the null hypothesis that the correlation was not different from zero. P values from multiple comparisons were combined using Fisher's Method where appropriate.

PCA. Each antibody-related spot on the Phospho-RTK and phosphokinase arrays was quantified using Image J. After background subtraction, the duplicate spots for each antibody were averaged, and antibodies with negligible signal were removed. The data were unit normalized, and principal components were calculated in R.

ACKNOWLEDGMENTS. We thank members of the O.N.W. laboratory for helpful comments and discussion on the manuscript. We thank Mireille Riedinger for purifying the 4G10 antibody used in mass spectrometry studies. We thank the Tissue Procurement Core Laboratory at UCLA for assistance on tissue processing and H&E staining. J.M.D. and T.S. are supported by the Department of Defense Prostate Cancer Research Program (W81XWH-11-1-0504 and W81XWH-12-1-0100, respectively). N.A.G. is supported by UCLA Scholars in Oncologic Molecular Imaging (SOMI) program, National Institutes of Health (NIH) Grant R25T CA098010. J.K.L. is supported by NIH Training Grant 5T32CA009297-28 and the UCLA Specialty Training and Advanced Research (STAR) Program. C.M.F. is supported by the UCLA Medical Scientist Training Program. J.H. is supported by the Department of Defense Prostate Cancer Research Program W81XWH-11-1-0227 and W81XWH-12-1-0206, UCLA Specialized Program in Research Excellence (SPORE) in prostate cancer, National Cancer Institute (NCI) 1R01CA158627, Stand Up to Cancer/AACR Dream Team Award, and Prostate Cancer Foundation Honorable A. David Mazzone Special Challenge Award. K.J.P. is supported by NIH U54 CA163124, NIH 1 U01CA143055-01A1, NIH 2 P50 CA69568, and NIH 1 PO1 CA093900 and receives support from the Prostate Cancer Foundation, the Taubman Research Institute as a Taubman Scholar, and the American Cancer Society as a Clinical Research Professor. T.G.G. is supported by NCI/NIH P01 CA168585 and R21 CA169993, American Cancer Society Research Scholar Award RSG-12-257-01-TBE, the CalTech–UCLA Joint Center for Translational Medicine, the UCLA Jonsson Cancer Center Foundation, the UCLA Institute for Molecular Medicine, the National Center for Advancing Translational Sciences UCLA Clinical and Translational Science Institute (CTSI) Grant UL1TR000124, and a Concern Fondation CONquer CanCER Now Award. J.H. and O.N.W. are supported by a Prostate Cancer Foundation Challenge Award. O.N.W. is an Investigator of the Howard Hughes Medical Institute and co–principal investigator of the West Coast Prostate Cancer Dream Team supported by Stand Up to Cancer/American Association for Cancer Research (AACR)/Prostate Cancer Foundation.

1. Kan Z, et al. (2010) Diverse somatic mutation patterns and pathway alterations in human cancers. *Nature* 466(7308):869–873.
2. Kim KS, et al. (2005) Predictors of the response to gefitinib in refractory non-small cell lung cancer. *Clin Cancer Res* 11(6):2244–2251.
3. Mass RD, et al. (2005) Evaluation of clinical outcomes according to HER2 detection by fluorescence in situ hybridization in women with metastatic breast cancer treated with trastuzumab. *Clin Breast Cancer* 6(3):240–246.
4. Taylor BS, et al. (2010) Integrative genomic profiling of human prostate cancer. *Cancer Cell* 18(1):11–22.
5. Kumar A, et al. (2011) Exome sequencing identifies a spectrum of mutation frequencies in advanced and lethal prostate cancers. *Proc Natl Acad Sci USA* 108(41): 17087–17092.
6. Grasso CS, et al. (2012) The mutational landscape of lethal castration-resistant prostate cancer. *Nature* 487(7406):239–243.
7. Cai H, Babic I, Wei X, Huang J, Witte ON (2011) Invasive prostate carcinoma driven by c-Src and androgen receptor synergy. *Cancer Res* 71(3):862–872.
8. Drake JM, et al. (2012) Oncogene-specific activation of tyrosine kinase networks during prostate cancer progression. *Proc Natl Acad Sci USA* 109(5):1643–1648.
9. Kuukasjärvi T, et al. (1997) Genetic heterogeneity and clonal evolution underlying development of asynchronous metastasis in human breast cancer. *Cancer Res* 57(8): 1597–1604.
10. Fidler IJ, Talmadge JE (1986) Evidence that intravenously derived murine pulmonary melanoma metastases can originate from the expansion of a single tumor cell. *Cancer Res* 46(10):5167–5171.
11. Shah RB, et al. (2004) Androgen-independent prostate cancer is a heterogeneous group of diseases: Lessons from a rapid autopsy program. *Cancer Res* 64(24):9209–9216.
12. Liu W, et al. (2009) Copy number analysis indicates monoclonal origin of lethal metastatic prostate cancer. *Nat Med* 15(5):559–565.
13. Aryee MJ, et al. (2013) DNA methylation alterations exhibit intraindividual stability and interindividual heterogeneity in prostate cancer metastases. *Sci Transl Med* 5(169):69ra10.
14. Mehra R, et al. (2008) Characterization of TMPRSS2-ETS gene aberrations in androgen-independent metastatic prostate cancer. *Cancer Res* 68(10):3584–3590.
15. Rubin MA, et al. (2000) Rapid ("warm") autopsy study for procurement of metastatic prostate cancer. *Clin Cancer Res* 6(3):1038–1045.
16. Cortes JE, et al. (2012) Bosutinib versus imatinib in newly diagnosed chronic-phase chronic myeloid leukemia: Results from the BELA trial. *J Clin Oncol* 30(28):3486–3492.
17. Cortes JE, et al. (2012) Ponatinib in refractory Philadelphia chromosome-positive leukemias. *N Engl J Med* 367(22):2075–2088.
18. Kantarjian H, et al. (2010) Dasatinib versus imatinib in newly diagnosed chronic-phase chronic myeloid leukemia. *N Engl J Med* 362(24):2260–2270.
19. Cohen MH, et al. (2010) Approval summary: Erlotinib maintenance therapy of advanced/metastatic non-small cell lung cancer (NSCLC). *Oncologist* 15(12):1344–1351.
20. O'Bryant CL, Wenger SD, Kim M, Thompson LA (2013) Crizotinib: A new treatment option for ALK-positive non-small cell lung cancer. *Ann Pharmacother* 47(2):189–197.
21. Flaherty KT, et al.; METRIC Study Group (2012) Improved survival with MEK inhibition in BRAF-mutated melanoma. *N Engl J Med* 367(2):107–114.
22. Mascarenhas J, Hoffman R (2012) Ruxolitinib: The first FDA approved therapy for the treatment of myelofibrosis. *Clin Cancer Res* 18(11):3008–3014.
23. Tai S, et al. (2011) PC3 is a cell line characteristic of prostatic small cell carcinoma. *Prostate* 71(15):1668–1679.
24. Anonymous; Cancer Genome Atlas Network (2012) Comprehensive molecular characterization of human colon and rectal cancer. *Nature* 487(7407):330–337.
25. Anonymous; Cancer Genome Atlas Network (2012) Comprehensive molecular portraits of human breast tumours. *Nature* 490(7418):61–70.
26. Rubbi L, et al. (2011) Global phosphoproteomics reveals crosstalk between Bcr-Abl and negative feedback mechanisms controlling Src signaling. *Sci Signal* 4(166):ra18.
27. Wolf-Yadlin A, et al. (2006) Effects of HER2 overexpression on cell signaling networks governing proliferation and migration. *Mol Syst Biol* 2:54.
28. Bai Y, et al. (2012) Phosphoproteomics identifies driver tyrosine kinases in sarcoma cell lines and tumors. *Cancer Res* 72(10):2501–2511.
29. Guha U, et al. (2008) Comparisons of tyrosine phosphorylated proteins in cells expressing lung cancer-specific alleles of EGFR and KRAS. *Proc Natl Acad Sci USA* 105(37):14112–14117.
30. Walters DK, et al. (2006) Activating alleles of JAK3 in acute megakaryoblastic leukemia. *Cancer Cell* 10(1):65–75.
31. Rikova K, et al. (2007) Global survey of phosphotyrosine signaling identifies oncogenic kinases in lung cancer. *Cell* 131(6):1190–1203.
32. Daniel VC, et al. (2009) A primary xenograft model of small-cell lung cancer reveals irreversible changes in gene expression imposed by culture in vitro. *Cancer Res* 69(8): 3364–3373.
33. Sirvent A, Vigy O, Orsetti B, Urbach S, Roche S (2012) Analysis of SRC oncogenic signaling in colorectal cancer by stable isotope labeling with heavy amino acids in mouse xenografts. *Mol Cell Proteomics* 11(12):1937–1950.
34. Nabhan C, et al. (2009) Erlotinib has moderate single-agent activity in chemotherapy-naïve castration-resistant prostate cancer: Final results of a phase II trial. *Urology* 74(3):665–671.
35. Ziada A, et al. (2004) The use of trastuzumab in the treatment of hormone refractory prostate cancer; phase II trial. *Prostate* 60(4):332–337.
36. Smith DC, et al. (2013) Cabozantinib in patients with advanced prostate cancer: Results of a phase II randomized discontinuation trial. *J Clin Oncol* 31(4):412–419.
37. Yakes FM, et al. (2011) Cabozantinib (XL184), a novel MET and VEGFR2 inhibitor, simultaneously suppresses metastasis, angiogenesis, and tumor growth. *Mol Cancer Ther* 10(12):2298–2308.
38. Friedlander TW, et al. (2012) Common structural and epigenetic changes in the genome of castration-resistant prostate cancer. *Cancer Res* 72(3):616–625.
39. Mehra R, et al. (2011) Characterization of bone metastases from rapid autopsies of prostate cancer patients. *Clin Cancer Res* 17(12):3924–3932.
40. Psaila B, Lyden D (2009) The metastatic niche: Adapting the foreign soil. *Nat Rev Cancer* 9(4):285–293.
41. Drake JM, Gabriel CL, Henry MD (2005) Assessing tumor growth and distribution in a model of prostate cancer metastasis using bioluminescence imaging. *Clin Exp Metastasis* 22(8):674–684.
42. Goldstein AS, et al. (2011) Purification and direct transformation of epithelial progenitor cells from primary human prostate. *Nat Protoc* 6(5):656–667.
43. Stoyanova T, et al. (2012) Regulated proteolysis of Trop2 drives epithelial hyperplasia and stem cell self-renewal via β-catenin signaling. *Genes Dev* 26(20):2271–2285.
44. Goldstein AS, Huang J, Guo C, Garraway IP, Witte ON (2010) Identification of a cell of origin for human prostate cancer. *Science* 329(5991):568–571.
45. Graham NA, et al. (2012) Glucose deprivation activates a metabolic and signaling amplification loop leading to cell death. *Mol Syst Biol* 8:589.
46. Spivak M, Weston J, Bottou L, Käll L, Noble WS (2009) Improvements to the percolator algorithm for Peptide identification from shotgun proteomics data sets. *J Proteome Res* 8(7):3737–3745.
47. Taus T, et al. (2011) Universal and confident phosphorylation site localization using phosphoRS. *J Proteome Res* 10(12):5354–5362.
48. Vizcaíno JA, et al. (2013) The PRoteomics IDEntifications (PRIDE) database and associated tools: Status in 2013. *Nucleic Acids Res* 41(Database issue):D1063–D1069.
49. Eisen MB, Spellman PT, Brown PO, Botstein D (1998) Cluster analysis and display of genome-wide expression patterns. *Proc Natl Acad Sci USA* 95(25):14863–14868.
50. Saldanha AJ (2004) Java Treeview—Extensible visualization of microarray data. *Bioinformatics* 20(17):3246–3248.

Supporting Information

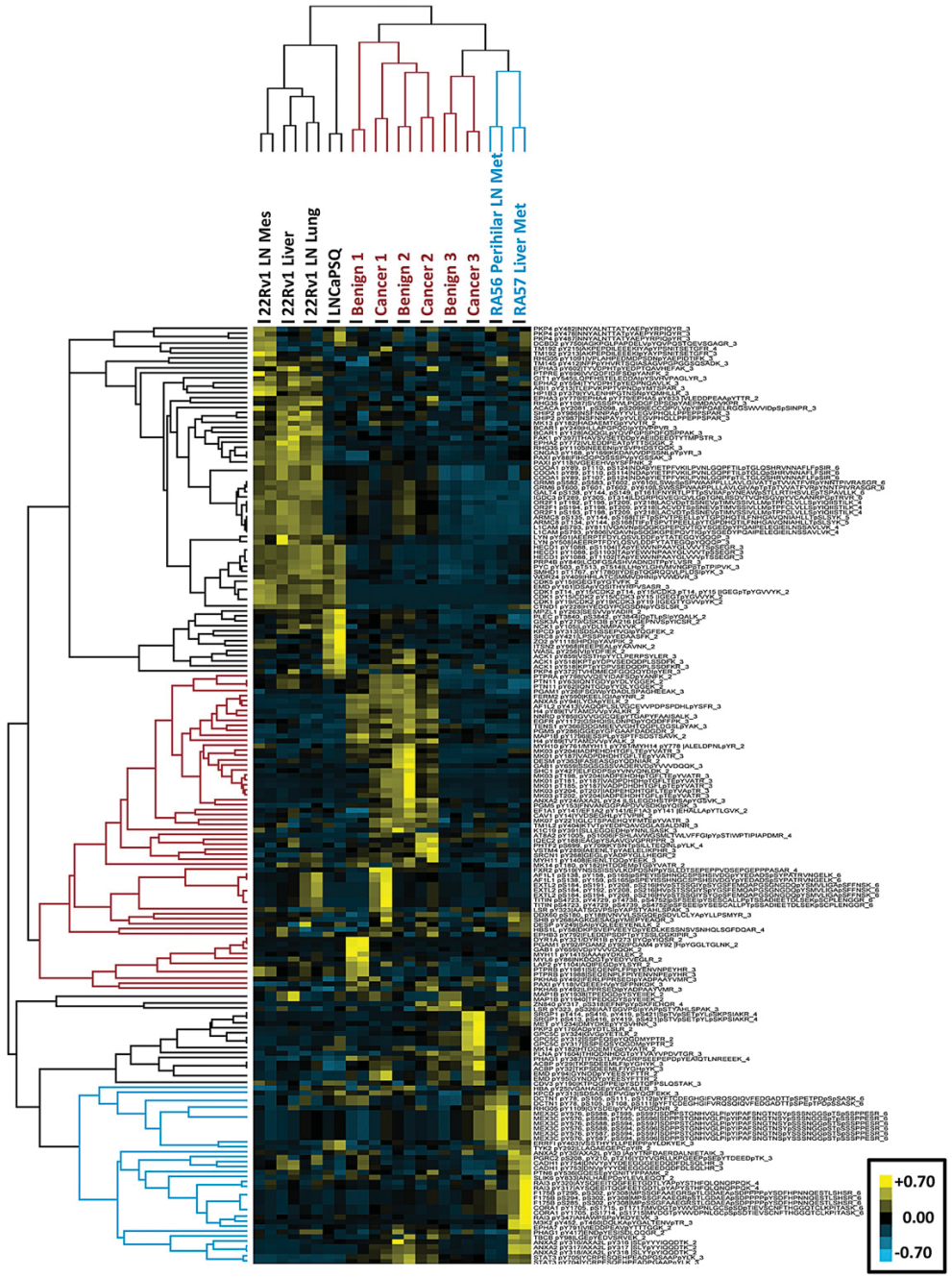

Fig. S1. Phosphoproteomic analysis exhibits distinct clusters of phosphorylation between the cell line-derived xenografts and primary prostate tissues. Unsupervised hierarchical clustering does not group cell line-derived metastatic xenograft tumors with either organ confined or metastatic castration-resistant prostate cancer (CRPC). In addition, treatment-naïve patient-matched benign and cancerous prostates display indistinguishable phosphopeptide signatures. The phosphoprofiling heatmap from Fig. 2*A* with the protein and residue identities of the phosphorylation events are listed. For all heatmaps, the labels are as follows: UniProt ID, phosphosite residue number, phosphopeptide (charge state of mass spectrometry ion). If the phosphopeptide has multiple identities, a slash separates each protein and phosphorylation residue number. The vertical line separates the proteins from the phospho-peptide. Yellow, hyperphosphorylation; blue, hypophosphorylation.

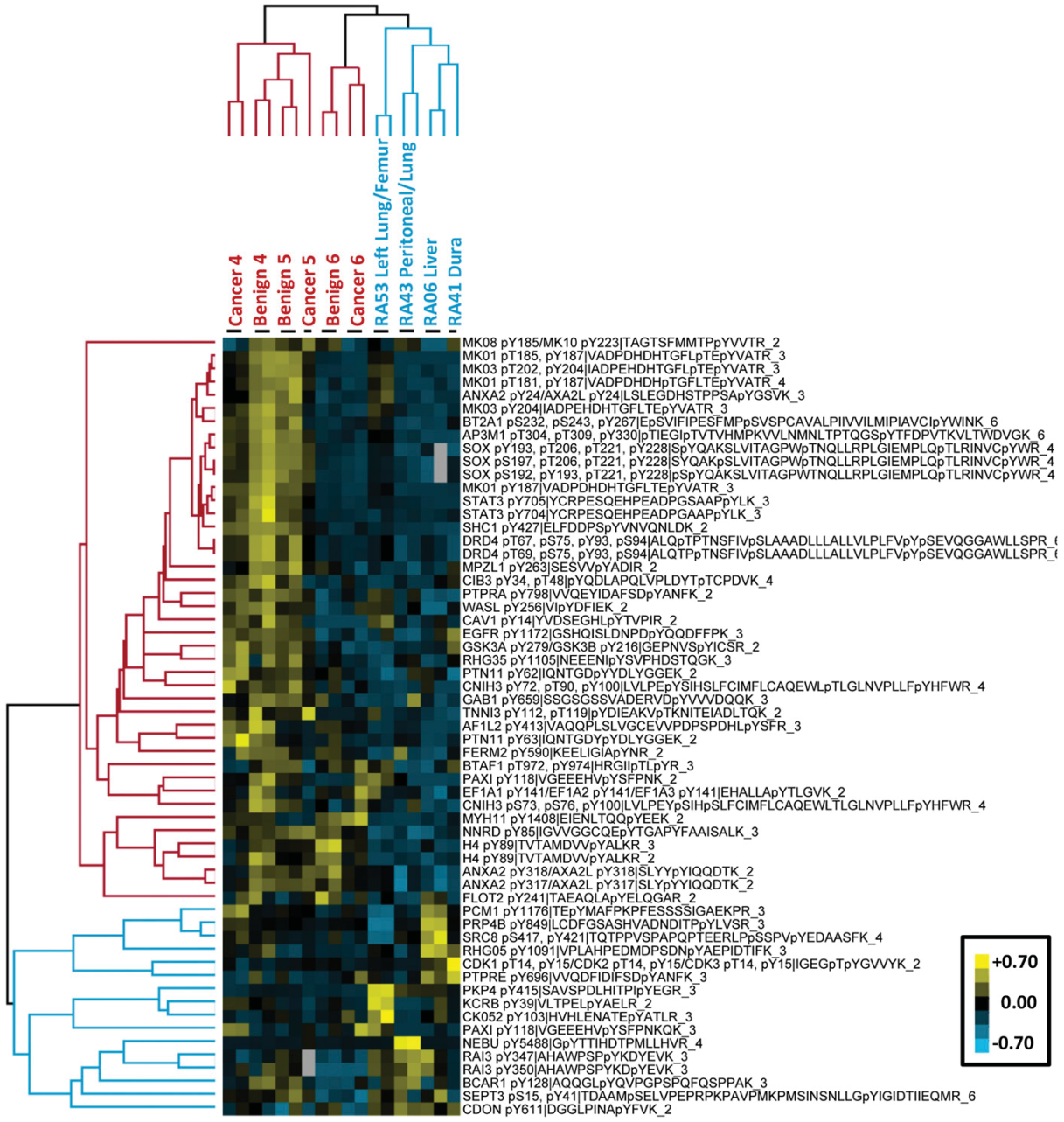

Fig. S2. Phosphoproteomic analysis exhibits distinct clusters of phosphorylation between treatment-naïve prostate cancer and metastatic CRPC. Unsupervised hierarchical clustering does not group organ-confined prostate benign or cancerous prostates with metastatic CRPC. Also, treatment-naïve patient-matched benign and cancerous prostates display indistinguishable phosphopeptide signatures. The phosphoprofiling heatmap from batch 2 with the protein and residue identities of the phosphorylation events are listed. For all heatmaps, the labels are as follows: UniProt ID, phosphosite residue number, phosphopeptide (charge state of mass spectrometry ion). If the phosphopeptide has multiple identities, a slash separates each protein and phosphorylation residue number. The vertical line separates the proteins from the phosphopeptide. Yellow, hyperphosphorylation; blue, hypophosphorylation.

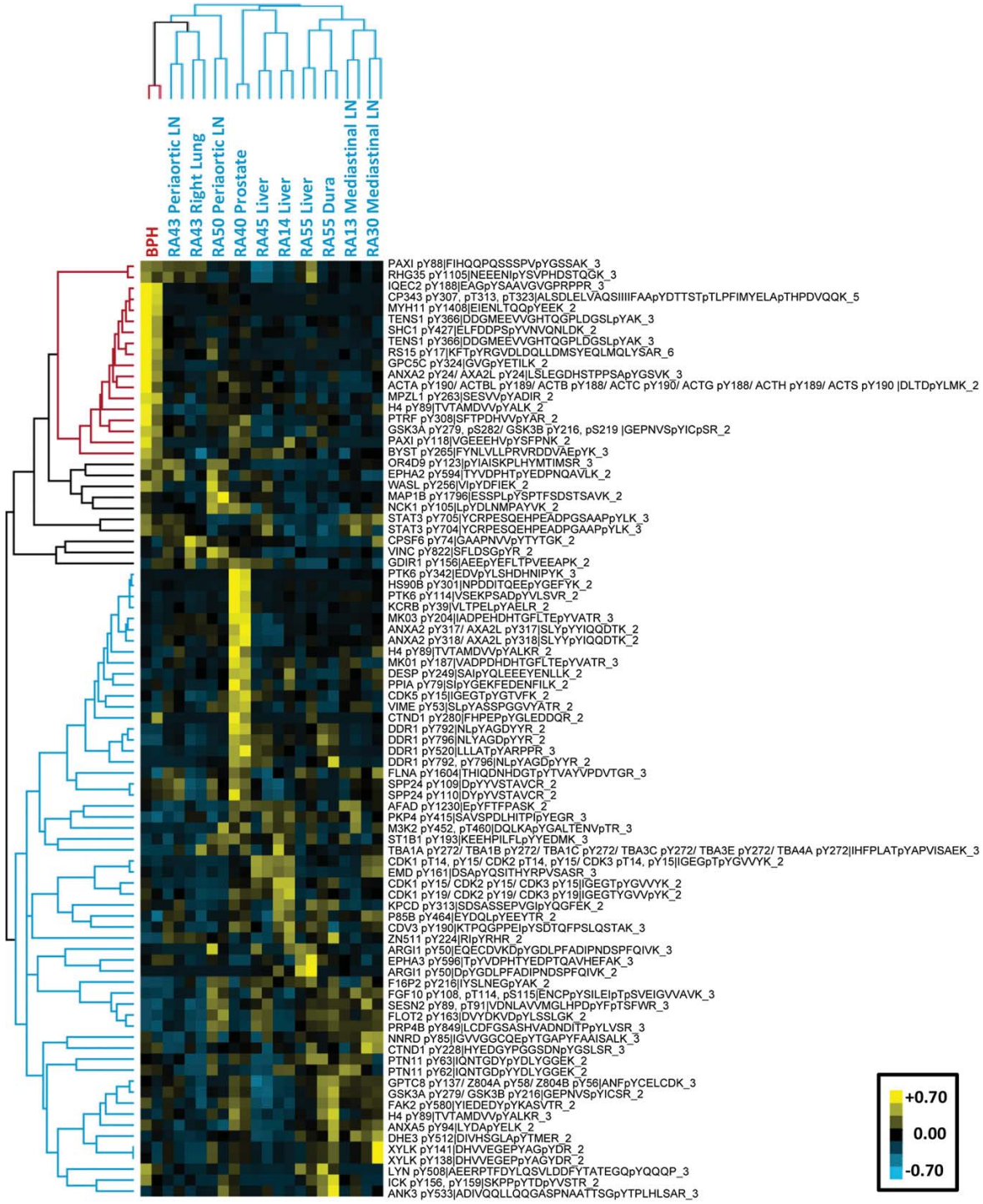

Fig. S3. Phosphoproteomic analysis exhibits both patient-specific and metastatic site-specific patterns of tyrosine kinase activation in metastatic CRPC. Unsupervised hierarchical clustering groups by organ site of metastases as well as by intrapatient metastatic lesions. Benign prostatic hyperplasia (BPH) was used as the treatment-naïve tissue for comparison. The phosphoprofiling heatmap from Fig. 2*B* with the protein and residue identities of the phosphorylation events is listed. For all heatmaps, the labels are as follows: UniProt ID, phosphosite residue number, phosphopeptide (charge state of mass spectrometry ion). If the phosphopeptide has multiple identities, a slash separates each protein and phosphorylation residue number. The vertical line separates the proteins from the phosphopeptide. Yellow, hyperphosphorylation; blue, hypophosphorylation.

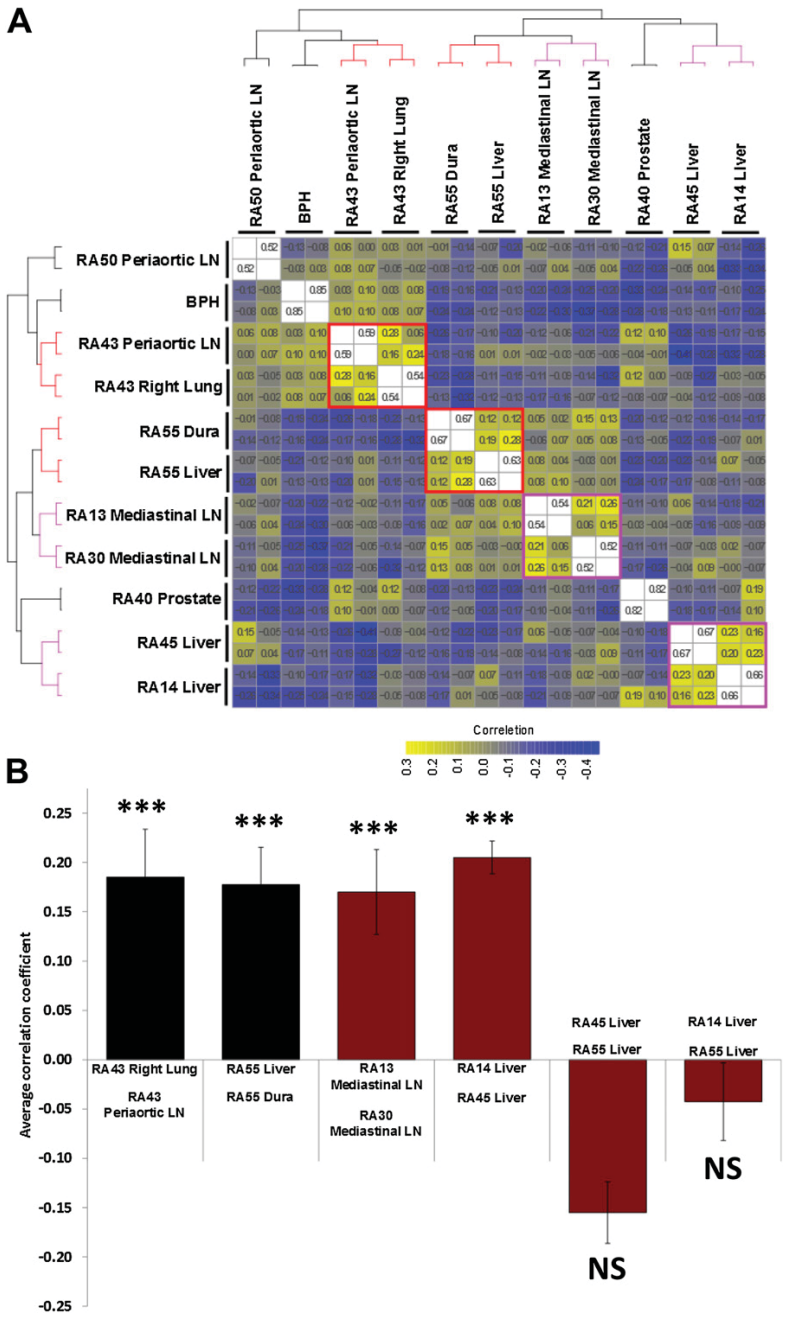

Fig. S4. Phosphoproteomic data reveal high levels of intrapatient similarity and occasional high levels of intraanatomical site similarity. (*A*) Pairwise Pearson correlation coefficients for each phosphotyrosine sample (including technical duplicates) were calculated and then clustered. The correlation coefficients are superimposed on each color-coded square. The correlation coefficients on the diagonal and the correlation coefficients for technical replicates were omitted from the color scale. (*B*) Pairwise correlation coefficients, excluding technical replicates, were averaged, and the statistical significance against the null hypothesis that the correlation was not greater than zero was calculated. Error bars are the SE. ***$P < 0.001$; NS, not significant.

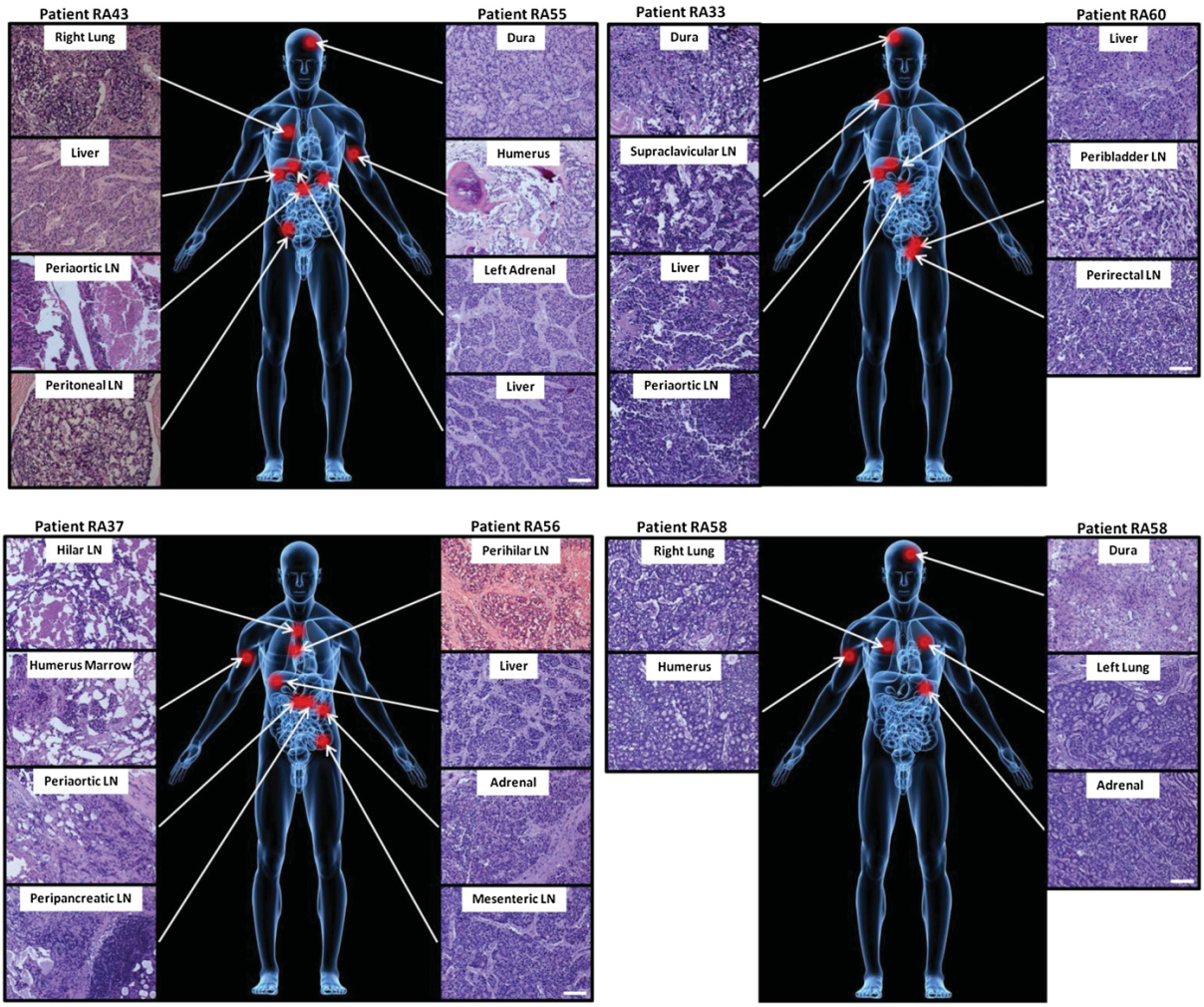

Fig. S5. Location and histological characterization of seven patients with anatomically distinct metastatic CRPC lesions. Seven separate patients' metastatic lesions are depicted with representative histology. These samples were used for western blot and phospho–receptor tyrosine kinase (RTK) and phosphokinase arrays. Red dots indicate the approximate location of the metastatic lesions analyzed. Tissues with greater than 50% tumor content were evaluated. (Scale bar, 50 μm.)

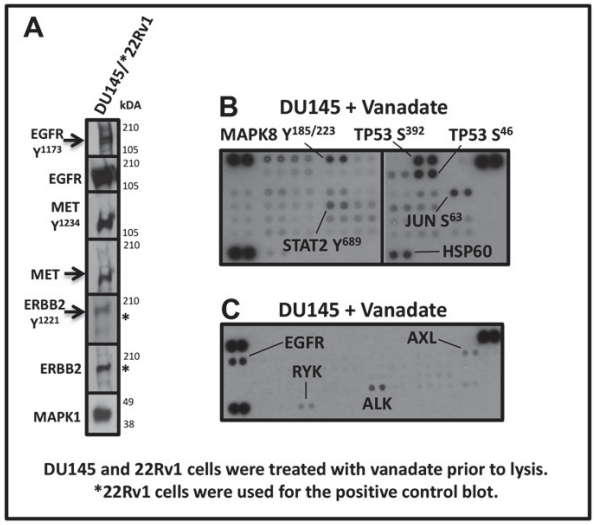

Fig. S6. Evaluation of RTK epidermal growth factor receptor (EGFR), erythroblastic leukemia viral oncogene homolog 2 (ERBB2 or HER2/neu), and hepatocyte growth factor receptor (HGFR or MET) and phospho-kinase and phospho-RTK arrays using positive control prostate cancer cell lines. Western blot analyses from DU145 or 22Rv1 cells treated with the phosphatase inhibitor, vanadate, were evaluated for the activated states of the RTKs EGFR, ERBB2, and MET (*A*); phosphokinase (*B*); or phospho-RTK arrays (*C*). DU145 or 22Rv1 (indicated by an asterisk next to the blot) cells were used as positive controls.

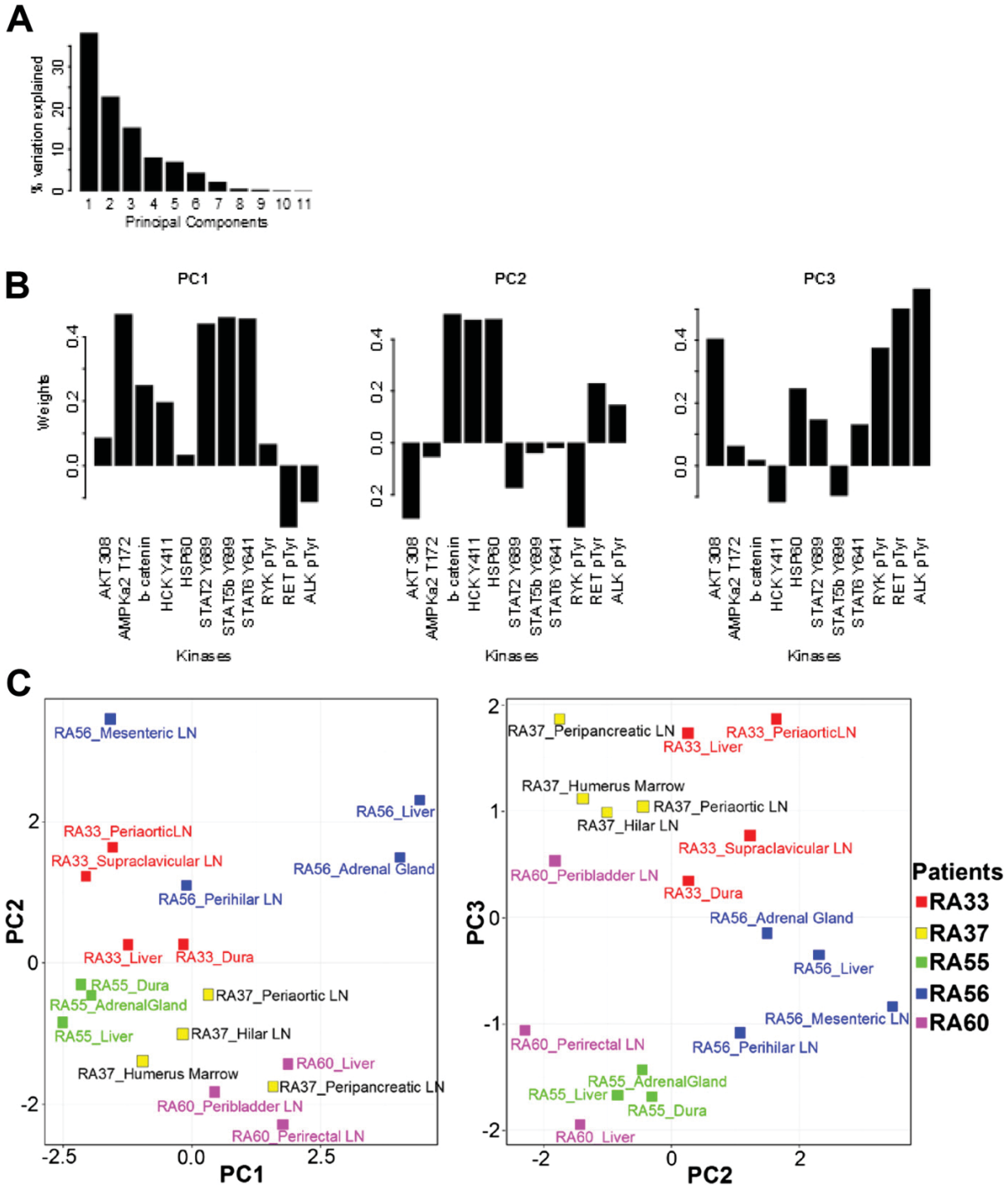

Fig. S7. Principal component (PC) analysis of phosphokinase arrays. Data from CRPC metastatic samples analyzed by phosphokinase arrays were subjected to PC analysis. After removal of antibodies with negligible signal, 11 kinases remained: AKT T^{308}, protein kinase, AMP-activated, alpha 1 catalytic subunit (PRKAA1 or AMPKa) T^{172}, β-catenin, hemopoietic cell kinase (HCK) Y^{411}, STAT2 Y^{689}, STAT5b Y^{699}, STAT6 Y^{641}, receptor-like tyrosine kinase (RYK) phosphotyrosine, rearranged during transfection (RET) phosphotyrosine, and anaplastic lymphoma kinase (ALK) phosphotyrosine. (*A*) Schematic of the loadings vectors for the first three PCs. (*B*) The percentages listed for each PC indicated the amount of variance explained by that PC. (*C*) Plots of the PC analysis for all five patients analyzed demonstrate intrapatient kinase expression similarity and individual differences.

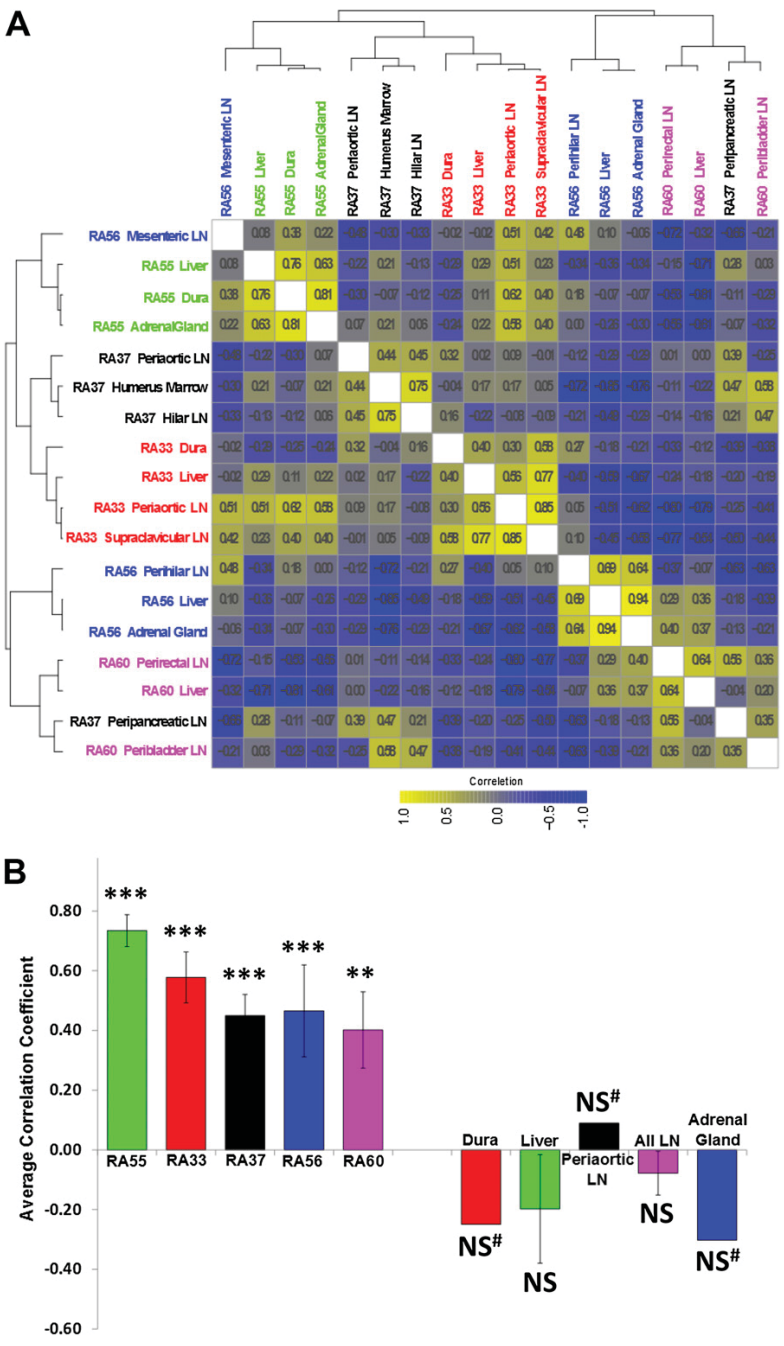

Fig. S8. Phosphokinase arrays demonstrate high levels of intrapatient but not interpatient similarity. (*A*) Pairwise Pearson correlation coefficients for each sample measured on the phosphokinase and phospho-RTK arrays were calculated and then clustered. The correlation coefficients are superimposed on each color-coded square. The correlation coefficients on the diagonal were omitted for readability. (*B*) Pairwise correlation coefficients were averaged, and the statistical significance against the null hypothesis that the correlation was not greater than zero was calculated. Error bars are the SE. Multiple *P* values were combined using Fisher's Method. ***$P < 0.001$, **$P < 0.01$; NS, not significant; #, single *P* value, not Fisher's combined.

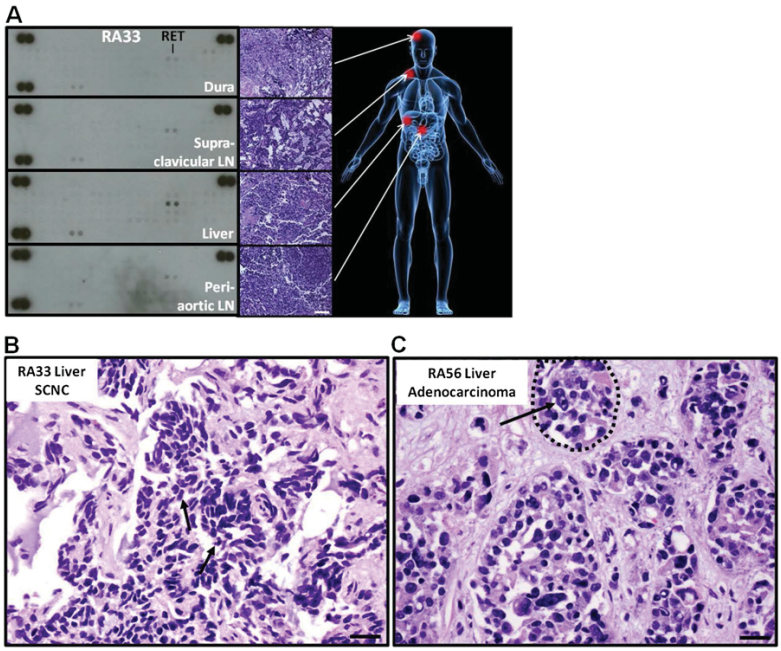

Fig. S9. Tyrosine phosphorylation of RTK RET in small cell neuroendocrine carcinoma (SCNC). (*A*) Analysis of patient RA33 using RTK arrays revealed the tyrosine phosphorylation of neuronal tyrosine kinase RET. (*B*) Metastatic tumor cells in this patient demonstrate typical nuclear morphology of SCNC including a darkly stained nucleus with a homogeneous chromatin pattern, high nuclear/cytoplasmice ratio, lack of nucleoli, and frequent mitotic figures (*B*, arrows). These characteristics are in sharp contrast to the nuclear morphology of adenocarcinoma tumor cells (*C*) that have open and vesicular chromatin patterns and prominent nuclei (*C*, arrow) and glandular formation (*C*, dashed circle). (Scale bar, 25 μm.)

Chapter 4:

N-Myc Drives Neuroendocrine Prostate Cancer Initiated from Human Prostate Epithelial Cells

Cancer Cell (2016) 29:536-47

N-Myc Drives Neuroendocrine Prostate Cancer Initiated from Human Prostate Epithelial Cells

John K. Lee,[1,2] John W. Phillips,[3] Bryan A. Smith,[3] Jung Wook Park,[3] Tanya Stoyanova,[3] Erin F. McCaffrey,[3] Robert Baertsch,[4] Artem Sokolov,[4] Justin G. Meyerowitz,[5,6,7] Colleen Mathis,[3] Donghui Cheng,[8] Joshua M. Stuart,[4] Kevan M. Shokat,[5,7,12] W. Clay Gustafson,[5,9] Jiaoti Huang,[8,10] and Owen N. Witte[3,8,11,12,*]

[1]Division of Hematology and Oncology, Department of Medicine, University of California, Los Angeles, Los Angeles, CA 90095, USA
[2]Molecular Biology Institute, University of California, Los Angeles, Los Angeles, CA 90095, USA
[3]Department of Microbiology, Immunology, and Medical Genetics, University of California, Los Angeles, Los Angeles, CA 90095, USA
[4]Center for Biomolecular Science and Engineering, Jack Baskin School of Engineering, University of California, Santa Cruz, Santa Cruz, CA 95064, USA
[5]Helen Diller Family Comprehensive Cancer Center, University of California, San Francisco, San Francisco, CA 94158, USA
[6]Departments of Neurology and Neurological Surgery, University of California, San Francisco, San Francisco, CA 94158, USA
[7]Department of Cellular and Molecular Pharmacology, University of California, San Francisco, San Francisco, CA 94158, USA
[8]Eli and Edythe Broad Center of Regenerative Medicine and Stem Cell Research, University of California, Los Angeles, Los Angeles, CA 90095, USA
[9]Department of Pediatrics, UCSF Benioff Children's Hospital, University of California, San Francisco, San Francisco, CA 94158, USA
[10]Department of Pathology and Laboratory Medicine, University of California, Los Angeles, Los Angeles, CA 90095, USA
[11]Department of Molecular and Medical Pharmacology, University of California, Los Angeles, Los Angeles, CA 90095, USA
[12]Howard Hughes Medical Institute, University of California, Los Angeles, Los Angeles, CA 90095, USA
*Correspondence: owenwitte@mednet.ucla.edu
http://dx.doi.org/10.1016/j.ccell.2016.03.001

SUMMARY

MYCN **amplification and overexpression are common in neuroendocrine prostate cancer (NEPC). However, the impact of aberrant N-Myc expression in prostate tumorigenesis and the cellular origin of NEPC have not been established. We define N-Myc and activated AKT1 as oncogenic components sufficient to transform human prostate epithelial cells to prostate adenocarcinoma and NEPC with phenotypic and molecular features of aggressive, late-stage human disease. We directly show that prostate adenocarcinoma and NEPC can arise from a common epithelial clone. Further, N-Myc is required for tumor maintenance, and destabilization of N-Myc through Aurora A kinase inhibition reduces tumor burden. Our findings establish N-Myc as a driver of NEPC and a target for therapeutic intervention.**

INTRODUCTION

Neuroendocrine prostate cancer (NEPC) makes up less than 2% of all primary prostate cancers (Helpap et al., 1999). However, treatment-related NEPC often emerges during androgen deprivation therapy for prostate adenocarcinoma, the predominant subtype of prostate cancer (Beltran et al., 2014). The term NEPC describes a heterogeneous group of neuroendocrine tumors defined morphologically that include well-differentiated carcinoid, adenocarcinoma with neuroendocrine differentiation, adenocarcinoma with Paneth cell-like neuroendocrine differentiation, mixed neuroendocrine carcinoma-acinar adenocarcinoma, and the more aggressive large-cell carcinoma and small-cell carcinoma (Epstein et al., 2014). NEPC is also distinguished from prostate adenocarcinoma by the expression of neuroendocrine differentiation markers and the loss of expression of the androgen receptor (AR) and prostate-specific antigen (Wang and Epstein, 2008). Patients with aggressive NEPC have limited treatment options and succumb to the disease within a year (Spiess et al., 2007).

Significance

Our studies underscore the functional significance of the *MYCN* oncogene in NEPC. Deregulated expression of *MYCN* combined with myristoylated *AKT1* drives the development of prostate adenocarcinoma and NEPC from human prostate epithelial cells. We present direct evidence that both tumor subtypes can be derived from a common epithelial precursor. N-Myc expression is essential to maintain the tumor state, indicating that N-Myc may be a therapeutic target in *MYCN*-amplified NEPC. Pharmacologic disruption of N-Myc by the targeted inhibition of Aurora A kinase causes a marked reduction in tumor growth. In summary, we provide insight into the pathogenesis of NEPC and the rationale for a therapeutic strategy in this deadly disease.

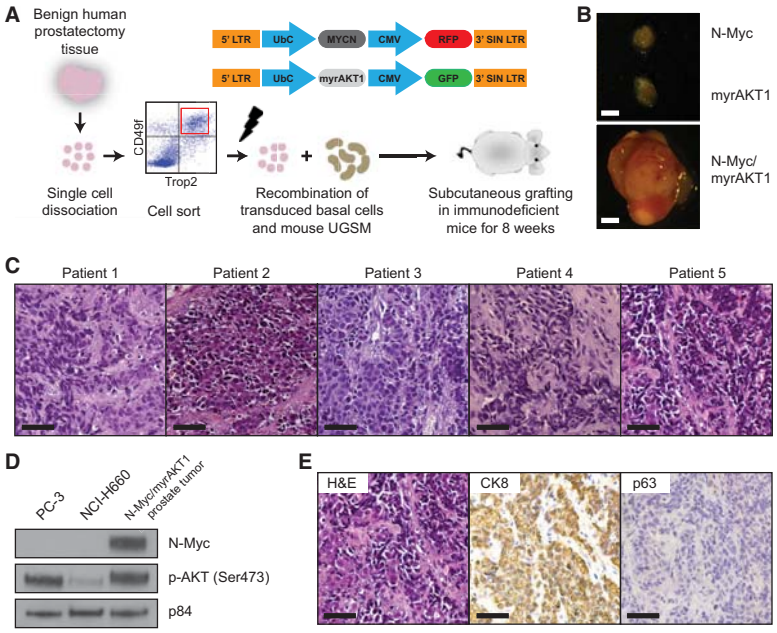

Figure 1. N-Myc and myrAKT1 Initiate NEPC from Human Prostate Basal Epithelial Cells

(A) Schematic of a human prostate regeneration and transformation assay (UbC, human ubiquitin C promoter; CMV, cytomegalovirus promoter; SIN, self-inactivating). The red square outlines the Trop2^{+}CD49f^{hi} basal epithelial cell population.

(B) Grafts transduced with N-Myc, myrAKT1, and N-Myc/myrAKT1 harvested after 8 weeks. Scale bar, 2 mm.

(C) H&E-stained sections of N-Myc/myrAKT1 tumors derived from individual patient prostatectomy samples. Scale bar, 100 μm.

(D) Immunoblot of the human NEPC cell lines PC-3 and NCI-H660 and an N-Myc/myrAKT1 tumor with antibodies against N-Myc, p-AKT (Ser473), and p84 as a loading control.

(E) H&E and immunohistochemical stains of an N-Myc/myrAKT1 tumor for CK8 and p63. Scale bar, 100 μm.

See also Figure S1 and Table S1.

Aggressive NEPC represents a lethal endpoint in the progression of prostate cancer from prostate adenocarcinoma to castration-resistant prostate cancer (CRPC) to NEPC. Neuroendocrine transdifferentiation is an adaptive mechanism of resistance to androgen withdrawal observed in vitro and in vivo (Lin et al., 2014; Shen et al., 1997). The phenotypic conversion to NEPC is associated with recurrent genetic lesions including mutation or deletion of *RB1* and *TP53* as well as the overexpression and genomic amplification of *MYCN* and *AURKA* (Beltran et al., 2011; Tan et al., 2014). NEPCs also harbor genetic abnormalities present in prostate adenocarcinomas such as *ETS* rearrangements and *PTEN* mutations (Beltran et al., 2011; Tan et al., 2014), indicating that these cancer types may arise from a common clonal origin.

Prior work has identified multipotent stem and progenitor cells within the basal epithelial compartment of the mouse and human prostate that give rise to basal, luminal, and neuroendocrine cells (Goldstein et al., 2008, 2010). Others have shown through lineage tracing studies that both basal and luminal cells in the mouse prostate can be cell types of origin of cancer (Choi et al., 2012; Wang et al., 2009). Importantly, we have demonstrated that naive basal cells in the human prostate can serve as targets of direct transformation. The overexpression of ERG and constitutively active myristoylated AKT1 (myrAKT1) initiated prostate cancer from human prostate basal cells (Goldstein et al., 2010). Loss of the tumor suppressor PTEN is found in 70% of prostate cancers and leads to the activation of AKT1, a common early event in prostate cancer tumorigenesis (Gray et al., 1998; Wu et al., 1998). Further studies showed that the deregulated expression of c-Myc and myrAKT1 in human basal cells generated prostate adenocarcinoma and squamous cell carcinoma from a common precursor (Stoyanova et al., 2013). The c-Myc/myrAKT1 human prostate cancer model highlights the potential for biphenotypic tumors to arise from divergent differentiation during tumorigenesis.

The Myc family of proto-oncogenes (*MYC*, *MYCL*, and *MYCN*) encodes a group of multi-functional transcription factors whose deregulation plays a role in the initiation and maintenance of most human cancers (Dang, 2012). *MYC* is commonly overexpressed and amplified in prostate cancer (Fleming et al., 1986; Jenkins et al., 1997). A recent study has demonstrated recurrent, focal amplification of *MYCL* in 27% of localized prostate cancers (Boutros et al., 2015). *MYCN* has been shown to be overexpressed and amplified in approximately 40% of NEPCs but only 5% of prostate adenocarcinomas (Beltran et al., 2011). Numerous studies have implicated N-Myc as a critical oncoprotein required for the development of neural and neuroendocrine tumors (Beltran, 2014). Here, we sought to evaluate the functional role of N-Myc in the initiation and maintenance of human NEPC.

RESULTS

N-Myc and myrAKT1 Overexpression in Human Prostate Basal Cells Initiates NEPC and Prostate Adenocarcinoma

To investigate whether N-Myc can initiate prostate cancer from human prostate epithelial cells, we used a tissue regeneration model of prostate cancer developed by our group (Figure 1A) (Goldstein et al., 2010; Stoyanova et al., 2013). Benign regions of prostate tissue from patients undergoing prostatectomy were dissociated to single cells. Basal epithelial cells were purified based on cell surface markers (CD45^{-}Trop2^{+}CD49f^{hi}). AKT1 was introduced as a sensitizing oncogenic event as it is frequently activated in prostate cancers including NEPCs (Figure 1D) and the overexpression of myrAKT1 initiates pre-malignant prostatic intraepithelial neoplasia in our human prostate transformation assay (Stoyanova et al., 2013). Enforced expression of N-Myc and activated AKT1 in the epithelial cells was

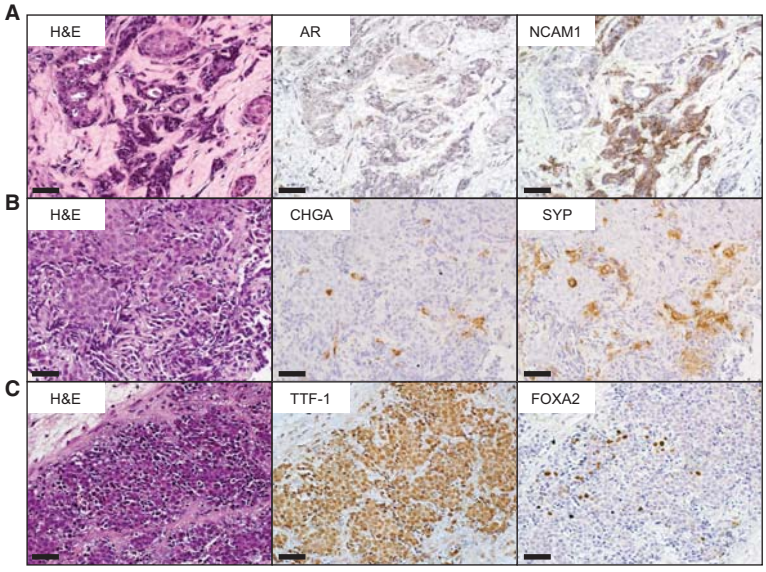

D

	AR	NCAM1	CHGA	SYP	TTF1	FOXA2
NA 1	-	+	+	+	+	+
NA 2	-	-	-	-	+	+
NA 3	-	+	-	+	-	+
NA 4	-	-	-	-	+	+
NA 5	-	+	-	-	-	+

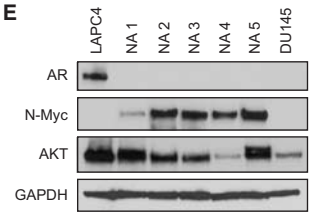

Figure 2. Prostate Tumors Initiated by N-Myc and myrAKT1 Lack AR Expression and Exhibit Neuroendocrine Markers

(A–C) Photomicrographs of N-Myc/myrAKT1 tumor sections containing regions of neuroendocrine carcinoma with H&E stains and immunohistochemical staining for AR and NCAM1, CHGA and SYP, and TTF-1 and FOXA2. Scale bar, 100 μm.

(D) Summary of the immunohistochemical staining for neuroendocrine markers in the regenerated tumors derived from five independent patient prostate samples. Positive staining represents visible staining in at least 5% of the tumor cells.

(E) Immunoblot of the AR-positive human prostate cancer cell line LNCaP, five different N-Myc/myrAKT1 (NA) tumors, and the AR-null human prostate cancer cell line DU145 with antibodies against AR, N-Myc, AKT, and GAPDH as a loading control.

achieved by lentiviral transduction. Transduced epithelial cells were mixed with mouse urogenital sinus mesenchyme (UGSM) and implanted subcutaneously in NOD-SCID-IL2Rγ^{null} (NSG) mice supplemented with testosterone.

The overexpression of N-Myc and myrAKT1 in sets of prostate basal cells from five human prostatectomy specimens (Table S1) produced tumors (Figure 1B) after 6–10 weeks with no evidence of metastatic disease. Histology of the N-Myc/myrAKT1 tumors revealed regions of high-grade adenocarcinoma and infrequent squamous cell carcinoma like the human c-Myc/myrAKT1 tumors described previously (Stoyanova et al., 2013). Some regions exhibited high nuclear-to-cytoplasmic ratio, frequent mitotic figures, and apoptotic features consistent with NEPC, including areas of small-cell prostate carcinoma (SCPC) (Figures 1C and S1A) (Wang and Epstein, 2008). Other regions of the tumors were consistent with mixed neuroendocrine carcinoma-acinar adenocarcinoma (Figure 2B). The tumors expressed N-Myc and activated AKT1 (Figure 1D), and their human origin was confirmed by immunostaining for human leukocyte antigen (HLA) class I ABC (Figure S1C). N-Myc/myrAKT1 tumors also expressed the luminal marker cytokeratin 8 (CK8) but lacked the basal marker p63 (Figure 1E), indicating loss of the basal cell layer that is a hallmark of prostate cancer.

To evaluate whether luminal prostate epithelial cells could also be transformed by N-Myc and myrAKT1, we isolated luminal cells from four benign human prostates based on cell surface markers (CD45^{-}Trop2^{+}CD49f^{low}) and transduced them in a comparable manner. Similar to prior studies (Goldstein et al., 2010; Stoyanova et al., 2013), human luminal cells did not produce tumors after oncogenic challenge (data not shown).

While the diagnosis of NEPC is usually made by the recognition of classic histologic features, assessment of neuroendocrine marker expression by immunohistochemistry (IHC) is often performed to confirm the clinical diagnosis (Epstein et al., 2014). The neuroendocrine carcinoma in the N-Myc/myrAKT1 tumors demonstrated expression of neural cell adhesion molecule 1 (NCAM1), chromogranin A (CHGA), synaptophysin (SYP), thyroid transcription factor-1 (TTF-1), and forkhead box A2 (FOXA2) (Mirosevich et al., 2006; Yao et al., 2006). We detected immunostaining of these proteins in the regions of neuroendocrine carcinoma but not of adenocarcinoma in the N-Myc/myrAKT1 tumors (Figures 2A–2C). While all tumors showed morphologic evidence of NEPC, the expression pattern of the neuroendocrine markers was heterogeneous with only one tumor expressing all five markers (Figure 2D). This heterogeneity in expression of markers is similar to what is appreciated in human NEPC specimens (Yao et al., 2006).

N-Myc/myrAKT1 Tumors Are Castration Resistant

An invariant feature of late-stage human prostate cancer including NEPC is castration-resistant proliferation. The N-Myc/myrAKT1 tumors exhibited absent AR expression by IHC (Figure 2A), by immunoblotting (Figure 2E), and by gene expression (Figure 4D). We assessed the functional dependence of N-Myc/myrAKT1 tumor growth on androgens by subcutaneously injecting the CD49f^{low} tumor cells in intact or castrate animals. Passage of CD49f^{low} cells (Stoyanova et al., 2013) from N-Myc/myrAKT1 tumors gave rise to tumors demonstrating mixed neuroendocrine carcinoma and adenocarcinoma (Figure S1B). No difference in the growth kinetics of the tumors was observed in intact and castrate hosts (Figure 3A), indicating that the N-Myc/myrAKT1 tumors are castration resistant. In contrast, the androgen-dependent human prostate cancer cell line LNCaP formed tumors

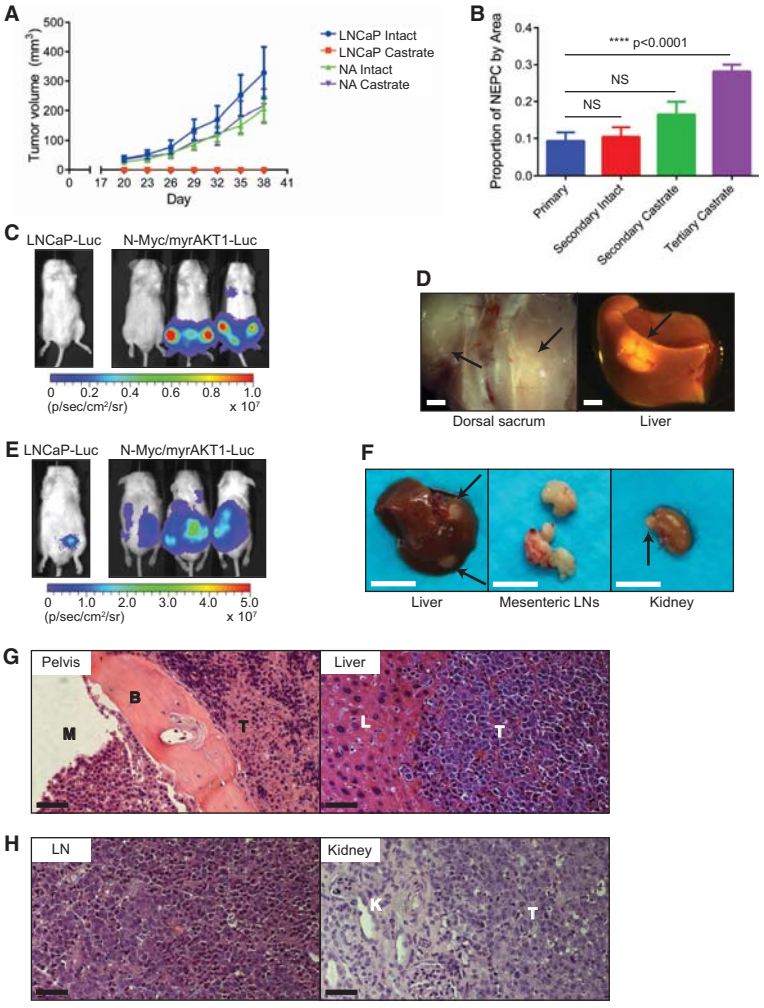

Figure 3. N-Myc/myrAKT1 Prostate Tumors Are Castration Resistant and Metastasize Widely

(A) LNCaP and transplanted N-Myc/myrAKT1 (NA) tumor volumes ± SD (n = 4 for each condition) in intact and surgically castrate mice over time.

(B) Average percentage of neuroendocrine carcinoma identified by smart image segmentation ± SEM in sections of primary, secondary, and tertiary N-Myc/myrAKT1 prostate tumors. p values were calculated from a one-way ANOVA.

(C) Bioluminescent imaging of mice 21 days after tail vein injection with the LNCaP-Luc or N-Myc/myrAKT1-Luc cell lines (signal intensity is represented by radiance, p/s/cm^2/sr).

(D) Gross tumor deposits marked by closed arrows localized to the sacrum and liver in N-Myc/myrAKT1-Luc-injected mice. Scale bar, 2 mm.

(E) Bioluminescent imaging of mice 74 days after orthotopic injection with the LNCaP-Luc or N-Myc/myrAKT1-Luc cell lines.

(F) Gross metastatic tumors marked by closed arrows involving the liver, mesenteric lymph nodes (LNs), and kidney of N-Myc/myrAKT1-Luc mice. Scale bar, 1 cm.

(G) H&E-stained sections of metastatic N-Myc/myrAKT1-Luc tumors in the pelvis and liver. M, marrow space; B, bone; L, liver; and T, tumor. Scale bar, 100 μm.

(H) H&E-stained sections of metastatic N-Myc/myrAKT1-Luc tumors in a mesenteric LN and kidney. K, kidney; T, tumor. Scale bar, 100 μm.

See also Figure S2.

in intact animals but showed no growth in castrate animals (Figure 3A).

The histology of the N-Myc/myrAKT1 tumors passaged in castrate mice also showed mixed neuroendocrine carcinoma and adenocarcinoma on a background of necrosis (Figure S1B). To quantify the relative percentage of each cancer subtype by area in the tumors, we implemented smart image segmentation to differentiate neuroendocrine carcinoma and adenocarcinoma on H&E-stained sections (Figures S2A–S2C). We noted a progressive enrichment of the neuroendocrine carcinoma within the tumor with successive passage in castrate mice, from 9% in the primary tumor to 28% in the tertiary tumor (Figure 3B). These results suggest a statistically significant but subtle competitive advantage of NEPC upon serial propagation in castrate conditions.

N-Myc/myrAKT1 Tumors Are Invasive and Metastatic

To gauge the metastatic potential of the N-Myc/myrAKT1 tumors, we first used a tail vein assay to model the invasion-metastasis cascade (Valastyan and Weinberg, 2011). As a source of tumor cells, we dissociated an N-Myc/myrAKT1 tumor to single cells and propagated them in HITES media (Carney et al., 1981). N-Myc/myrAKT1 tumor cells and the non-metastatic human prostate cancer cell line LNCaP were transduced with a lentivirus expressing firefly luciferase (Luc) to produce the N-Myc/myrAKT1-Luc and LNCaP-Luc sublines. Tumor cells were injected into the tail veins of NSG mice. Bioluminescence was detected in the hindlimbs and pelvis in two of three N-Myc/myrAKT1-Luc mice on day 21, whereas signal was absent in LNCaP-Luc mice (Figure 3C). Necropsy of the mice showed tumors involving limb bones, sacrum, and liver (Figure 3D). We did not appreciate macrometastatic disease in the lungs despite bioluminescent imaging showing localization of N-Myc/myrAKT1-Luc cells to the lungs immediately after tail vein injection (Figure S2D). However, microscopic review of lung sections revealed numerous foci of micrometastatic disease (Figure S2E).

To confirm these findings, we performed an orthotopic injection assay of metastasis, which necessitates local invasion and intravasation, in addition to metastatic processes required for the tail vein assay. N-Myc/myrAKT1-Luc or LNCaP-Luc tumor cells were implanted into the left lateral lobes of the prostates of NSG mice. Mice were sacrificed on day 74 because of

abdominal distention of the N-Myc/myrAKT1-Luc mice. Imaging prior to euthanasia revealed multiple areas of bioluminescence in three of three N-Myc/myrAKT1-Luc mice while signal was confined to the prostate in LNCaP-Luc mice (Figure 3E). Necropsy of the N-Myc/myrAKT1-Luc mice showed extensive disease in lymph nodes and vital organs including liver and kidney (Figure 3F).

The tumors from the metastasis models exhibited a mixed phenotype of neuroendocrine carcinoma and adenocarcinoma identical to the parental tumor (Figures 3G and 3H). They also retained expression of the linked fluorescent markers from the N-Myc and myrAKT1 proviruses, HLA Class I ABC, and the neuroendocrine marker FOXA2 (Figures S2F–S2G). Collectively, these findings indicate that N-Myc/myrAKT1 tumor cells are highly aggressive and proficient in the multi-step process of metastatic dissemination.

Molecular Characterization of N-Myc/myrAKT1 Tumors

We then questioned whether the N-Myc/myrAKT1 tumors demonstrated molecular properties of human NEPC. Previously, Beltran et al. (2011) analyzed seven NEPCs (five SCPCs) and 30 prostate adenocarcinomas by next-generation RNA sequencing (RNA-seq) to illustrate gene networks involving AR signaling, neuroendocrine processes, and cell-cycle regulation that distinguish these entities. To evaluate global transcriptome features in the N-Myc/myrAKT1 tumors, we harvested three N-Myc/myrAKT1 tumors, isolated regions of neuroendocrine carcinoma and adenocarcinoma from frozen sections by laser capture microdissection, and processed the specimens for RNA-seq analysis (Figure 4A).

Within each of the tumors, we identified fewer than 1,500 genes differentially expressed (>4-fold) between the neuroendocrine carcinoma and adenocarcinoma. Gene set enrichment analysis of differentially expressed genes (>4-fold) in the N-Myc/myrAKT1 tumor derived from patient 1 showed enrichment for neuronal pathways including targets of *NRSF/REST*, a master repressor of neural genes (Chong et al., 1995), in the neuroendocrine carcinoma (Figure 4B). The adenocarcinoma was enriched in stem cell-associated pathways involving *BMI1*, *SHH*, *NANOG*, and *WNT*. On the other hand, the neuroendocrine carcinoma and adenocarcinoma components of the N-Myc/myrAKT1 tumors generated from patients 2 and 4 showed differential expression (>4-fold) of only 114 and 80 genes.

We generated a weighted 50-gene predictor to identify the gene expression features that most discriminate NEPCs from prostate adenocarcinomas in the Beltran et al. (2011) dataset (Table S2). Gene ontology of this NEPC gene signature identified biological processes such as secretion, neurotransmitter transport, neuron differentiation, and glial and oligodendrocyte fate. The predictor was applied to the N-Myc/myrAKT1 tumors to derive gene signature scores that approximate their likeness to NEPC. Both the neuroendocrine carcinoma and adenocarcinoma components of the N-Myc/myrAKT1 tumors scored positively but intermediate in value to the Beltran et al. (2011) tumors (Figure 4C).

Like the NEPCs profiled by Beltran et al. (2011), both components of the N-Myc/myrAKT1 tumors showed low levels of expression of the epithelial marker *TACSTD2*, *AR*, and the androgen-regulated genes *NKX3-1*, *KLK3*, and *TMPRSS2* (Figure 4D). Consistent with our IHC results, expression of the neuroendocrine markers *CHGA*, *SYP*, *NCAM1*, and *ENO2* was heterogeneous (Figures 2D and 4D). *MYCN* was highly expressed from the integrated proviruses in the N-Myc/myrAKT1 tumors. We also identified elevated levels of the cell-cycle regulation gene *AURKA* (Beltran et al., 2011; Mosquera et al., 2013). Our gene expression analysis also demonstrated that the polycomb genes *CBX2* and *EZH2* and other recently identified NEPC epigenetic regulators (Clermont et al., 2015) are upregulated in the N-Myc/myrAKT1 tumors and the Beltran et al. (2011) NEPCs (Figure 4D). These results show that the N-Myc/myrAKT1 tumors exhibit many of the defining molecular attributes that exemplify human NEPC.

To determine whether significant genomic abnormalities occur during progression to NEPC in our model, we performed high-resolution copy number analysis on three N-Myc/myrAKT1 tumors by array comparative genomic hybridization (aCGH). Two tumors exhibited no large chromosomal anomalies while one tumor showed a gain in chromosome 7 (Figure S3 and Table S3). Copy number alterations were identified in more than one tumor but these mapped to genomic regions of copy number polymorphism based on the dbVar and DGVa databases (Table S3). These findings suggest that N-Myc and myrAKT1 drive the transformation of human prostate epithelial cells to NEPC without the need for large-scale genetic abnormalities.

We also performed whole-exome sequencing of the tumors with an average of ~70-fold coverage to evaluate for mutations acquired during tumorigenesis. We calculated a mutation rate of 3.5 per megabase which is higher than the 2.0 per megabase described in heavily treated CRPC (Grasso et al., 2012). This value may be inflated due to the lack of matched benign samples in our analysis and the dependence on SNP filters. Unique mutations were identified in *CCDC168*, *GLYAT*, *OR2W3*, *SMARCA2*, and *ZFPM1* in more than one tumor (Table S4). Loss of *SMARCA2*, a catalytic subunit of the SWI/SNF chromatin remodeling complex, promotes androgen-independent proliferation in mouse prostate epithelial cells via E2F1 (E2F transcription factor 1) deregulation (Shen et al., 2008). Our analysis did not reveal mutations in genes altered at high frequency in advanced prostate cancer such as *AR*, *TP53*, *RB1*, and *FOXA1* (Grasso et al., 2012).

Human N-Myc/myrAKT1 Prostate Cancer Cells Are Highly Tumorigenic and Demonstrate Plasticity

The propagation of N-Myc/myrAKT1 tumor cells in vitro led to the establishment of a cell line named LASCPC-01. These cells grow rapidly in suspension (doubling time ~18 hr) as floating and attached clusters reminiscent of small-cell lung cancer cell lines (Figure 5A) (Carney et al., 1981). Immunoblot analysis of LASCPC-01 cells showed expression of N-Myc and activated AKT1, AURKA, and the neuroendocrine markers ASCL1 and NSE (Figure 5B). ASCL1 is a pro-neural transcription factor expressed in NEPC (Rapa et al., 2008). Conventional karyotyping of LASCPC-01 cells showed a 46 X,Y male karyotype without chromosomal abnormalities (Figure 5C). Copy number analysis of the LASCPC-01 cell line revealed a mosaic gain of 1q23.1-1q44 (Figure S3 and Table S3).

To evaluate the capacity of N-Myc/myrAKT1 prostate cancer cells to propagate tumors, we performed a limiting dilution

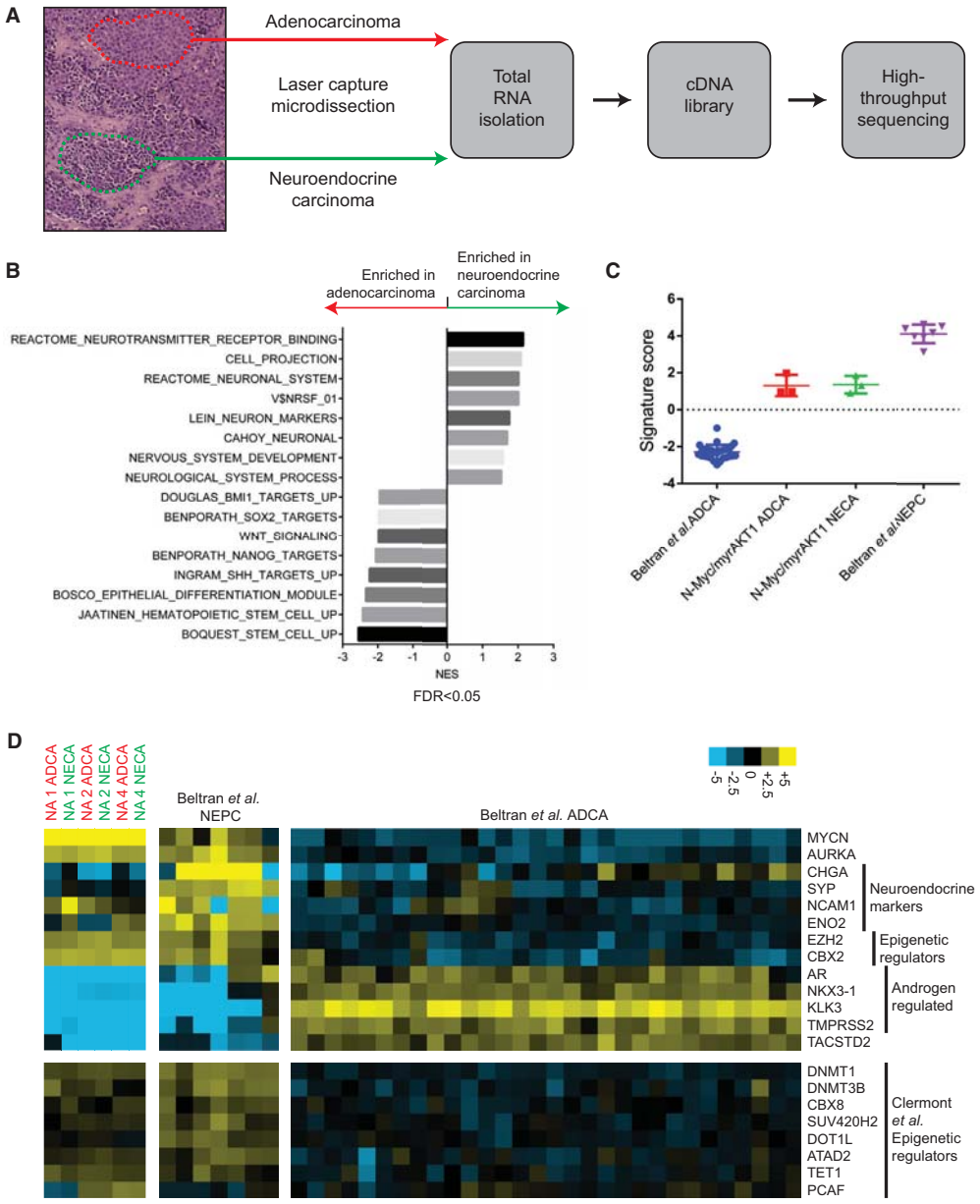

Figure 4. Transcriptome Profiling of the N-Myc/myrAKT1 Tumors Demonstrates Similarity to Human NEPC

(A) Schematic of the laser capture microdissection of matched regions of adenocarcinoma and neuroendocrine carcinoma in an N-Myc/myrAKT1 tumor and the workflow for whole-transcriptome shotgun sequencing.

(B) Gene set enrichment analysis for genes differentially expressed (>4-fold) in the adenocarcinoma or neuroendocrine carcinoma from the N-Myc/myrAKT1 tumor derived from patient 1.

(C) Neuroendocrine prostate cancer signature scores ± SD for Beltran et al. (2011) neuroendocrine prostate cancer (NEPC, n = 7), N-Myc/myrAKT1 adenocarcinoma (NA ADCA, n = 3), N-Myc/myrAKT1 neuroendocrine carcinoma (NA NECA, n = 3), and Beltran et al. (2011) adenocarcinoma (ADCA, n = 30).

(D) Heatmap of a selection of genes in NA ADCA, NA NECA, Beltran et al. (2011) NEPC, and Beltran et al. (2011) ADCA samples (contrast = $\pm 2^5$).

See also Figure S3 and Tables S2, S3, and S4.

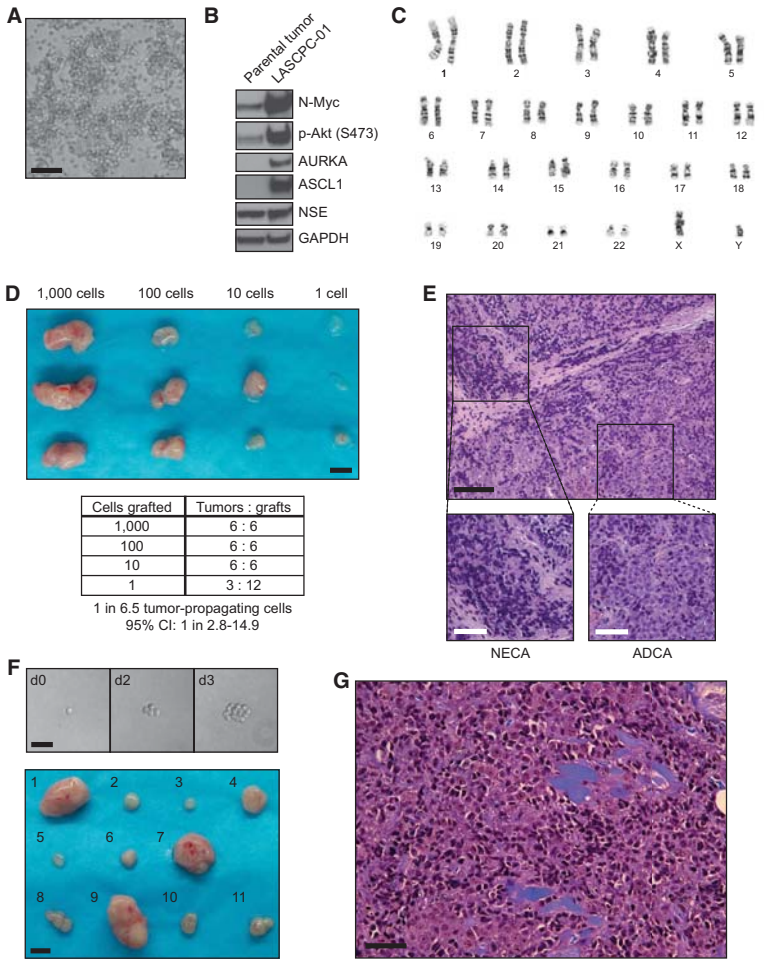

Figure 5. Establishment of a Human NEPC Cell Line LASCPC-01 with Cancer Stem Cell-like Features

(A) Photomicrograph of the LASCPC-01 cell line growing in suspension. Scale bar, 100 μm.

(B) Immunoblot analysis of the parental N-Myc/myrAKT1 tumor from which LASCPC-01 was derived and the LASCPC-01 cell line with antibodies against N-Myc, p-AKT (Ser473), AURKA, ASCL1, NSE, and GAPDH as a loading control.

(C) Conventional karyotyping of the LASCPC-01 cell.

(D) Gross tumors generated from the subcutaneous xenotransplantation of serially diluted LASCPC-01 cells after 5 weeks. Scale bar, 5 mm.

(E) Representative H&E-stained section of LASCPC-01 xenograft tumors with regions of neuroendocrine carcinoma (NECA) and adenocarcinoma (ADCA). Black scale bar, 200 μm; white scale bar, 100 μm.

(F) Top panel: photomicrographs of LASCPC-01 cells in culture after single-cell sorting, deposition, and culture. Scale bar, 50 μm. Bottom panel: gross tumors from the subcutaneous xenotransplantation of 11 clonal LASCPC-01 sublines after 4 weeks. Scale bar, 5 mm.

(G) Representative H&E-stained section of a xenograft tumor derived from a clonal LASCPC-01 subline. Scale bar, 100 μm.

See also Figure S4.

xenograft assay (Figure 5D). We estimated that 1 in 6.5 cells (95% confidence interval [CI], 2.8–14.9) exhibited tumor regenerative capacity (Hu and Smyth, 2009). In all tumors, including those from singly xenografted N-Myc/myrAKT1 tumor cells, we discovered mixed neuroendocrine carcinoma and adenocarcinoma similar to the parental N-Myc/myrAKT1 tumor (Figures 5E, S1A, and S4A). This finding suggested that a single N-Myc/myrAKT1 tumor clone could give rise to neuroendocrine carcinoma and adenocarcinoma.

To confirm this observation, we performed single-cell sorting to expand individual N-Myc/myrAKT1 tumor cell clones from the LASCPC-01 cell line (Figure 5F). Eleven clonal sublines of LASCPC-01 were subcutaneously xenografted in NSG mice and generated tumors in 4 weeks (Figure 5F). Histologic examination showed that all clonal subline xenograft tumors exhibited both neuroendocrine carcinoma and adenocarcinoma phenotypes (Figures 5G and S4B). These results indicate that N-Myc and myrAKT1 cooperate to produce cancer cells marked by high tumor-propagating potential and the capacity to generate biphenotypic prostate tumors.

N-Myc Expression Is Essential for Tumor Maintenance in N-Myc/myrAKT1 Tumors

We next questioned whether N-Myc expression is required for tumor maintenance. Studies in *MYC*-driven mouse models of osteogenic sarcoma, lymphoma, and hepatocellular carcinoma have shown that inactivation of c-Myc reverses tumorigenesis through the induction of proliferative arrest, differentiation, cellular senescence, and apoptosis (Jain et al., 2002; Wu et al., 2007). To address the question of N-Myc dependence, we used a lentivirus with doxycycline-inducible N-Myc expression and a lentivirus with constitutive myrAKT1 expression (Figure 6A) in our tissue regeneration model of prostate cancer (Figure 1A). Eight weeks after implantation of the graft in an NSG mouse supplemented with a doxycycline diet, we harvested an inducible N-Myc/myrAKT1 tumor with the same histologic features of mixed NEPC as the constitutive N-Myc/myrAKT1 tumors (Figures 6B and S1A).

While dissociated cells from the inducible N-Myc/myrAKT1 tumor propagated tumors in mice fed doxycycline, they did not form tumors in mice that were not fed doxycycline (Figure 6C). In mice that were initially supplemented with doxycycline and allowed to establish inducible N-Myc/myrAKT1 tumors, doxycycline withdrawal led to a rapid and significant regression of the tumors within 96 hr (Figure 6C). Immunoblot analysis of these tumors after doxycycline withdrawal revealed a dramatic decrease in N-Myc protein levels (Figure 6D). Further, histologic evaluation of the tumors 72 hr after doxycycline withdrawal showed significant necrosis with a remarkable decline in cellularity (Figure 6E).

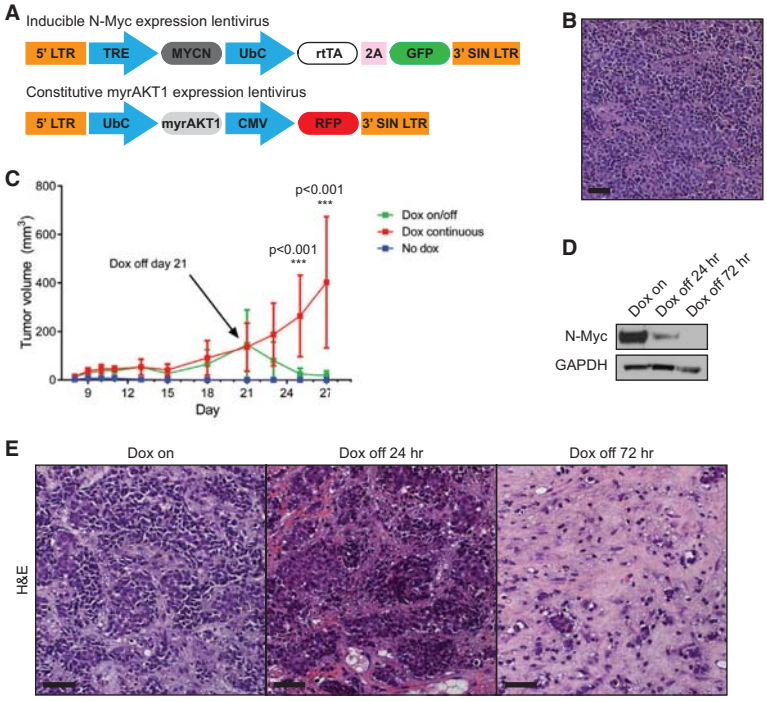

Figure 6. N-Myc Expression Is Required for Tumor Maintenance in the N-Myc/myrAKT1 Tumors

(A) Lentiviral constructs used for doxycycline-inducible expression of N-Myc and constitutive expression of myrAKT1 (TRE, tetracycline response element; rtTA, reverse tetracycline-controlled transactivator).

(B) H&E-stained section of an inducible N-Myc/myrAKT1 tumor. Scale bar, 100 μm.

(C) Average tumor volume of passaged inducible N-Myc/myrAKT1 tumors ± SD over time under conditions of no doxycycline (No dox, n = 13), continuous doxycycline (Dox continuous, n = 11), and doxycycline withdrawal on day 21 after initial doxycycline (Dox on/off, n = 11). p values were calculated from a paired t test.

(D) Immunoblot analysis of inducible N-Myc/myrAKT1 tumors after continuous doxycycline or initial doxycycline followed by withdrawal using antibodies against N-Myc and GAPDH as a loading control.

(E) Representative H&E-stained sections of inducible N-Myc/myrAKT1 tumors after continuous doxycycline and after doxycycline withdrawal. Scale bar, 100 μm.

These results demonstrate that N-Myc is necessary for tumor maintenance in our human transformation model of NEPC and suggest that N-Myc is an important therapeutic target in *MYCN*-amplified NEPC.

Pharmacologic Inhibition of N-Myc Dependence in NEPC

AURKA expression in the N-Myc/myrAKT1 tumors (Figure 4D) and LASCPC-01 cell line (Figure 5B) is consistent with the concept of a feedforward loop between N-Myc and AURKA identified in childhood neuroblastoma (Otto et al., 2009). N-Myc induces the expression of AURKA, and AURKA regulates the stability of N-Myc through a kinase-independent protein interaction with N-Myc and the Fbxw7 ubiquitin ligase that prevents N-Myc proteolysis. Treatment of *MYCN*-amplified neuroblastoma cell lines with the Aurora A kinase inhibitor MLN8237 reduced N-Myc protein levels by up to 60% and suppressed growth (Brockmann et al., 2013). MLN8237 is now being evaluated in a clinical trial for NEPC (Beltran et al., 2011). Recently, a class of conformation-disrupting (CD) AURKA inhibitors was designed and optimized to potently destabilize N-Myc (Gustafson et al., 2014). The lead compound, CD532, directly interacts with AURKA and induces a global conformational shift, disrupting the AURKA/N-Myc protein complex and promoting the degradation of N-Myc by the ubiquitin-proteasome pathway. Further, the cytotoxic activity of CD532 was evaluated in human cancer cell lines, and sensitivity to CD532 strongly correlated with amplification and expression of *MYCN*. Human prostate cancer cell lines were not tested.

We therefore sought to test CD532 in our N-Myc/myrAKT1 prostate cancer model to evaluate its therapeutic potential in NEPC. After 3 hr of treatment with CD532, LASCPC-01 cells showed a dose-dependent decline in N-Myc protein levels, inhibition of Aurora A kinase activity (phosphorylation of histone H3), and induction of cleaved PARP (Figure 7A). Diminished N-Myc protein expression was identified in LASCPC-01 cells treated with CD532 at doses of 250 nM and greater. On the other hand, treatment with the pan-Aurora kinase inhibitor VX-680 and MLN8237 did not reduce N-Myc protein levels over the same time frame (Figure 7B) and across a range of doses and time points (Figure S5A), showing differences in the ability of these AURKA inhibitors to destabilize N-Myc and inhibit Aurora A kinase activity. CD532 induced a log reduction in LASCPC-01 cell viability at 3 hr (Figure 7C) coincident with a rapid decline in N-Myc protein levels and accompanied by increased cleaved caspase-3 (Figure 7D). Cell-cycle analysis also confirmed a significantly increased sub-G1 population consistent with cell death (Figure 7E). Treatment with MLN8237 or cabazitaxel, a taxane approved for the treatment of metastatic CRPC, showed minimal early effects relative to DMSO treatment (Figures 7C and 7E).

The half-maximal effective concentration (EC_{50}) of CD532 in LASCPC-01 cells was 99.4 nM (95% CI, 81.7–120.8 nM) at 48 hr (Figure 7F). In contrast, the EC_{50} values of the LNCaP and DU145 human prostate cancer cell lines were approximately 20-fold higher (Figure S5B). These findings suggest that the inhibitory effect of CD532 is more specific for N-Myc-driven prostate cancer. To show that the ubiquitin-proteasome pathway is critical for N-Myc destabilization by CD532, LASCPC-01 cells were treated with a dose range of CD532 and the proteasomal inhibitor MG-132. MG-132 stabilized N-Myc but did not affect the inhibition of Aurora A kinase activity (Figure S5C).

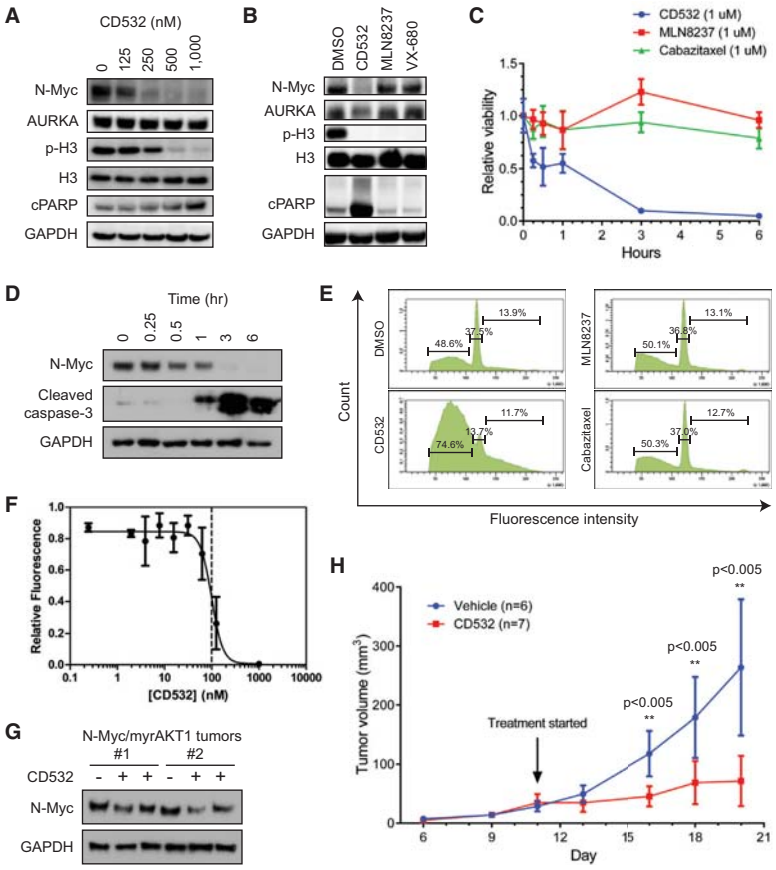

Figure 7. Therapeutic Targeting of N-Myc Dependence in the N-Myc/myrAKT1 Model of NEPC

(A) Immunoblot analysis of LASCPC-01 cells treated with a dose range of CD532 with antibodies against N-Myc, AURKA, phosphorylated histone H3 (p-H3), histone H3, cleaved PARP (cPARP), and GAPDH as a loading control.

(B) Immunoblot of LASCPC-01 treated with DMSO or 500 nM CD532, MLN8237, or VX-680 for 3 hr with antibodies against, N-Myc, AURKA, p-H3, H3, cPARP, and GAPDH as a loading control.

(C) LASCPC-01 cell viability ± SD after 3 hr of treatment with 1 μM CD532, MLN8237, or cabazitaxel relative to treatment with DMSO (n = 6 for each condition).

(D) Immunoblot of LASCPC-01 cells treated with 1 μM CD532 over a time course with antibodies against N-Myc, cleaved caspase-3, and GAPDH as a loading control.

(E) Cell-cycle analysis of LASCPC-01 cells after 3 hr of treatment with DMSO or 1 μM CD532, MLN8237, or cabazitaxel. Quantification of the sub-G1, G1, and S/G2/M fractions is shown.

(F) Dose response of CD532 ± SD (normalized to DMSO treatment only) at 48 hr using the CellTiter-Glo cell viability assay in LASCPC-01 cells.

(G) Immunoblot analysis of N-Myc/myrAKT1 tumors after treatment with vehicle or CD532 for 24 hr with antibodies against N-Myc and GAPDH as a loading control.

(H) Average tumor volume of LASCPC-01 subcutaneous xenografts ± SD with vehicle (n = 6) or CD532 (n = 7) treatment initiated on day 11. p values were calculated from a paired t test.

See also Figure S5 and Table S5.

We also assessed the human kinome interaction profile of CD532 using an active site-directed competition binding assay to characterize off-target interactions (Karaman et al., 2008). Aside from AURKA, CD532 kinase interactors include cyclin-dependent kinases like CDK2 and CDK7, KIT, FLT3, PDGFRB, RET, and FGF receptors (Figure S5D and Table S5). Inhibition of these targets may potentiate the N-Myc destabilizing effects of CD532. Relative to clinical kinase inhibitors, CD532 exhibited a favorable kinase selectivity profile comparable with crizotinib (Figure S5E).

To examine the in vivo effect of CD532, mice harboring passaged N-Myc/myrAKT1 tumors derived from two individual patient samples were treated with either vehicle or CD532 60 mg/kg daily for two doses. To confirm the on-target effect of CD532, the tumors were harvested and assayed for N-Myc expression normalized to GAPDH expression. CD532-treated tumors exhibited a 31.3% mean reduction in N-Myc protein levels relative to vehicle-treated tumors (Figure 7G). Treatment of a larger cohort of mice bearing subcutaneous LASCPC-01 xenograft tumors with CD532 25 mg/kg twice per week significantly reduced tumor burden over vehicle treatment (Figure 7H). Our results show that disruption of N-Myc stability through AURKA inhibition in *MYCN*-amplified NEPC may be a rational and promising therapeutic strategy.

DISCUSSION

Models of NEPC have been limited to human tumor xenografts with poorly defined genetic drivers and genetically engineered mouse models (i.e., TRAMP and prostate-specific conditional knockouts) that inactivate p53 and Rb (Berman-Booty and Knudsen, 2015). However, the protracted tumor latencies of these mouse models reflect the need for secondary oncogenic events to promote prostate tumorigenesis. In these systems, pinpointing the function of driver oncogenes that are activated during prostate cancer progression is challenging. We report that the deregulated expression of N-Myc and myrAKT1 in primary human prostate epithelial cells is sufficient to produce tumors with the characteristics of end-stage prostate cancer in the form of mixed NEPC and prostate adenocarcinoma. The abbreviated tumor latency and repeated observation of this phenotype in tumors derived from multiple unique human prostate samples indicate that N-Myc and activated AKT1 together are penetrant drivers of progression to NEPC.

Rapid castration-resistant proliferation and absence of AR expression are defining properties of the disease. N-Myc overexpression in the androgen-dependent LNCaP cell line has been shown to diminish AR expression levels (Beltran et al., 2011). The N-Myc/myrAKT1 tumors also showed low or absent

AR expression and demonstrated primary androgen independence. These findings suggest that the acquisition of *MYCN* gene amplification and overexpression during prostate cancer evolution may allow escape from AR dependence and promote the emergence of CRPC and NEPC. Reciprocal regulation of c-Myc and AR expression has been described in prostate cancer (Gao et al., 2013; Ni et al., 2013), but the relationship between N-Myc and AR has not been explored.

Metastatic invasion of visceral organs is largely responsible for the exceedingly poor survival of patients with aggressive NEPC. N-Myc expression correlates with invasive and metastatic behavior in neuroblastoma, and the N-Myc transcriptional program in neuroblastoma appears to regulate multiple aspects of metastasis (Huang and Weiss, 2013). While primary N-Myc/myrAKT1 tumors in the subcutaneous compartment did not demonstrate invasion or metastasis, dissociated tumor cells introduced into the tail veins or prostates of mice readily colonized bone, lymph nodes, and visceral organs. Although the microenvironment likely accounts for the absence of distant spread from the subcutaneous xenograft tumors (Stephenson et al., 1992), secondary genetic events and clonal selection during culture may have also contributed to the metastatic phenotype.

The cellular origin of NEPC has not been clearly defined. The prevailing hypothesis is that prostate adenocarcinomas undergo transdifferentiation to NEPC, especially under the selective pressure of androgen deprivation (Beltran et al., 2014; Lin et al., 2014; Shen et al., 1997). This theory is supported by genetic analyses of human prostate tumors with concurrent neuroendocrine carcinoma and adenocarcinoma where common *TP53* mutations and *TMPRSS2-ERG* rearrangements have been identified in both cancer types, suggesting a shared clonal origin (Hansel et al., 2009; Williamson et al., 2011). Our results functionally demonstrate that NEPC and prostate adenocarcinoma can both arise from a single N-Myc/myrAKT1 tumor cell clone derived from a prostate epithelial cell. Further, propagation of tumor cells in castrate conditions leads to enrichment of the NEPC over the prostate adenocarcinoma. These findings show directly an epithelial-to-neuroendocrine transition and prove that a common clone gives rise to these cancer subtypes in human prostate cancer, as has been proposed by prior studies (Beltran et al., 2014; Lin et al., 2014). Our data suggest that a subset of primary prostate adenocarcinoma with *MYCN* amplification and overexpression may acquire cancer stem cell properties that allow them to act as lurking clones capable of repopulating the tumor with NEPC after treatment. Consistent with this idea, previous work has shown that concurrent *MYCN* and *AURKA* amplification was identified in 65% of prostate adenocarcinomas from patients who later developed NEPC but in only 5% from an unselected population (Mosquera et al., 2013).

Our collective studies do not rule out the possibility that a benign neuroendocrine cell could also be a target of transformation giving rise to NEPC. In small-cell lung cancer, neuroendocrine cells and non-neuroendocrine epithelial cells have been found to be targets of transformation in a mouse model system, albeit with different efficiencies (Sutherland et al., 2011). Evaluation of this hypothesis in the human prostate with direct transformation studies is technically challenging due to the rarity of neuroendocrine cells in benign tissues and the lack of homogeneously expressed cell surface markers. In addition, we were unable to obtain outgrowths from human prostate luminal epithelial cells after introducing the oncogenes N-Myc and myrAKT1. This may reflect a limitation of our in vivo transformation assay as prior attempts to directly transform human luminal cells using this system have also been unsuccessful (Goldstein et al., 2010; Stoyanova et al., 2013). The advent of organoid cultures that enable the growth of luminal progenitor cells (Karthaus et al., 2014) may in the near future provide an opportunity to understand the functional impact of N-Myc overexpression and PI3K/AKT pathway activation in this population.

For decades, platinum-based chemotherapy has been the mainstay of treatment for aggressive human NEPC such as SCPC with dismal outcomes. In our studies, we functionally demonstrate that N-Myc drives NEPC and continuous expression of N-Myc is necessary for tumor maintenance. We propose that N-Myc is an attractive therapeutic target in this disease. Once considered impossible to target, the Myc family of oncoproteins can now be inhibited through a number of pharmacologic strategies (Dang, 2012). The positive feedback loop between N-Myc and Aurora A kinase identified in neuroblastoma (Otto et al., 2009) and NEPC (Beltran et al., 2011) provides one such opportunity. Our studies show that CD532 is highly active in our N-Myc/myrAKT1 tumor cells. CD532 potently inhibits Aurora A kinase activity and reduces N-Myc protein levels at sub-micromolar doses in vitro and substantially slows tumor growth in vivo. Based on these pre-clinical data, we believe that dual inhibition of N-Myc and Aurora A kinase warrants future clinical evaluation in patients with NEPC.

Lastly, the importance of N-Myc in the development of NEPC is highlighted by our prior contrasting finding that c-Myc combined with myrAKT1 in the same system generates adenosquamous carcinoma of the prostate but not NEPC (Stoyanova et al., 2013). The notion that Myc family members can drive distinct oncogenic differentiation pathways has been inferred from the amplification of specific Myc family members in several human cancers (Beltran, 2014). Compelling functional data in support of this idea has also come from a mouse model system in which the overexpression of *MYC* or *MYCN* combined with the loss of *TP53* in mouse cerebellar neural progenitor cells produced distinct tumors akin to two different subgroups of human medulloblastoma (Kawauchi et al., 2012). The differential regulation of Myc transcriptional programs in human cancers and the mechanisms by which N-Myc initiates a neuroendocrine transformation program in prostate cancer warrant further study.

EXPERIMENTAL PROCEDURES

Human Prostate Transformation Assay

De-identified human prostate tissues were obtained from the UCLA Translation Pathology Core Laboratory and are exempt from UCLA Institutional Review Board approval. The processing of human prostate tissue, acquisition of epithelial subpopulations, lentiviral transduction, recombination with mouse UGSM, and subcutaneous grafting in NSG mice were performed as previously described (Goldstein et al., 2010). Subcutaneous implantation of transduced human prostate epithelial cell and UGSM grafts was performed in accordance with a protocol approved by the Animal Research Committee at UCLA. Mice were obtained from The Jackson Laboratory and mouse care and husbandry were performed according to the regulations of the Division of Laboratory Animal Medicine at UCLA.

Lentiviral Constructs

The cloning of lentiviral constructs is described in the Supplemental Experimental Procedures.

Cell Lines

Information on cell lines and culture conditions are provided in the Supplemental Experimental Procedures.

Histology, Immunohistochemistry, and Immunoblotting

Protocols and antibodies used for histology, immunohistochemistry, and immunoblotting of tissues and cell lines are described in the Supplemental Experimental Procedures.

Castration-Resistance and Metastasis Assays

Protocols for castration-resistance and metastasis assays are provided in the Supplemental Experimental Procedures.

Whole-Transcriptome Sequencing Analysis

Details regarding laser capture microdissection, RNA isolation, library preparation, RNA sequencing analysis, and generation of the NEPC gene signature are described in the Supplemental Experimental Procedures.

Copy Number Variation and Whole-Exome Sequencing Analysis

Protocols for copy number variation and whole-exome sequencing analysis are presented in the Supplemental Experimental Procedures.

Serial Dilution, Clonal Subline, and N-Myc Dependence Xenograft Studies

Protocols for serial dilution, clonal subline, and N-Myc dependence xenograft studies are described in the Supplemental Experimental Procedures.

Small Molecule Inhibitors

The sources of small molecule inhibitors and protocols for in vitro and in vivo CD532 studies are provided in the Supplemental Experimental Procedures.

ACCESSION NUMBERS

The RNA-seq and aCGH data reported in this article have been deposited in NCBI GEO: GSE77624 and GSE77368.

SUPPLEMENTAL INFORMATION

Supplemental Information includes Supplemental Experimental Procedures, five figures, and five tables and can be found with this article online at http://dx.doi.org/10.1016/j.ccell.2016.03.001.

AUTHOR CONTRIBUTIONS

J.K.L. and O.N.W. conceived the project; J.K.L, J.W.P., B.A.S., J.W.P., T.S., E.F.M., and W.C.G. performed the experiments; R.B., A.S., J.G.M, J.M.S., K.M.S., W.C.G., and J.H. assisted with data interpretation; C.M. and D.C. provided technical assistance with human tissue processing; J.K.L. and O.N.W. wrote the manuscript.

ACKNOWLEDGMENTS

We thank Drs. Himisha Beltran and Mark Rubin at the Weill Medical College of Cornell University for sharing primary data from their human prostate cancer RNA-seq dataset. We thank the Translational Pathology Core Laboratory at UCLA, the California NanoSystems Institute Advanced Light Microscopy and Spectroscopy Shared Resource Facility, the UCLA Clinical Microarray Core, the High Throughput Sequencing Core at the Broad Stem Cell Research Center at UCLA, and the Clinical and Molecular Cytogenetics Laboratories at UCLA for core services. We thank the Harvard Medical School LINCS Center, which is funded by NIH grants (U54 HG006097, U54 HL127365), for use of publically available KINOME*scan* data. This research was supported by the UCLA Hal Gaba Director's Fund for Cancer Stem Cell Research. J.K.L. is supported by the Tower Cancer Research Foundation Career Development Award, a Prostate Cancer Foundation Young Investigator Award, and the UCLA Subspecialty Training and Advanced Research Program, J.W. Phillips is supported by the UCLA Tumor Cell Biology Training Grant (T32CA09056), B.A.S. is supported by the UCLA Tumor Immunology Training Grant (T32CA009120), J.W. Park is supported by a UCLA Broad Stem Cell Research Center Training Grant, and T.S. is supported by a Prostate Cancer Foundation Young Investigator Award and an NCI/NIH K99 Award (K99CA184397). W.C.G. is supported by a NIH K08 Award (K08NS079485) and the Alex's Lemonade Stand Foundation. J.H. is supported by NIH grants (5R01CA172603-02, 2P30CA016042-39, 1R01CA181242-01A1, 1R01CA195505), the Department of Defense Prostate Cancer Research Program (W81XWH-12-1-0206), UCLA SPORE in Prostate Cancer, Prostate Cancer Foundation Honorable A. David Mazzone Special Challenge Award, and UCLA Jonsson Comprehensive Cancer Center Impact Grant. K.M.S and O.N.W. are Investigators of the Howard Hughes Medical Institute. O.N.W. is supported by an NIH grant (U01 CA164188-01A) and a Prostate Cancer Foundation Challenge Award. A.S., J.M.S., K.M.S., J.H., and O.N.W. are supported by a Stand Up To Cancer/Prostate Cancer Foundation/Prostate Dream Team Translational Cancer Research Grant (SU2C-AACR-DT0812). This research grant is made possible by the generous support of the Movember Foundation. Stand Up To Cancer is a program of the Entertainment Industry Foundation administered by the American Association for Cancer Research.

Received: September 21, 2015
Revised: December 15, 2015
Accepted: March 1, 2016
Published: March 31, 2016

REFERENCES

Beltran, H. (2014). The N-myc oncogene: maximizing its targets, regulation, and therapeutic potential. Mol. Cancer Res. *12*, 815–822.

Beltran, H., Rickman, D.S., Park, K., Chae, S.S., Sboner, A., MacDonald, T.Y., Wang, Y., Sheikh, K.L., Terry, S., Tagawa, S.T., et al. (2011). Molecular characterization of neuroendocrine prostate cancer and identification of new drug targets. Cancer Discov. *1*, 487–495.

Beltran, H., Tomlins, S., Aparicio, A., Arora, V., Rickman, D., Ayala, G., Huang, J., True, L., Gleave, M.E., Soule, H., et al. (2014). Aggressive variants of castration-resistant prostate cancer. Clin. Cancer Res. *20*, 2846–2850.

Berman-Booty, L.D., and Knudsen, K.E. (2015). Models of neuroendocrine prostate cancer. Endocr. Relat. Cancer *22*, R33–R49.

Boutros, P.C., Fraser, M., Harding, N.J., de Borja, R., Trudel, D., Lalonde, E., Meng, A., Hennings-Yeomans, P.H., McPherson, A., Sabelnykova, V.Y., et al. (2015). Spatial genomic heterogeneity within localized, multifocal prostate cancer. Nat. Genet. *47*, 736–745.

Brockmann, M., Poon, E., Berry, T., Carstensen, A., Deubzer, H.E., Rycak, L., Jamin, Y., Thway, K., Robinson, S.P., Roels, F., et al. (2013). Small molecule inhibitors of aurora-a induce proteasomal degradation of N-myc in childhood neuroblastoma. Cancer Cell *24*, 75–89.

Carney, D.N., Bunn, P.A., Jr., Gazdar, A.F., Pagan, J.A., and Minna, J.D. (1981). Selective growth in serum-free hormone-supplemented medium of tumor cells obtained by biopsy from patients with small cell carcinoma of the lung. Proc. Natl. Acad. Sci. USA *78*, 3185–3189.

Choi, N., Zhang, B., Zhang, L., Ittmann, M., and Xin, L. (2012). Adult murine prostate basal and luminal cells are self-sustained lineages that can both serve as targets for prostate cancer initiation. Cancer Cell *21*, 253–265.

Chong, J.A., Tapia-Ramirez, J., Kim, S., Toledo-Aral, J.J., Zheng, Y., Boutros, M.C., Altshuller, Y.M., Frohman, M.A., Kraner, S.D., and Mandel, G. (1995). REST: a mammalian silencer protein that restricts sodium channel gene expression to neurons. Cell *80*, 949–957.

Clermont, P.L., Lin, D., Crea, F., Wu, R., Xue, H., Wang, Y., Thu, K.L., Lam, W.L., Collins, C.C., Wang, Y., et al. (2015). Polycomb-mediated silencing in neuroendocrine prostate cancer. Clin. Epigenetics *7*, 40.

Dang, C.V. (2012). MYC on the path to cancer. Cell *149*, 22–35.

Epstein, J.I., Amin, M.B., Beltran, H., Lotan, T.L., Mosquera, J.-M., Reuter, V.E., Robinson, B.D., Troncoso, P., and Rubin, M.A. (2014). Proposed

morphologic classification of prostate cancer with neuroendocrine differentiation. Am. J. Surg. Pathol. *38*, 756–767.

Fleming, W.H., Hamel, A., MacDonald, R., Ramsey, E., Pettigrew, N.M., Johnston, B., Dodd, J.G., and Matusik, R.J. (1986). Expression of the c-myc protooncogene in human prostatic carcinoma and benign prostatic hyperplasia. Cancer Res. *46*, 1535–1538.

Gao, L., Schwartzman, J., Gibbs, A., Lisac, R., Kleinschmidt, R., Wilmot, B., Bottomly, D., Coleman, I., Nelson, P., McWeeney, S., et al. (2013). Androgen receptor promotes ligand-independent prostate cancer progression through c-Myc upregulation. PLoS One *8*, e63563.

Goldstein, A.S., Lawson, D.A., Cheng, D., Sun, W., Garraway, I.P., and Witte, O.N. (2008). Trop2 identifies a subpopulation of murine and human prostate basal cells with stem cell characteristics. Proc. Natl. Acad. Sci. USA *105*, 20882–20887.

Goldstein, A.S., Huang, J., Guo, C., Garraway, I.P., and Witte, O.N. (2010). Identification of a cell of origin for human prostate cancer. Science *329*, 568–571.

Grasso, C.S., Wu, Y.M., Robinson, D.R., Cao, X., Dhanasekaran, S.M., Khan, A.P., Quist, M.J., Jing, X., Lonigro, R.J., Brenner, J.C., et al. (2012). The mutational landscape of lethal castration-resistant prostate cancer. Nature *487*, 239–243.

Gray, I.C., Stewart, L.M., Phillips, S.M., Hamilton, J.A., Gray, N.E., Watson, G.J., Spurr, N.K., and Snary, D. (1998). Mutation and expression analysis of the putative prostate tumour-suppressor gene PTEN. Br. J. Cancer *78*, 1296–1300.

Gustafson, W.C., Meyerowitz, J.G., Nekritz, E.A., Chen, J., Benes, C., Charron, E., Simonds, E.F., Seeger, R., Matthay, K.K., Hertz, N.T., et al. (2014). Drugging MYCN through an allosteric transition in Aurora kinase A. Cancer Cell *26*, 414–427.

Hansel, D.E., Nakayama, M., Luo, J., Abukhdeir, A.M., Park, B.H., Bieberich, C.J., Hicks, J.L., Eisenberger, M., Nelson, W.G., Mostwin, J.L., et al. (2009). Shared TP53 gene mutation in morphologically and phenotypically distinct concurrent primary small cell neuroendocrine carcinoma and adenocarcinoma of the prostate. Prostate *69*, 603–609.

Helpap, B., Kollermann, J., and Oehler, U. (1999). Neuroendocrine differentiation in prostatic carcinomas: histogenesis, biology, clinical relevance, and future therapeutical perspectives. Urol. Int. *62*, 133–138.

Hu, Y., and Smyth, G.K. (2009). ELDA: extreme limiting dilution analysis for comparing depleted and enriched populations in stem cell and other assays. J. Immunol. Methods *347*, 70–78.

Huang, M., and Weiss, W.A. (2013). Neuroblastoma and MYCN. Cold Spring Harbor Perspect. Med. *3*, a014415.

Jain, M., Arvanitis, C., Chu, K., Dewey, W., Leonhardt, E., Trinh, M., Sundberg, C.D., Bishop, J.M., and Felsher, D.W. (2002). Sustained loss of a neoplastic phenotype by brief inactivation of MYC. Science *297*, 102–104.

Jenkins, R.B., Qian, J., Lieber, M.M., and Bostwick, D.G. (1997). Detection of c-myc oncogene amplification and chromosomal anomalies in metastatic prostatic carcinoma by fluorescence in situ hybridization. Cancer Res. *57*, 524–531.

Karaman, M.W., Herrgard, S., Treiber, D.K., Gallant, P., Atteridge, C.E., Campbell, B.T., Chan, K.W., Ciceri, P., Davis, M.I., Edeen, P.T., et al. (2008). A quantitative analysis of kinase inhibitor selectivity. Nat. Biotechnol. *26*, 127–132.

Karthaus, W.R., Iaquinta, P.J., Drost, J., Gracanin, A., van Boxtel, R., Wongvipat, J., Dowling, C.M., Gao, D., Begthel, H., Sachs, N., et al. (2014). Identification of multipotent luminal progenitor cells in human prostate organoid cultures. Cell *159*, 163–175.

Kawauchi, D., Robinson, G., Uziel, T., Gibson, P., Rehg, J., Gao, C., Finkelstein, D., Qu, C., Pounds, S., Ellison, D.W., et al. (2012). A mouse model of the most aggressive subgroup of human medulloblastoma. Cancer Cell *21*, 168–180.

Lin, D., Wyatt, A.W., Xue, H., Wang, Y., Dong, X., Haegert, A., Wu, R., Brahmbhatt, S., Mo, F., Jong, L., et al. (2014). High fidelity patient-derived xenografts for accelerating prostate cancer discovery and drug development. Cancer Res. *74*, 1272–1283.

Mirosevich, J., Gao, N., Gupta, A., Shappell, S.B., Jove, R., and Matusik, R.J. (2006). Expression and role of Foxa proteins in prostate cancer. Prostate *66*, 1013–1028.

Mosquera, J.M., Beltran, H., Park, K., MacDonald, T.Y., Robinson, B.D., Tagawa, S.T., Perner, S., Bismar, T.A., Erbersdobler, A., Dhir, R., et al. (2013). Concurrent AURKA and MYCN gene amplifications are harbingers of lethal treatment-related neuroendocrine prostate cancer. Neoplasia *15*, 1–10.

Ni, M., Chen, Y., Fei, T., Li, D., Lim, E., Liu, X.S., and Brown, M. (2013). Amplitude modulation of androgen signaling by c-MYC. Genes Dev. *27*, 734–748.

Otto, T., Horn, S., Brockmann, M., Eilers, U., Schuttrumpf, L., Popov, N., Kenney, A.M., Schulte, J.H., Beijersbergen, R., Christiansen, H., et al. (2009). Stabilization of N-Myc is a critical function of Aurora A in human neuroblastoma. Cancer Cell *15*, 67–78.

Rapa, I., Ceppi, P., Bollito, E., Rosas, R., Cappia, S., Bacillo, E., Porpiglia, F., Berruti, A., Papotti, M., and Volante, M. (2008). Human ASH1 expression in prostate cancer with neuroendocrine differentiation. Mod. Pathol. *21*, 700–707.

Shen, R., Dorai, T., Szaboles, M., Katz, A.E., Olsson, C.A., and Buttyan, R. (1997). Transdifferentiation of cultured human prostate cancer cells to a neuroendocrine cell phenotype in a hormone-depleted medium. Urol. Oncol. *3*, 67–75.

Shen, H., Powers, N., Saini, N., Comstock, C.E., Sharma, A., Weaver, K., Revelo, M.P., Gerald, W., Williams, E., Jessen, W.J., et al. (2008). The SWI/SNF ATPase Brm is a gatekeeper of proliferative control in prostate cancer. Cancer Res. *68*, 10154–10162.

Spiess, P.E., Pettaway, C.A., Vakar-Lopez, F., Kassouf, W., Wang, X., Busby, J.E., Do, K.A., Davuluri, R., and Tannir, N.M. (2007). Treatment outcomes of small cell carcinoma of the prostate: a single-center study. Cancer *110*, 1729–1737.

Stephenson, R.A., Dinney, C.P., Gohji, K., Ordonez, N.G., Killion, J.J., and Fidler, I.J. (1992). Metastatic model for human prostate cancer using orthotopic implantation in nude mice. J. Natl. Cancer Inst. *84*, 951–957.

Stoyanova, T., Cooper, A.R., Drake, J.M., Liu, X., Armstrong, A.J., Pienta, K.J., Zhang, H., Kohn, D.B., Huang, J., Witte, O.N., et al. (2013). Prostate cancer originating in basal cells progresses to adenocarcinoma propagated by luminal-like cells. Proc. Natl. Acad. Sci. USA *110*, 20111–20116.

Sutherland, K.D., Proost, N., Brouns, I., Adriaensen, D., Song, J.Y., and Berns, A. (2011). Cell of origin of small cell lung cancer: inactivation of Trp53 and Rb1 in distinct cell types of adult mouse lung. Cancer Cell *19*, 754–764.

Tan, H.L., Sood, A., Rahimi, H.A., Wang, W., Gupta, N., Hicks, J., Mosier, S., Gocke, C.D., Epstein, J.I., Netto, G.J., et al. (2014). Rb loss is characteristic of prostatic small cell neuroendocrine carcinoma. Clin. Cancer Res. *20*, 890–903.

Valastyan, S., and Weinberg, R.A. (2011). Tumor metastasis: molecular insights and evolving paradigms. Cell *147*, 275–292.

Wang, W., and Epstein, J.I. (2008). Small cell carcinoma of the prostate. A morphologic and immunohistochemical study of 95 cases. Am. J. Surg. Pathol. *32*, 65–71.

Wang, X., Julio, M.K.-d., Economides, K.D., Walker, D., Yu, H., Halili, M.V., Hu, Y.-P., Price, S.M., Abate-Shen, C., and Shen, M.M. (2009). A luminal epithelial stem cell that is a cell of origin for prostate cancer. Nature *461*, 495–500.

Williamson, S.R., Zhang, S., Yao, J.L., Huang, J., Lopez-Beltran, A., Shen, S., Osunkoya, A.O., MacLennan, G.T., Montironi, R., and Cheng, L. (2011). ERG-TMPRSS2 rearrangement is shared by concurrent prostatic adenocarcinoma and prostatic small cell carcinoma and absent in small cell carcinoma of the urinary bladder: evidence supporting monoclonal origin. Mod. Pathol. *24*, 1120–1127.

Wu, X., Senechal, K., Neshat, M.S., Whang, Y.E., and Sawyers, C.L. (1998). The PTEN/MMAC1 tumor suppressor phosphatase functions as a negative regulator of the phosphoinositide 3-kinase/Akt pathway. Proc. Natl. Acad. Sci. USA *95*, 15587–15591.

Wu, C.H., van Riggelen, J., Yetil, A., Fan, A.C., Bachireddy, P., and Felsher, D.W. (2007). Cellular senescence is an important mechanism of tumor regression upon c-Myc inactivation. Proc. Natl. Acad. Sci. USA *104*, 13028–13033.

Yao, J.L., Madeb, R., Bourne, P., Lei, J., Yang, X., Tickoo, S., Liu, Z., Tan, D., Cheng, L., Hatem, F., et al. (2006). Small cell carcinoma of the prostate: an immunohistochemical study. Am. J. Surg. Pathol. *30*, 705–712.

Supplemental Information

N-Myc Drives Neuroendocrine Prostate Cancer Initiated from Human Prostate Epithelial Cells

John K. Lee, John W. Phillips, Bryan A. Smith, Jung Wook Park, Tanya Stoyanova, Erin F. McCaffrey, Robert Baertsch, Artem Sokolov, Justin G. Meyerowitz, Colleen Mathis, Donghui Cheng, Joshua M. Stuart, Kevan M. Shokat, W. Clay Gustafson, Jiaoti Huang, and Owen N. Witte

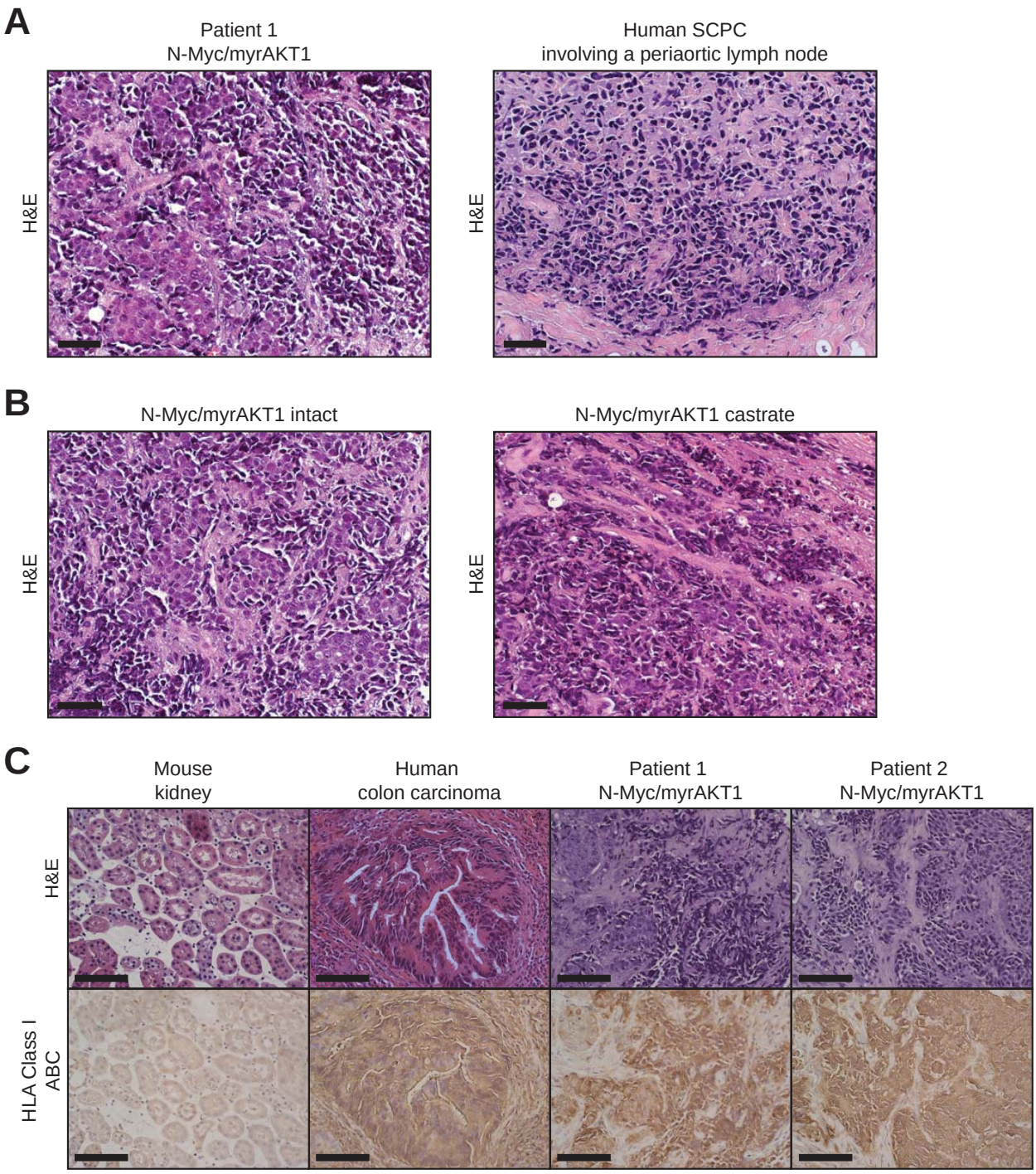

Figure S1, related to Figure 1. N-Myc/myrAKT1 prostate tumors demonstrate histologic features of human small cell prostate carcinoma and are of a human cellular origin. (A) H&E-stained sections obtained from an N-Myc/myrAKT1 tumor and an extensive stage human small cell prostate carcinoma specimen from a periaortic lymph node (scale bar=100 μm). (B) H&E-stained sections of N-Myc/myrAKT1 transplanted tumors from intact and castrate conditions (scale bar=100 μm). (C) H&E and HLA Class I ABC stains of mouse kidney, human colon carcinoma, and N-Myc/myrAKT1 tumors generated from two different patient samples (scale bar=100 μm).

Table S1, related to Figure 1. Characteristics of human prostate specimens.

Patient	Age Range	Race	Diagnosis	Gleason Score (Tumor Size)	Pre-operative PSA
1	65-70	White	Prostatic adenocarcinoma	3+3=6 (N/A)	7.4
2	75-80	White	Prostatic adenocarcinoma	Focus 1: 4+5=9 (1.2 cm) Focus 2: 4+3=7 (1.1 cm) Focus 3: 3+3=6 (0.1 cm) Focus 4: 3+3=6 (0.1 cm)	<0.01
3	60-65	White	Prostatic adenocarcinoma	Focus 1: 3+4=7 with tertiary 5 (3.2 cm) Focus 2: 3+3=6 (0.25 cm)	9.4
4	60-65	White	Benign prostate gland	N/A (N/A)	N/A
5	65-70	White	Prostatic adenocarcinoma	3+4=7 (1.5 cm)	N/A
6	60-65	White	Prostatic adenocarcinoma	3+4=7 (N/A)	3.4

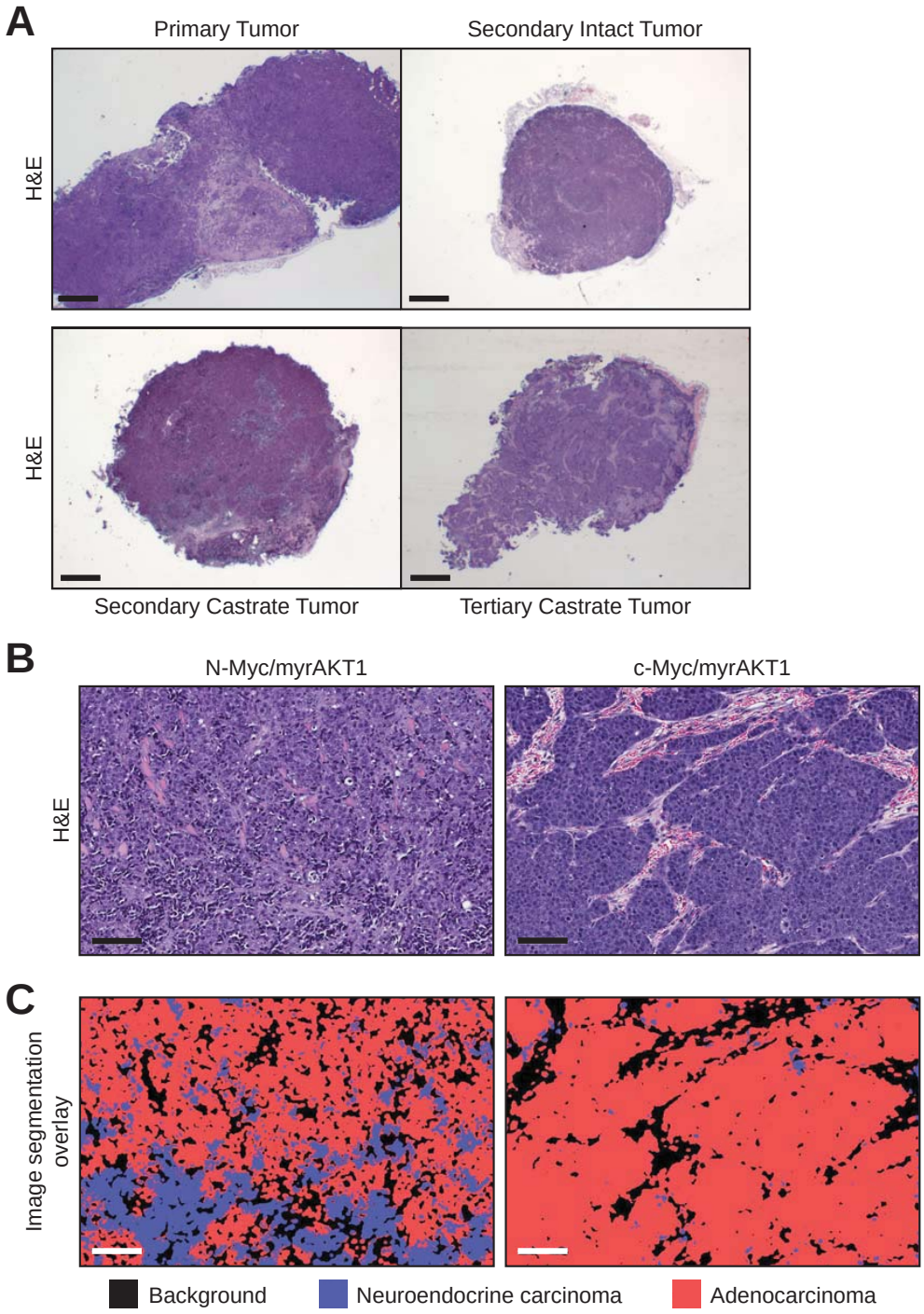
A
Primary Tumor
Secondary Intact Tumor
H&E
H&E
Secondary Castrate Tumor
Tertiary Castrate Tumor
B
N-Myc/myrAKT1
c-Myc/myrAKT1
H&E
C
Image segmentation overlay
Background
Neuroendocrine carcinoma
Adenocarcinoma

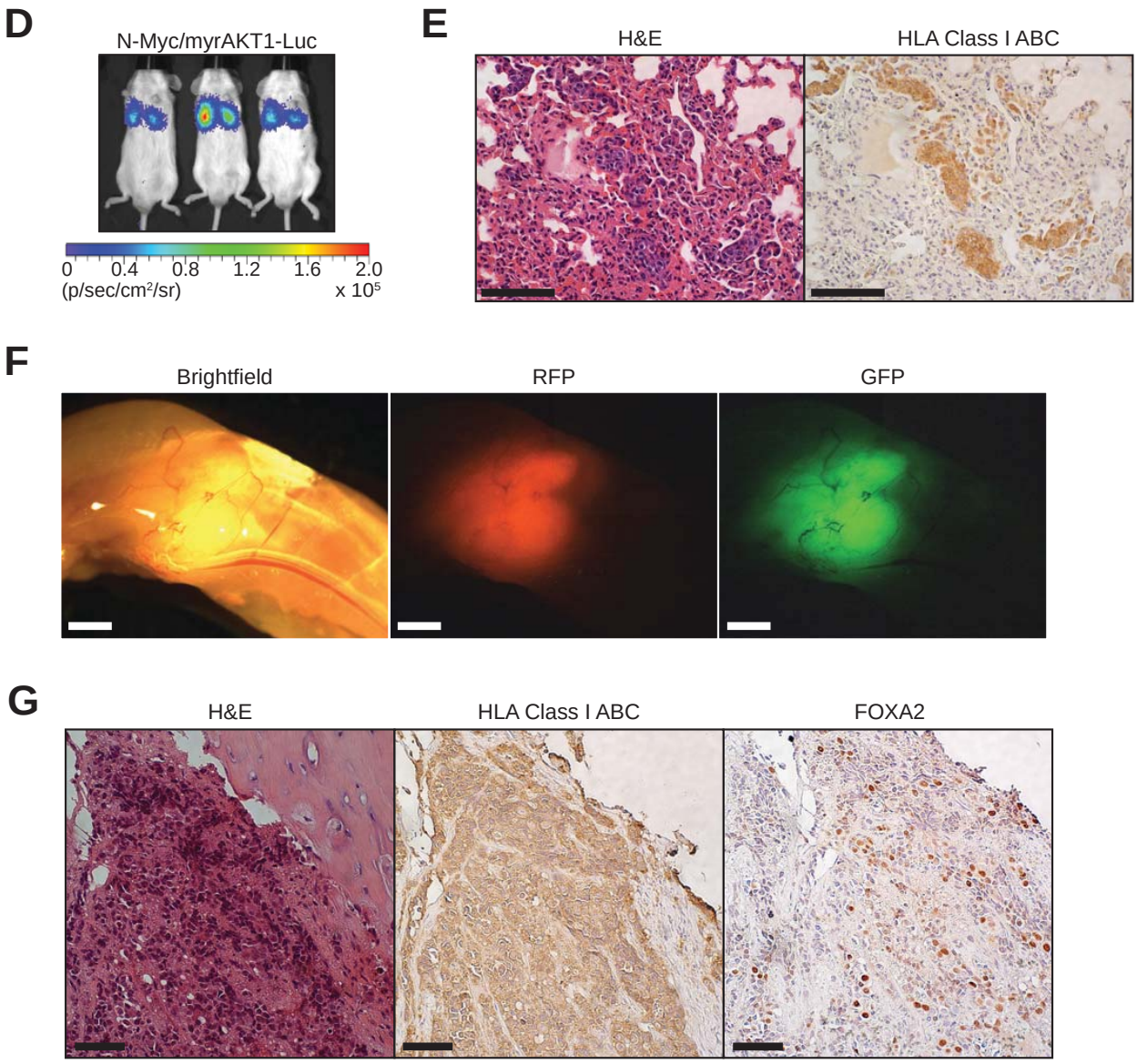

Figure S2, related to Figure 3. N-Myc/myrAKT1 prostate tumors are enriched for NEPC after castration and demonstrate widespread metastases marked by HLA Class I ABC and neuroendocrine marker FOXA2 expression. (A) H&E-stained sections of primary, secondary, and tertiary N-Myc/myrAKT1 prostate tumors at low magnification (scale bar=800 μm). (B) Representative H&E-stained sections of N-Myc/myrAKT1 and c-Myc/myrAKT1 tumors (scale bar=100 μm). (C) Image segmentation overlay of the photomicrographs in (B) with features characterized as background (black), neuroendocrine carcinoma (blue), and adenocarcinoma (red) (scale bar=100 μm). (D) Bioluminescent imaging of mice immediately post-tail vein injection with the N-Myc/myrAKT1-Luc cell line (signal intensity is represented by radiance, p/sec/cm2/sr). (E) H&E and HLA Class I ABC immunostaining of lung sections from mice 21 days after tail vein injection with the N-Myc/myrAKT1-Luc cell line (scale bar=100 μm). (F) Brightfield, red fluorescent, and green fluorescent images of a hind limb from an N-Myc/myrAKT1-Luc mouse bearing a tumor deposit (scale bar=2 mm). (G) H&E, HLA Class I ABC, and FOXA2 immunostaining of tissue sections from metastatic N-Myc/myrAKT1-Luc tumors involving the femur (scale bar=100 μm).

Table S2, related to Figure 4. Weighted 50-gene NEPC signature.

Gene	Weight
CPLX2	0.054237
ACTL6B	0.0397921
CA9	0.0390316
MYT1	0.0355834
UNC13A	0.0326315
TNNT1	0.0318484
DPYSL5	0.0293946
LRTM2	0.0273999
SYT4	0.0254472
XKR7	0.0234302
CHRNB2	0.0211502
SRRM4	0.0206361
ATP1A3	0.0193364
CDK5R2	0.0151874
FAM123C	0.0147568
MARCH4	0.0104644
RTBDN	0.0091143
RUNDC3A	0.0084861
GRM4	0.008138
VGF	0.0080349
NKX2-2	0.0065812
SEZ6	0.0065713
ASCL1	0.0060928
SCRT1	0.005412
HMP19	0.003171
LHX2	0.0025981
MAST1	0.0025208
SYT5	7.45E-05

Gene	Weight
POTEH	-0.001174
ANO7	-0.001527
AZGP1	-0.00187
OR51E2	-0.002243
TARP	-0.004231
SRD5A2	-0.004461
ALOX15B	-0.004484
POTEG	-0.005139
ACPP	-0.005406
GDEP	-0.006899
PAGE4	-0.00748
P704P	-0.007655
ACSM1	-0.009399
DES	-0.009427
KLK2	-0.014421
C15orf21	-0.015193
MSMB	-0.016603
PCGEM1	-0.018376
NPY	-0.024701
PCA3	-0.027402
KLK3	-0.034047
MYBPC1	-0.036665

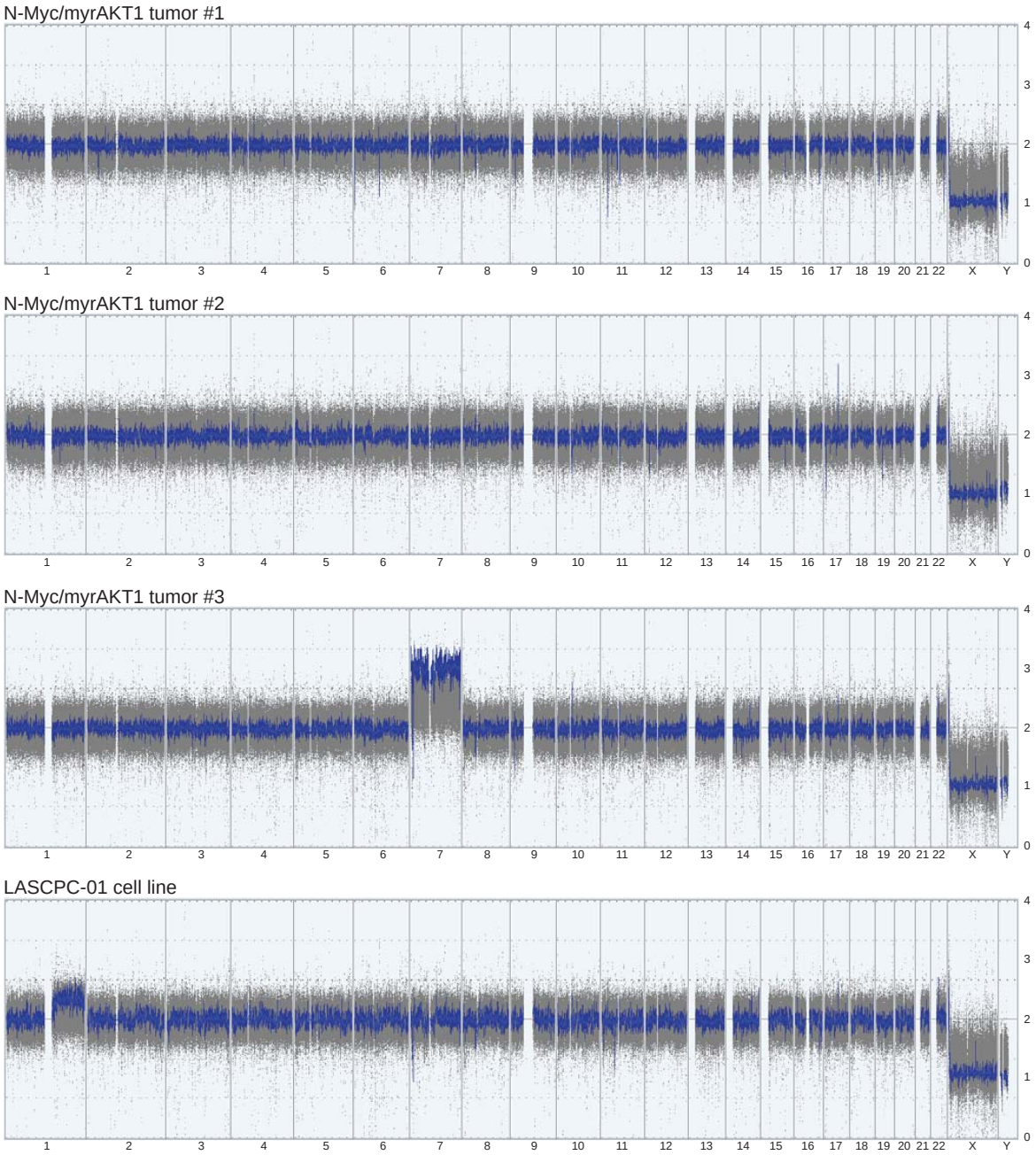

Figure S3, related to Figure 4. N-Myc/myrAKT1 tumors and the LASCPC-01 cell line exhibit few chromosomal abnormalities. Whole genome array CGH plots showing chromosomal location and copy number of three N-Myc/myrAKT1 tumors and the LASCPC-01 cell line analyzed using the high-resolution Affymetrix CytoScan HD platform (blue line represents the smoothed copy number profile).

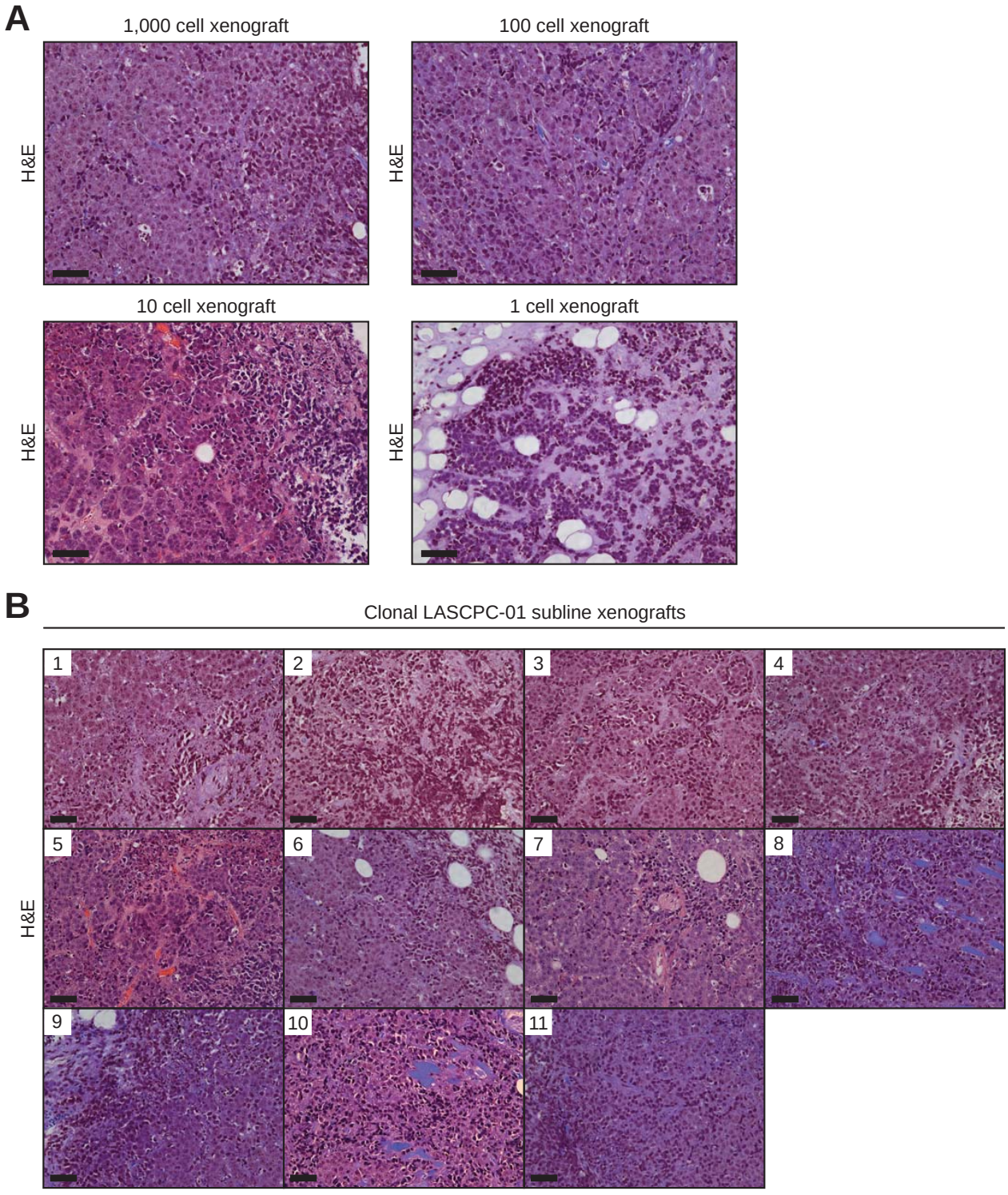

Figure S4, related to Figure 5. N-Myc/myrAKT1 tumor cells are highly tumorigenic and demonstrate plasticity. (A) H&E-stained sections of xenograft tumors derived from the implantation of 1,000, 100, 10, or 1 LASPC-01 tumor cell. (B) H&E-stained sections of xenograft tumors from each of eleven clonal LASCPC-01 sublines demonstrating mixed neuroendocrine carcinoma and adenocarcinoma.

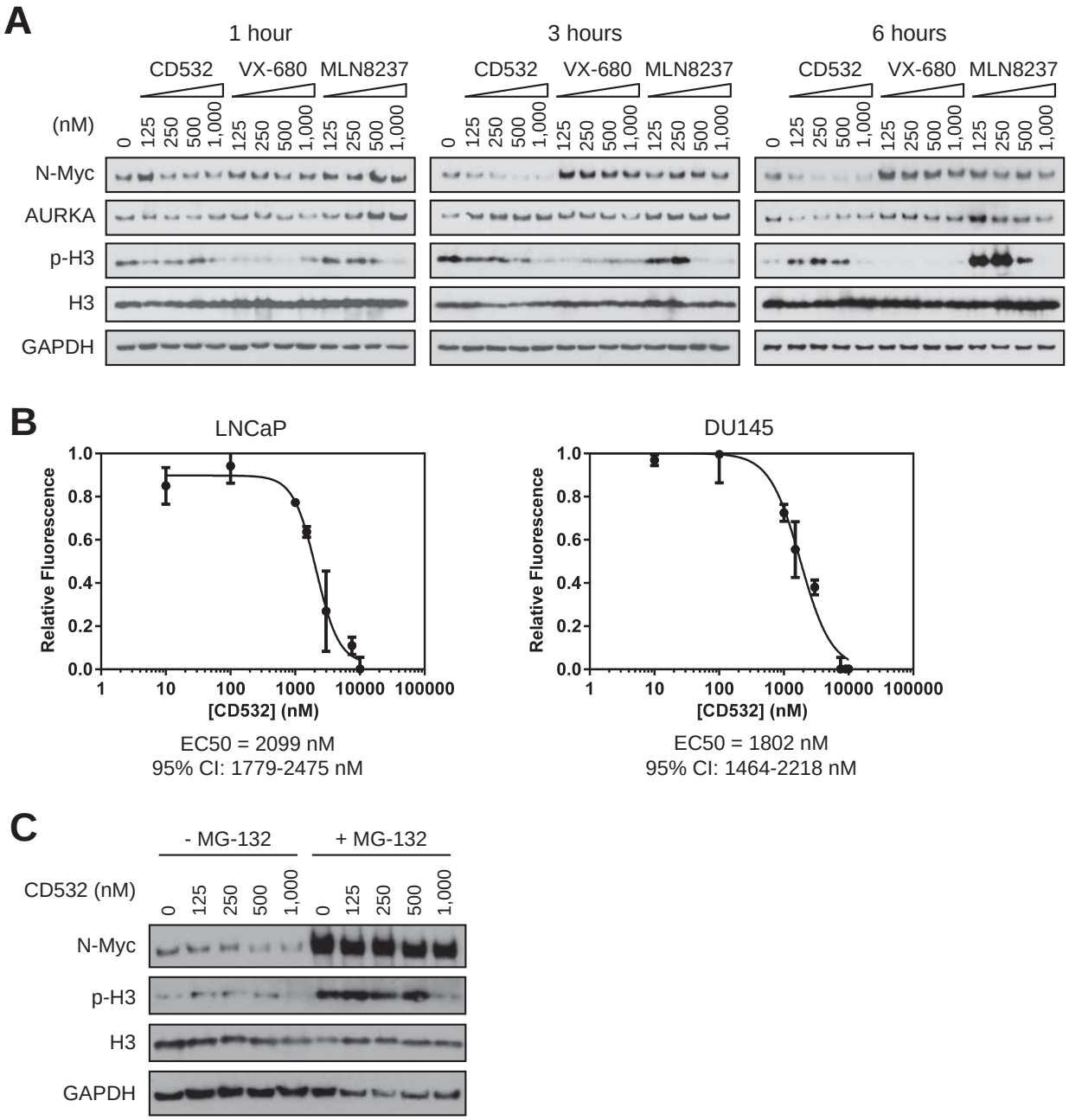
A
1 hour
3 hours
6 hours
CD532
VX-680
MLN8237
(nM)
0
125
250
500
1,000
N-Myc
AURKA
p-H3
H3
GAPDH
B
LNCaP
DU145
Relative Fluorescence
[CD532] (nM)
EC50 = 2099 nM
95% CI: 1779-2475 nM
EC50 = 1802 nM
95% CI: 1464-2218 nM
C
- MG-132
+ MG-132
CD532 (nM)
N-Myc
p-H3
H3
GAPDH

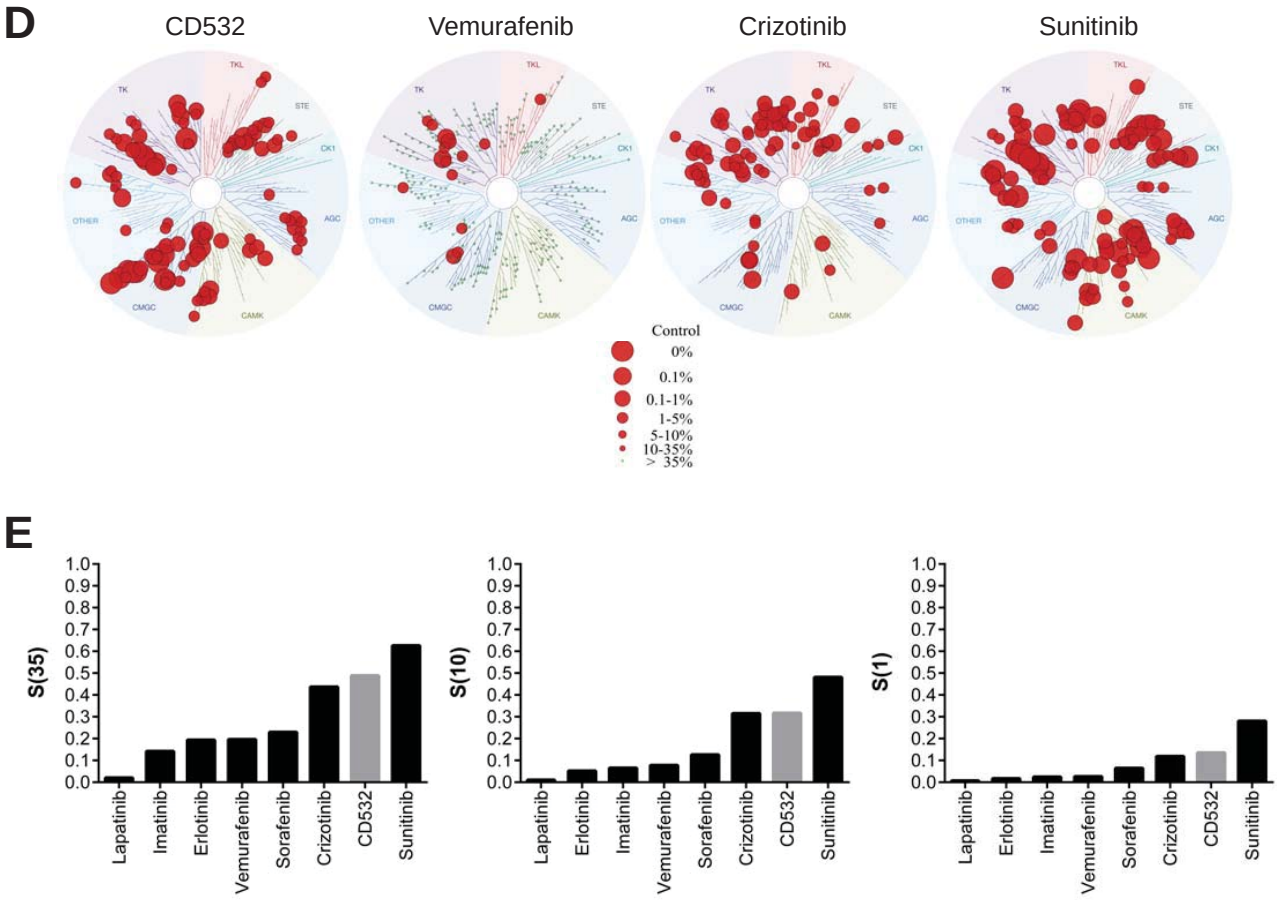

Figure S5, related to Figure 7. On-target effects of CD532 on N-Myc destabilization and Aurora A kinase inhibition and kinase selectivity of CD532. (A) Immunoblot analysis of LASCPC-01 cells treated with the indicated inhibitors and doses for the indicated periods of time with antibodies against N-Myc, AURKA, phosphorylated histone H3 (p-H3), histone H3, and GAPDH as a loading control. (B) Dose response of CD532 +/- SD (normalized to DMSO treatment only) at 48 hours using the CellTiter-Glo cell viability assay in LNCaP cells and DU145 cells. (C) Immunoblot analysis of LASCPC-01 cells treated with increasing concentrations of CD532 for 3 hours in the presence or absence of 10 μM MG-132 pre-treated for 3 hours. (D) Small molecule kinase interaction map for CD532 after screening a panel of >400 human kinases at a dose of 10 μM using the DiscoveRx KINOME*scan* platform. Also shown are maps for vemurafenib, crizotinib, and sunitinib generated from Karaman *et al.* (Nature Biotechnology, 2008) and publically available data from the Harvard Medical School LINCS Center. Red circles represent small molecule-kinase interactions and the size of the circles indicates relative binding, represented as percent of control [(test compound signal - positive control signal)/(negative control signal - positive control signal) x 100]. (E) Selectivity scores of kinase inhibitors for binding interactions with S_{35} or S_{10} or S_1 [(number of non-mutated kinases with percent of control <35 or <10 or <1)/(number of non-mutated kinases tested)].

SUPPLEMENTAL EXPERIMENTAL PROCEDURES

Lentiviral Constructs

The myrAKT1 lentiviral vector has been described previously (Xin et al., 2005). The N-Myc lentiviral vector was cloned by PCR amplification of pMXs-hu-N-Myc (Plasmid 50772, Addgene) with the forward primer 5'-AGTTCTAGAACCATGCCGAGCTGCTCCACG-3' and reverse primer 5'-AGTGA ATTCTTAGCAAGTCCGAGCGTGTTC-3'. The PCR product was cloned into pCR2.1-TOPO using the TOPO TA Cloning Kit (Life Technologies). The *MYCN* insert was then released by digestion with XbaI and EcoRI and cloned into the XbaI and EcoRI sites of the FU-CRW lentiviral backbone (Memarzadeh et al., 2007). The final plasmid was named FU-MYCN-CRW. The FU-IYLW lentiviral vector was used for ectopic expression of firefly luciferase. The inducible N-Myc lentiviral vector was cloned by inserting *MYCN* into the BamHI site of the PSTV lentiviral backbone. The final plasmid was named PSTV-MYCN-CGW. Lentiviruses were prepared and titered as described (Xin et al., 2005).

Cell Lines

DU145, LNCaP, and PC-3 (ATCC) were grown in RPMI with 10% FBS. LAPC4 (gift from Robert Reiter, UCLA) was grown in Iscove's with 20% FBS. NCI-H660 (ATCC) was grown in HITES media containing RPMI, 5% FBS, 10 nM hydrocortisone, 10 nM beta-estradiol (Sigma), insulin-transferrin-selenium, and Glutamax (Life Technologies). LASCPC-01 was established by dissociating an N-Myc/myrAKT1 tumor as previously described (Stoyanova et al., 2013) and plating cells in HITES media. Clonal sublines of LASCPC-01 were established by singly sorting the LASCPC-01 cells on a BD FACS ARIA II (BD Biosciences) into individual wells of a 96-

well plate each containing 100 µl of HITES media. Single cell deposition was verified by direct microscopic visualization and cultures were monitored daily for colony formation.

Histology, Immunohistochemistry, and Immunoblotting

Tumor samples were formalin-fixed, paraffin-embedded, sectioned to 4 µm thickness, and mounted on glass slides. For each tumor, sections were stained with a standard H&E protocol. For immunohistochemistry, unstained sections were deparaffinized, hydrated, and subjected to heat-induced antigen retrieval using 40 mM sodium citrate buffer pH 6. Primary and secondary antibodies for immunohistochemistry are listed below. For immunoblot analysis, tumor tissues and prostate cancer cell lines were homogenized and lysed in either urea lysis buffer (20 mM HEPES pH 8.0, 9 M urea, 2.5 mM sodium pyrophosphate, 1.0 M beta-glycerophosphate, 1% N-octyl glycoside, 2 mM sodium orthovanadate) or TNN lysis buffer (50 nM Tris pH 8, 120 nM NaC1, 0.5% NP-40, 1 mM dithiothreitol, and protease inhibitors). Primary and secondary antibodies for immunoblotting are listed below. Films were scanned on an HP Scanjet G4050 for analysis. Densitometry was performed using Adobe Photoshop CS5 and corrected for background intensity.

Antibodies for Immunohistochemistry and Immunoblotting

Primary antibodies used for immunohistochemistry include CK8 (1:1,000, Covance MMS-162P), p63 (1:250, Santa Cruz sc-8431), AR (1:250, Santa Cruz sc-816), CHGA (1:600, Dako M0869), NCAM1 (1:100, Novocastra NCL-CD56-504), SYP (1:200, Novocastra NCL-SYNAP-299), TTF-1 (1:5,000, Upstate #07-601), FOXA2 (1:200, Abcam ab108422), and HLA Class I ABC (1:200, Abcam ab70328). Secondary antibodies used were ImmPRESS Anti-Rabbit Ig

Peroxidase and Anti-Mouse Ig Peroxidase (Vector Labs). Liquid DAB+ substrate reagent (Dako) was used to perform direct chromogenic visualization. Primary antibodies used for immunoblotting include N-Myc (1:1,000, Santa Cruz B8.4.B), AURKA (1:1,000, Abcam ab1287), NSE (1:1,000, Abcam ab139749), ASCL1 (1:1,000, BD Pharmingen 24B72D11.1), AKT (1:1,000, Cell Signaling #4691), phospho-AKT Ser473 (1:1,000, Cell Signaling #9271), phospho-histone H3 Ser10 (1:1,000, Cell Signaling #3642), histone H3 (1:5,000, Cell Signaling #4499), cleaved PARP (1:1,000, Cell Signaling #5625), cleaved caspase-3 (1:1,000, Cell Signaling #9661), GAPDH (1:5,000, GeneTex GT239) and p84 (1:2,000, GeneTex 5E10). Secondary antibodies used were Goat Anti-Rabbit-HRP Conjugate and Goat Anti-Mouse-HRP Conjugate (BioRad) and Rabbit anti-Chicken Secondary Antibody (Thermo Scientific).

Castration-Resistance Assay

Dissociated N-Myc/myrAKT1 tumor cells were incubated with CD49f-APC antibody (eBiosciences) at 4ºC for 15 minutes. Cells were sorted on a BD FACS ARIA II to isolate the GFP^+, RFP^+, and $CD49f^{low}$ population. 10^5 GFP^+, RFP^+, and $CD49f^{low}$ tumor cells or LNCaP cells were resuspended in 50 µl of cold Matrigel (BD Biosciences) and implanted subcutaneously in intact or surgically castrated NSG mice. Surgical castration (orchiectomy) of mice was performed in accordance with a protocol approved by the Animal Research Committee at UCLA.

Metastasis Assays

Dissociated N-Myc/myrAKT1 tumor cells were incubated in HITES media and propagated for two weeks in culture prior to infection with lentivirus expressing firefly luciferase. 10^6 N-Myc/myrAKT1 or LNCaP cells expressing luciferase were washed twice with PBS, resuspended

in 100 µl of Hank's buffered saline solution (HBSS), and injected into the tail veins of NSG mice. 10^4 N-Myc/myrAKT1 or LNCaP cells expressing luciferase were also washed in PBS, resuspended in 50 µl of HBSS, and injected into the left anterior lobe of the prostate of NSG mice. Mice were injected with 150 µl of 15 mg/ml luciferin intraperitoneally five minutes prior to live bioluminescent imaging with an IVIS Lumina II (Caliper Life Sciences) under inhaled isoflurane anesthesia. Metastasis assays and live bioluminescent imaging of mice were performed in accordance with a protocol approved by the Animal Research Committee at UCLA.

Image Segmentation Analysis

Primary, secondary, and tertiary N-Myc/myrAKT1 tumors passaged in intact and castrate mice were harvested and fixed in 10% buffered formalin for 16 hours. Two tumors for each condition were embedded in paraffin, sectioned and mounted on glass slides, and stained with H&E. High-resolution scans of whole stained sections were obtained using an Aperio ScanScope AT (Leica Biosystems). For each tumor section, ten randomly selected fields of 20X magnification were exported in TIFF format. For image segmentation, the smart segmentation feature of Image-Pro Premier (Media Cybernetics) was trained to classify two classes of cell objects (neuroendocrine carcinoma or adenocarcinoma) and background in H&E-stained sections of human prostate adenocarcinoma and small cell prostate carcinoma using the supervised class assignment of at least 50 individual cellular objects. TIFF images of each H&E-stained N-Myc/myrAKT1 tumor section were processed and the total pixel area of each class type was exported for quantification.

Laser Capture Microdissection and RNA Isolation

Tumor tissues were embedded and frozen in O.C.T. freezing compound. 10 μm sections of tumor were cryosectioned and mounted on laser capture microdissection slides. The slides were stained using the Arcturus Histogene LCM Frozen Section Staining Kit (Life Technologies). Laser capture microdissection was performed on a Leica Microsystems LMD7000 with visualization at 5X and 10X magnification. Microdissected specimens were collected into sterile PCR tubes and RNA isolation was performed with the Arcturus PicoPure RNA Isolation Kit (Life Technologies). RNA was analyzed using an RNA Bioanalyzer Kit (Agilent Technologies).

Whole Transcriptome Sequencing Analysis

cDNA libraries were prepared from isolated RNA using the TruSeq RNA Sample Prep Kit v2 (Illumina). High-throughput sequencing with 75 bp paired-end reads was performed using an Illumina HiSeq 2500 in rapid run mode. Reads were mapped to human genome reference HG19 using MapSplice (Wang et al., 2010b). Gene expression was quantified using RSEM (Li and Dewey, 2011) and quantile normalized. Gene set enrichment analysis was performed using GSEA software from Broad Institute (Subramanian et al., 2005) with a pre-ranked list of genes differentially expressed (>4-fold) between neuroendocrine carcinoma carcinoma and adenocarcinoma in each tumor sample.

Neuroendocrine Gene Signature

A computational model was designed to discriminate the seven NEPC and 30 prostate adenocarcinoma samples from the Beltran *et al.* RNA-seq gene expression dataset. Using the dichotomy based on the clinical diagnoses, we trained a logistic regression model with elastic net regularization (Friedman et al., 2010). We characterized the elastic net regularization with

parameters for the ridge regression term and LASSO term. The ridge regression term was fixed at 1.0 given the absence of preceding information about its importance. A LASSO term was selected to generate a gene expression signature with 50 non-zero weights. The model evaluated *in silico* through leave-pair-out cross validation. This scheme evaluates all possible pairs of one neuroendocrine prostate cancer and one adenocarcinoma sample and withholds each pair from training. The model trains on all other samples and then is applied back to the withheld pair. The final weighted neuroendocrine gene signature score was able to accurately classify all pairs of NEPC and prostate adenocarcinoma samples. Gene ontology was performed with DAVID 6.7 (Dennis et al., 2003) using official gene symbols.

Copy Number Variation and Whole Exome Sequencing Analysis

Snap frozen tissues were manually homogenized with a Dounce homogenizer and DNA was extracted using the DNeasy Blood and Tissue Kit (QIAGEN). Copy number analysis was performed on an Affymetrix Cytoscan HD Array and data was processed using the Affymetrix Chromosome Analysis Suite v3.1.0.15 with the NA33 reference model and using the High-Resolution setting. Exomes were isolated with the SeqCap EZ Human Exome Library v3.0 (Roche) and libraries were prepared using the Low-Throughput Library Preparation Kit with standard PCR amplification module (KAPA Biosystems). High-throughput sequencing with 150 bp paired-end reads was performed using an Illumina HiSeq 3000. Sequence data were aligned to the GRCh37 human reference genome using BWA v0.7.7-r411 (Li and Durbin, 2009). PCR duplicates were marked using the MarkDuplicates program in the Picard-Tools-1.115 tool set. GATK v3.2-2 was used for INDEL realignment and base quality recalibration (McKenna et al., 2010). Exome coverage was calculated using BEDTools (Quinlan and Hall, 2010). SAMtools

was used to call the single nucleotide variants and small INDELs (Li et al., 2009). All variants were annotated using ANNOVAR (Wang et al., 2010a). Data was subsequently filtered for genotype quality score, read depth (>15), and single nucleotide polymorphisms using the dbSNP and 1000 Genomes databases (Sherry et al., 1999).

Serial Dilution and Clonal Subline Xenografts

For serial dilution experiments, 1, 10, 100, or 1,000 LASCPC-01 cells were resuspended in 20 µl of cold Matrigel and implanted subcutaneously in NSG mice. For clonal subline xenografts, 10^6 LASCPC-01 cells were resuspended in 50 µl of cold Matrigel and injected subcutaneously in NSG mice. All xenograft studies were performed in accordance with a protocol approved by the Animal Research Committee at UCLA.

N-Myc Tumor Dependence Studies

For inducible N-Myc/myrAKT1 experiments, 2 x 10^6 inducible N-Myc/myrAKT1 tumor cells were resuspended in 50 µl of cold Matrigel and implanted subcutaneously in NSG mice that were fed doxycycline food pellets (Bio-Serv) for induction and/or fed regular food pellets with daily changes in cages and bedding for doxycycline withdrawal. Tumor dimensions were measured by calipers and tumor volumes were calculated using the following equation, V=(L*W*H)/2.

***In vitro* Testing of Aurora A Kinase Inhibitors**

CD532 (EMD Millipore), MLN8237, VX-680, cabazitaxel, and MG-132 (Selleck Chemicals) were dissolved in DMSO. 5 x 10^6 LASCPC-01 cells were plated in a 10 cm dish in HITES media and incubated with the indicated dose of drug at 37º C prior to collection. For cell cycle analysis,

cells were washed with PBS and fixed in 70% ethanol in PBS overnight at -20ºC. Fixed cells were then stained with propidium iodide (50 µg/ml) and treated with RNase A (100 ng/ml) for 30 minutes at 37ºC. Cell cycle analysis was performed on a BD FACSCanto (BD Biosciences). Cell viability studies were performed by seeding 10^4 LASCP-01 cells in 100 µl of HITES media in each well of a 96-well white wall optical plate. Cell viability after drug treatment was analyzed relative to DMSO treatment using the CellTiter-Glo Luminescent Cell Viability Assay (Promega). For proteasome inhibition studies, 2 x 10^6 LASCPC-01 cells were plated in a 10 cm dish in HITES media and pre-treated with 10 µM MG-132 for three hours then treated with the indicated dose of CD532 for an additional three hours.

Kinase Selectivity Analysis

Kinase selectivity analysis of CD532 was performed using the KINOME*scan* screening and profiling service with the *scan*MAX panel (DiscoveRx) at a fixed dose of 10 µM (Davis et al., 2011). Small molecule kinase interaction maps were generated using TREE*spot* Compound Profile Visualization Tool and images were reprinted with permission from DiscoveRx Corporation. Quantitative selectivity scores were calculated by enumerating the small molecule kinase interactions at specific thresholds divided by the total number of kinases evaluated.

***In vivo* CD532 Studies**

For short-term CD532 treatment studies, 10^6 dissociated cells from two independent N-Myc/myrAKT1 tumors were resuspended in 50 µl of cold Matrigel and subcutaneously xenografted in NSG mice. Once tumors achieved a volume of 200 mm^3, mice were injected with CD532 60 mg/kg or vehicle (95% PEG 300 and 5% DMSO) intraperitoneally daily for two

doses. For CD532 tumor challenge experiments, 10^6 LASCPC-01 cells were resuspended in 50 µl of cold Matrigel and implanted subcutaneously in NSG mice. Once tumors achieved a volume of 35 mm^3, mice were injected with CD532 25 mg/kg or vehicle (95% PEG 300 and 5% DMSO) intraperitoneally twice per week. Tumor dimensions were measured by calipers and tumor volumes were calculated using the following equation, V=(L*W*H)/2. *In vivo* administration of CD532 and treatment monitoring were performed in accordance with a protocol approved by the Animal Research Committee at UCLA.

SUPPLEMENTAL REFERENCES

Davis, M.I., Hunt, J.P., Herrgard, S., Ciceri, P., Wodicka, L.M., Pallares, G., Hocker, M., Treiber, D.K., and Zarrinkar, P.P. (2011). Comprehensive analysis of kinase inhibitor selectivity. Nat Biotech *29*, 1046-1051.

Dennis, G., Jr., Sherman, B.T., Hosack, D.A., Yang, J., Gao, W., Lane, H.C., and Lempicki, R.A. (2003). DAVID: Database for Annotation, Visualization, and Integrated Discovery. Genome Biol *4*, P3.

Friedman, J., Hastie, T., and Tibshirani, R. (2010). Regularization Paths for Generalized Linear Models via Coordinate Descent. Journal of statistical software *33*, 1-22.

Li, B., and Dewey, C.N. (2011). RSEM: accurate transcript quantification from RNA-Seq data with or without a reference genome. BMC bioinformatics *12*, 323.

Li, H., and Durbin, R. (2009). Fast and accurate short read alignment with Burrows-Wheeler transform. Bioinformatics (Oxford, England) *25*, 1754-1760.

Li, H., Handsaker, B., Wysoker, A., Fennell, T., Ruan, J., Homer, N., Marth, G., Abecasis, G., and Durbin, R. (2009). The Sequence Alignment/Map format and SAMtools. Bioinformatics (Oxford, England) *25*, 2078-2079.

McKenna, A., Hanna, M., Banks, E., Sivachenko, A., Cibulskis, K., Kernytsky, A., Garimella, K., Altshuler, D., Gabriel, S., Daly, M., *et al.* (2010). The Genome Analysis Toolkit: a MapReduce framework for analyzing next-generation DNA sequencing data. Genome research *20*, 1297-1303.

Memarzadeh, S., Xin, L., Mulholland, D.J., Mansukhani, A., Wu, H., Teitell, M.A., and Witte, O.N. (2007). Enhanced paracrine FGF10 expression promotes formation of multifocal prostate adenocarcinoma and an increase in epithelial androgen receptor. Cancer cell *12*, 572-585.

Quinlan, A.R., and Hall, I.M. (2010). BEDTools: a flexible suite of utilities for comparing genomic features. Bioinformatics (Oxford, England) *26*, 841-842.

Sherry, S.T., Ward, M., and Sirotkin, K. (1999). dbSNP-database for single nucleotide polymorphisms and other classes of minor genetic variation. Genome research *9*, 677-679.

Subramanian, A., Tamayo, P., Mootha, V.K., Mukherjee, S., Ebert, B.L., Gillette, M.A., Paulovich, A., Pomeroy, S.L., Golub, T.R., Lander, E.S., *et al.* (2005). Gene set enrichment analysis: a knowledge-based approach for interpreting genome-wide expression profiles.

Proceedings of the National Academy of Sciences of the United States of America *102*, 15545-15550.

Wang, K., Li, M., and Hakonarson, H. (2010a). ANNOVAR: functional annotation of genetic variants from high-throughput sequencing data. Nucleic acids research *38*, e164.

Wang, K., Singh, D., Zeng, Z., Coleman, S.J., Huang, Y., Savich, G.L., He, X., Mieczkowski, P., Grimm, S.A., Perou, C.M., *et al.* (2010b). MapSplice: accurate mapping of RNA-seq reads for splice junction discovery. Nucleic acids research *38*, e178.

Xin, L., Lawson, D.A., and Witte, O.N. (2005). The Sca-1 cell surface marker enriches for a prostate-regenerating cell subpopulation that can initiate prostate tumorigenesis. Proceedings of the National Academy of Sciences of the United States of America *102*, 6942-6947.

Chapter 5:

Conclusion and Future Studies

The aim of the research presented here is to identify and characterize determinants of aggressive prostate cancer in order to pinpoint therapeutic vulnerabilities. In the prior chapters, we have explored how the target epithelial cell of transformation affects the prostate cancer differentiation state [1], outlined the tyrosine kinase signaling pathways active in lethal metastatic CRPC [2], and defined N-Myc as a genetic driver of NEPC and a promising therapeutic target [3].

We have developed a modified human prostate transformation using an organoid culture system that has enabled us to evaluate the response of both basal and luminal cells to transformation with oncogenic stress. Overexpression of c-Myc and myrAKT1 in basal cells produced xenograft tumors with a poorly-differentiated, high Gleason grade prostate adenocarcinoma phenotype that lacked AR expression. On the other hand, the same oncogenes overexpressed in luminal cells generated xenograft tumors with well-differentiated, low Gleason grade prostate adenocarcinoma that expressed AR. Our work provides the first evidence that human luminal cells can be a cell of origin of prostate cancer and that different cells of origin may modulate distinct phenotypes. We have established a platform that will allow the comparison of additional basal and luminal cell subpopulations in a defined transformation assay.

We have also performed phosphoproteomic analysis of prostate cancer samples to understand the network of active tyrosine kinases in advanced disease. In analyzing metastatic prostate tumors, primary prostate cancer tissue, and prostate cancer cell line xenografts, we identified distinct patterns of tyrosine phosphopeptide enrichment. Interestingly, metastatic tumors within patients demonstrated similar profiles but tumors across patients were dissimilar. These studies have led to a prioritized list of active kinases in advanced prostate cancer that should be considered for

further clinical development. However, investigation of kinase inhibition in prostate cancer must take into account the heterogeneity of kinase targets and should require rational combination therapy and patient selection.

Using the human prostate transformation assay, we have defined the overexpression of N-Myc and myrAKT1 as two oncogenic events sufficient to initiate NEPC from prostate epithelial cells. This advance represents the first genetically defined human model system of NEPC. Previously developed in vivo models of NEPC in mice involve the inactivation of p53 and Rb and rely on secondary genetic abnormalities given the long tumor latencies [4]. With the N-Myc/myrAKT1 model of human NEPC, we have demonstrated plasticity in prostate adenocarcinoma and NEPC and showed that N-Myc expression is required for tumor maintenance. Exploiting a feed forward loop and protein interaction between N-Myc and Aurora A kinase, we show that a conformation destabilizing inhibitor of Aurora A kinase induces the rapid degradation of N-Myc and leads to inhibition of tumor growth. In sum these studies provide evidence of a functional role for N-Myc in NEPC and indicate that N-Myc is a priority target for therapy.

Unanswered questions and future studies:

Profiling the comprehensive serine, threonine, and tyrosine kinase signaling networks in lethal, metastatic CRPC

Tyrosine kinases represent one class of protein kinases that account for only a small subset of total phosphorylation events. The relative abundance of serine phosphorylation to threonine

phosphorylation to tyrosine phosphorylation is thought to be 1,800:200:1 in vertebrate cells [5]. Like tyrosine phosphorylation, serine and threonine phosphorylation is important for the regulation of signaling pathways for numerous biological events including diseases such as cancer. The levels of phosphorylation and the moieties specifically phosphorylated on a given protein are of importance in the regulation of biologic activity and provide information about the activity of kinases and phosphatases.

Having reported the profile of tyrosine phosphorylation events and predicted tyrosine kinases active in metastatic CRPC, we are now investigating the active serine/threonine kinase signaling pathways in these tumors. We have generated a comprehensive map of the phosphoproteome in advanced prostate cancer and have demonstrated that integration of phosphoproteomic data with genomic and transcriptomic data provides additional complementary information that may be clinically relevant (Drake et al., submitted). We propose that this multi-omic approach provides pathway information that may be suitable for stratifying patients for targeted therapies in late-stage prostate cancer. Additionally, the prioritization of oncogenic signaling pathways enabled by this analysis may inform rational clinical trials for combinatorial kinase inhibition.

Clinical evaluation of conformation destabilizing inhibitors of Aurora A kinase in NEPC

Beltran et al. first demonstrated the activity of Aurora A kinase inhibition in NEPC in a pre-clinical NCI-H660 cell line xenograft model [6]. Given these pre-clinical data and relative overexpression and frequent amplification of *AURKA* in NEPC, the AURKA inhibitor MLN8237 is being tested in an early-phase clinical trial for NEPC at Cornell. Early indications suggest that

MLN8237 is not effective as a single agent in halting NEPC progression. However, in relapsed or resistant childhood neuroblastoma, a phase I clinical trial of MLN2387 administered with irinotecan produced a significant response rate [7]. Therefore, strategies to combine AURKA inhibition with either cytotoxic chemotherapy or other targeted inhibitors may be more effective in NEPC.

Our studies suggest that CD532 represents a different class of AURKA inhibitor that can target not only the kinase activity of AURKA but also influence its protein-protein interaction with N-Myc, leading to N-Myc destabilization. In a direct comparison of CD532 with MLN8237 in our model of NEPC, we have shown that MLN8237 does not demonstrate a similar effect on N-Myc. In *MYCN*-amplified neuroblastoma, CD532 was found to induce the near complete degradation of N-Myc while MLN8237 produced only a 50% reduction [8]. Further, the loss of cell viability in our N-Myc/myrAKT1 model associated with CD532 treatment was striking and substantially higher than with MLN8237 treatment. Regardless of the results of the MLN8237 trial in NEPC, CD532 or its pharmacodynamically optimized derivatives should be pushed forward to clinical studies for NEPC given its distinct and potent activity profile relative to MLN8237.

How do Myc paralogs differ in oncogenic function in prostate cancer?

The *Myc* family of proto-oncogenes (*MYC*, *MYCN*, *MYCL1*) encode highly regulated basic helix loop helix transcriptional factors (c-Myc, N-Myc, L-Myc) that act downstream of ligand-receptor complexes and signal transduction pathways [9]. Myc proteins heterodimerize with Max and interact with active or repressive regulatory networks that modulate transcriptional activity upon

binding to E-box consensus DNA sequences [10]. In cancer, the multi-faceted roles of Myc in promoting DNA replication, metabolic reprogramming, genomic instability, and metastasis are well-documented [9]. Overexpression of the *Myc* family of proto-oncogenes is critical for the genesis and progression of the majority of human cancers. Yet, the deregulation of *MYC*, *MYCN*, or *MYCL1* is each associated with only certain human cancers and their functions are not always interchangeable [11]. For instance, Burkitt's lymphoma, an aggressive non-Hodgkin's lymphoma, is nearly always associated with translocation of *MYC* but not *MYCN* or *MYCL1* [12]. In addition, *MYCN* amplification identifies a high-risk group of childhood neuroblastomas with poor clinical outcomes [13]. These observations suggest that Myc paralogs may exhibit many shared but also distinct functions in human cancer.

In prostate cancer, we have used the in vivo transformation assay to show that the overexpression of c-Myc or N-Myc in combination with myrAKT1 in prostate epithelial cells produces distinct prostate cancer phenotypes: adenosquamous carcinoma (c-Myc/myrAKT1) or adenocarcinoma and neuroendocrine carcinoma (N-Myc/myrAKT1) [3, 14]. We have now directed our efforts to investigate the unique oncogenic functions of c-Myc and N-Myc that generate these phenotypic differences. Given the complexity of Myc paralog functions in cancer, we have decided to pursue a broad-ranging approach with the simultaneous profiling of the Myc interactome, transcriptome, proteome, and phosphoproteome in our Myc-driven human models of advanced prostate cancer. Novel biocomputational analyses to integrate multi-omic datasets will be implemented to obtain a deeper understanding of how Myc paralogs and their regulatory networks drive distinct gene expression patterns and signaling pathways.

Targeting the neuroendocrine differentiation state of NEPC

The neuroendocrine differentiation state of NEPC is a defining characteristic that distinguishes it from conventional prostate adenocarcinoma. Therefore, we and others believe that inhibition of the pathways that govern and maintain neuroendocrine transdifferentiation represents a logical therapeutic strategy. Advances in the fields of epigenetics and stem cell biology have led to an understanding that epigenetic regulation of chromatin structure, via DNA methylation, histone tail modifications, and nucleosome remodeling, determines cellular identity [15]. Recent work from Clermont et al. and Beltran et al. have shown that Polycomb repressive complex expression and global methylation profiles can distinguish NEPC from prostate adenocarcinoma [16, 17]. Inhibition of the Polycomb protein CBX2 in advanced prostate cancer was shown to induce cell death [18]. Strikingly, inhibition of the Polycomb protein EZH2 in AR-negative NEPC led to the re-expression of AR and growth inhibition [19], suggesting that differentiation therapy may be a potent treatment strategy.

In the hematopoietic system, cell surface markers have been used to identify and isolate distinct stem cell and progenitor populations [20]. Recent proteomic profiling of cell surface protein (surfaceome) expression across a large number of cell types including cancer cells demonstrated that unique cell identities exhibit quantitative and qualitative differences in cell surface protein expression [21]. We hypothesize that the distinct differentiation states of NEPC and prostate adenocarcinoma should be reflected in the cell surfaceome, allowing for the identification of cell surface targets that are differentially expressed and could form the basis for antibody or chimeric antigen receptor T-cell therapies for NEPC. Support for this general strategy comes from the

development of an anti-DLL3 antibody-drug conjugate for SCLC where an early-phase clinical trial has shown a dramatic response rate [22]. DLL3 is a Notch ligand that is expressed in neural lineages. In current studies, we are performing combined transcriptome profiling and cell surface capture with proteomics to isolate cell surface proteins that are differentially expressed between NEPC and prostate adenocarcinoma cell lines and tumors.

References

1. Park, J.W., et al., *Prostate epithelial cell of origin determines cancer differentiation state in an organoid transformation assay.* Proc Natl Acad Sci U S A, 2016. **113**(16): p. 4482-7.

2. Drake, J.M., et al., *Metastatic castration-resistant prostate cancer reveals intrapatient similarity and interpatient heterogeneity of therapeutic kinase targets.* Proc Natl Acad Sci U S A, 2013. **110**(49): p. E4762-9.

3. Lee, J.K., et al., *N-Myc Drives Neuroendocrine Prostate Cancer Initiated from Human Prostate Epithelial Cells.* Cancer Cell, 2016. **29**(4): p. 536-47.

4. Berman-Booty, L.D. and K.E. Knudsen, *Models of neuroendocrine prostate cancer.* Endocr Relat Cancer, 2015. **22**(1): p. R33-49.

5. Hunter, T., *The Croonian Lecture 1997. The phosphorylation of proteins on tyrosine: its role in cell growth and disease.* Philos Trans R Soc Lond B Biol Sci, 1998. **353**(1368): p. 583-605.

6. Beltran, H., et al., *Molecular characterization of neuroendocrine prostate cancer and identification of new drug targets.* Cancer Discov, 2011. **1**(6): p. 487-95.

7. DuBois, S.G., et al., *Phase I Study of the Aurora A Kinase Inhibitor Alisertib in Combination With Irinotecan and Temozolomide for Patients With Relapsed or Refractory Neuroblastoma: A NANT (New Approaches to Neuroblastoma Therapy) Trial.* J Clin Oncol, 2016. **34**(12): p. 1368-75.

8. Gustafson, W.C., et al., *Drugging MYCN through an allosteric transition in Aurora kinase A.* Cancer Cell, 2014. **26**(3): p. 414-27.

9. Dang, C.V., *MYC on the path to cancer.* Cell, 2012. **149**(1): p. 22-35.

10. Diolaiti, D., et al., *Functional interactions among members of the MAX and MLX transcriptional network during oncogenesis.* Biochim Biophys Acta, 2015. **1849**(5): p. 484-500.

11. Nesbit, C.E., J.M. Tersak, and E.V. Prochownik, *MYC oncogenes and human neoplastic disease.* Oncogene, 1999. **18**(19): p. 3004-16.

12. Boxer, L.M. and C.V. Dang, *Translocations involving c-myc and c-myc function.* Oncogene, 2001. **20**(40): p. 5595-610.

13. Huang, M. and W.A. Weiss, *Neuroblastoma and MYCN.* Cold Spring Harb Perspect Med, 2013. **3**(10): p. a014415.

14. Stoyanova, T., et al., *Prostate cancer originating in basal cells progresses to adenocarcinoma propagated by luminal-like cells.* Proc Natl Acad Sci U S A, 2013. **110**(50): p. 20111-6.

15. Boland, M.J., K.L. Nazor, and J.F. Loring, *Epigenetic regulation of pluripotency and differentiation.* Circ Res, 2014. **115**(2): p. 311-24.

16. Clermont, P.L., et al., *Polycomb-mediated silencing in neuroendocrine prostate cancer.* Clin Epigenetics, 2015. **7**(1): p. 40.

17. Beltran, H., et al., *Divergent clonal evolution of castration-resistant neuroendocrine prostate cancer.* Nat Med, 2016. **22**(3): p. 298-305.

18. Clermont, P.L., et al., *Identification of the epigenetic reader CBX2 as a potential drug target in advanced prostate cancer.* Clin Epigenetics, 2016. **8**: p. 16.

19. Kleb, B., et al., *Differentially methylated genes and androgen receptor re-expression in small cell prostate carcinomas.* Epigenetics, 2016. **11**(3): p. 184-93.

20. Chao, M.P., J. Seita, and I.L. Weissman, *Establishment of a normal hematopoietic and leukemia stem cell hierarchy.* Cold Spring Harb Symp Quant Biol, 2008. **73**: p. 439-49.

21. Bausch-Fluck, D., et al., *A mass spectrometric-derived cell surface protein atlas.* PLoS One, 2015. **10**(3): p. e0121314.

22. Saunders, L.R., et al., *A DLL3-targeted antibody-drug conjugate eradicates high-grade pulmonary neuroendocrine tumor-initiating cells in vivo.* Sci Transl Med, 2015. **7**(302): p. 302ra136.